Thèse de Doctorat

Haiyang ZHANG

Mémoire présenté en vue de l'obtention
du grade de Docteur de l'Université de Nantes
Sous le label de l'Université Nantes Angers Le Mans

Discipline : Electronique
Spécialité : Télécommunications
Laboratoire : IETR UMR 6164

Soutenue le 17 octobre 2014

École doctorale Sciences et Technologies de l'Information et Mathématiques (STIM)

CONCEPTION ET RÉALISATION D'UN RÉSEAU D'ANTENNES À POINTAGE ÉLECTRONIQUE POUR LES COMMUNICATIONS PAR SATELLITE

JURY

Président	**M. Jean-Marc RIBERO,** Professeur, Université Nice Sophia Antipolis
Rapporteurs	**M. Fabien NDAGIJIMANA**, Professeur, INP Grenoble
	M. Patrick VAUDON, Professeur, Université de Limoges
Directeur de Thèse	**M. Tchanguiz RAZBAN**, Professeur, Ecole polytechnique de l'université de Nantes
Encadrant	**M. Yann MAHE**, Maître de Conférences Ecole polytechnique de l'université de Nantes

* * * * * *

A mes parents,
à ma femme,
pour leur soutien et leur confiance

A Monsieur Bo-nian LI

A mon grand-père

A toute ma famille

* * * * * *

Acknowledgments

I would like to express my gratitude to Tchanguiz RAZBAN and Yann MAHÉ, for their patient supervision and countless academic and professional guidance. When I was in trouble with my study and research, they have always helped me out with their rich knowledge. They have also provided me quantities of ideas and experimental conditions, thus I can progress with my work day by day.

I would like to thank also Prof. Serge TOUTAIN and Prof. Yide WANG, for their helpful suggestions and encouragement.

I would like also to thank the jury, for their patient review and for taking them too much time.

I'm sincerely grateful for all the help of Marc BRUNET, Guillaume LIRZIN, Anne CHOUSSEAUD, Sandrine CHARLIER and all the other staffs of IETR laboratory of Polytechnique de L'Université de Nantes.

Many thanks to my family for supporting my education for many years both before and after I came to study in France. They have always spirited me up and encouraged me to study hard to earn my better life.

I am so lucky to have Bin as my wife, she have always been supporting me and encouraging me during the last 7 years. I would like to thank her confidence.

I'm greatly indebted to the Chinese Scholarship Council (CSC), which provides me sufficient financial aides to live and pursuit my diploma abroad.

Finally, I want to thank all my colleagues and friends, we have had really wonderful time and great fun during the last 3 years.

The past three years is long, as it is consisted of over thousand of days and nights. Far away from my family. Always immersed in research and struggled to find the solutions in my study.

While three years is short when you look back on the time passed by. The life

was calm, real and fulfilling. Nantes is a piece of pure land both in reality and in my heart. I am sure I will miss this place, even if i haven't left.

Résumé long en Français

Actuellement, la réception de signaux télévisuels par satellite (DBS : Direct Broadcast from Satellite) est principalement réalisée à l'aide d'une antenne parabolique constituée d'un réflecteur métallique et d'un récepteur radio-fréquence situé au foyer de la parabole (LNB : Low Noise Block). Ce type d'antennes, reconnues pour leur structure simple et leur faible coût, présente un gain relativement constant en fréquence. D'un point de vue pratique, ces antennes sont installées au faîte ou sur les murs des maisons individuelles ou encore aux balcons des immeubles (contribuant ainsi à la pollution visuelle lorsque le nombre d'antennes installées est important). De plus, ces antennes souffrent de défauts inhérents à leur conception :

• elles sont volumiques (présence du LNB placé au foyer du réflecteur),

• elles ne permettent pas a priori de pointer automatiquement vers plus de deux satellites (utilisation de deux LNB). Au delà, l'utilisation de blocs motorisés permet de lever ce verrou au détriment de l'encombrement, du poids et du coût.

En effet, ces antennes possèdent un lobe principal fixe ne permettant de pointer (pour chaque tête LNB) que sur un seul satellite. Par conséquent, lorsqu'elles sont installées, les utilisateurs ne peuvent recevoir que les programmes diffusés par le satellite visé. Enfin, du fait de la difficulté de réglage du faisceau principal sur l'angle d'azimut et d'élévation du satellite recherché, la plupart des consommateurs font appel à des professionnels afin d'assurer une installation précise de l'antenne.

Ces dernières années, une nouvelle demande des consommateurs est apparue afin de proposer des solutions antennaires plus discrètes et s'intégrant mieux au paysage urbain. Pour lever les limites des antennes paraboliques volumiques et proposer une alternative crédible à ces dernières, la réalisation d'une antenne large bande, à gain élevé, dont le faisceau principal est orientable, à double polarisation et à faible coût est donc souhaitable. Dans ce travail de recherche, notre ambition est de démontrer la faisabilité de conception d'une antenne bi-polarisation pour réception satellite dans la bande de fréquence 10,7-12,7GHz. La solution retenue devra être la plus discrète possible et, par conséquent, la plus plate et la plus fine possible. De plus, son faisceau principal devra être orientable afin de rechercher et pointer automatiquement sur les satellites souhaités.

Dans ce manuscrit, nous présentons les principaux résultats obtenus lors de ce

travail de thèse. Deux topologies d'antennes réseaux ont été étudiées et optimisées pour permettre de répondre aux autres critères de ce projet :

• une antenne réseau de monopoles alimentés par accès coplanaire,

• une antenne réseau dont l'élément de base est une antenne microruban à résonateurs couplés en croix.

L'antenne élémentaire de type monopole à accès coplanaire est tout d'abord présentée. La structure de cette antenne est basée sur un monopole disque dont la bande passante est naturellement très importante pour un encombrement réduit. Afin de maîtriser la bande passante et ainsi s'affranchir de la réception de signaux hors bande, un élément parasite ainsi qu'une fente en forme d'arc sont introduits. La mise en œuvre d'un second élément, placé orthogonalement au premier, permet un fonctionnement bi-polarisation. L'introduction d'un mur électrique constitué de plusieurs vias métallisés permet de maîtriser l'isolation entre les accès (niveau supérieur à 18dB). Ainsi, dans un encombrement aussi réduit qu'un cercle de diamètre 6,2mm, cette antenne monopole répond aux critères de bande passante (10,5GHz-12,8GHz). Le seul critère qui n'est pas atteint est le gain : Cette problématique est résolue par la mise en réseau de cet élément de base, dans une configuration linéaire, puis étendue en exploitant la deuxième dimension. Cette étude fait l'objet du troisième chapitre du manuscrit. Il est à noter cependant que la configuration particulière de l'accès à l'antenne monopole impose une distribution série de la puissance. De plus, afin de contrôler les remontées des lobes secondaires sans contraindre de manière importante l'arbre de distribution, une loi de type Dolph-Chebyshev a été retenue. Ainsi, la répartition de puissance s'effectue au travers de l'utilisation d'un nombre important de transformateurs d'impédance. Ces transformateurs sont alors réalisés par des lignes quart d'ondes intrinsèquement faible bande. Lorsque le nombre d'éléments augmente, il devient alors complexe de maintenir une large bande passante. Néanmoins, il devrait être possible à terme de lever ce verrou et de proposer un réseau large bande basé sur cet élément.

Pour tenir compte de la difficulté de maintenir une bande passante suffisante, nous avons envisagé une autre solution utilisant l'association de plusieurs résonateurs couplés entre eux. L'antenne est alors constituée d'un patch rectangulaire alimenté par accès coaxial ainsi que de 4 éléments parasites résonants. La maîtrise de la bande passante est aussi assurée par l'utilisation d'une fente en forme de U inscrite au niveau de l'élément principal. Une bande passante relative de plus de 38% est alors obtenue couvrant 10GHz-14,7GHz. De la même manière que pour l'antenne monopole, afin de lever le problème de la réception d'une deuxième polarisation, une antenne identique est placée orthogonalement à la première. Pour limiter l'encombrement global, un des éléments parasites est partagé. Ce partage dégrade l'isolation entre les accès : afin de lutter contre cette remontée, plusieurs

solutions sont introduites telles que l'insertion de 4 fentes carrées au niveau de l'élément partagé, permettant ainsi de canaliser les courants se développant sur ce dernier, ou encore la découpe des angles des deux patchs principaux et du résonateur partagé. Une amélioration significative est alors observée et une isolation supérieure à 20dB est atteinte sur toute la bande de fréquence utile. Étant donné que cet élément de base est constitué de 4 résonateurs, ces derniers sont aussi contributifs en terme de rayonnement. Ainsi, un gain légèrement plus important que pour une antenne patch rectangulaire seule est obtenu. Cette antenne a été réalisée en couche supérieure sur un substrat de téflon d'épaisseur 1,524mm et l'excitation est reportée en couche inférieure sur un substrat téflon d'épaisseur 0,8mm. Une couche de masse entre ces deux parties permet d'assurer l'isolation, notamment au niveau du rayonnement. Par conséquent, cette solution présente un profil relativement fin et plat. De plus, la complexité de réalisation est limitée, et donc la solution relativement faible coût. Durant l'étude de cet élément, nous avons proposé une méthode simple permettant d'établir qu'il était possible de stabiliser le diagramme de rayonnement dans le demi-espace supérieur sur toute la bande passante de fonctionnement et d'atténuer de manière significative le rayonnement arrière. Le principe retenu est basé sur l'utilisation d'un anneau métallique de largeur $\lambda_g/4$ à la fréquence centrale (sur le même plan que l'antenne) et d'une fente en anneau elle aussi de largeur $\lambda_g/4$. L'antenne est alors située au centre des deux anneaux, à une distance de λ_g de l'anneau métallique (bord à bord). En utilisant ce principe, nous avons pu montrer, en simulation et en mesure, une amélioration incontestable du niveau des lobes secondaires, du niveau du rayonnement arrière ainsi que la stabilité en fréquence du diagramme de rayonnement dans le demi-plan supérieur.

Du fait des performances intéressantes de cette antenne à résonateurs couplés disposés en croix, et afin d'augmenter le niveau de gain, cet élément est mis en réseau. Afin de montrer la faisabilité d'un tel réseau, une première étude a consisté en une disposition linéaire de 4 éléments, puis une extension à la deuxième dimension est effectuée. L'inconvénient majeur de cette antenne réside dans son encombrement. En effet, sa taille effective est de l'ordre de $0{,}94\lambda_0$. La mise en réseau entraînera inévitablement l'apparition de lobes de réseaux. Aussi, le partage de résonateurs est introduit dans le chapitre 4 sur les deux configurations de réseaux. A l'aide de cette technique, la distance inter-élément a été diminuée de $0{,}94\lambda_0$ à seulement $0{,}7\lambda_0$ avec succès. Nous avons ainsi montré que l'utilisation de la technique de résonateurs partagés n'entraînait pas de modifications importantes ni en bande passante, ni sur le couplage entre les accès. En s'appuyant sur ces résultats encourageants, plusieurs topologies de réseaux de distribution ont été testées aussi bien sur la configuration 1D que sur la configuration 2D. Les distributions parallèles basées sur des jonctions en T entraînent une diminution significative de

la bande passante du réseau du fait de l'utilisation d'inverseurs d'impédance quart d'onde. Aussi, leur remplacement par des diviseurs de puissance de Wilkinson s'est avérée beaucoup plus intéressante afin de maintenir la bande passante. Une bande passante de 10,2GHz-13,3GHz est ainsi observée en mesure. L'utilisation d'une technologie polymère multicouches innovante (intégration de couches minces résistives enterrées) a permis l'intégration des deux réseaux de distributions (un pour chaque polarisation) en évitant les problèmes de couplages et de croisements des lignes. Le design et l'agencement des différentes couches est présentée et une réalisation est fournie par la société GTID-Protecno, située à Brest. Les mesures effectuées ont montré que, sur les deux polarisations, la bande passante est préservée et que l'isolation entre les accès est supérieure à 20dB sur toute la bande de fonctionnement. Cette solution d'intégration reste ainsi extrêmement intéressante en terme d'encombrement dans la mesure où l'épaisseur du multicouche n'excède pas 3,6mm. Le réseau 4×4 éléments réalisé présente ainsi un gain de 18,9dBi. Dans cette configuration, l'augmentation du gain, bien que significative, n'atteint pas les 12dB attendus par rapport à l'élément seul. Ceci se justifie par l'utilisation de la technique des résonateurs partagés. Ainsi, dans la configuration du réseau 4×4 éléments, le nombre d'éléments n'est pas, dans l'absolu, augmenté d'un facteur 16. Quoiqu'il en soit, nous avons démontré tout l'intérêt de cette technique et les objectifs de gain devraient être atteints en augmentant dans les bonnes proportions le nombre d'éléments.

La dernière partie de ce travail est consacrée au problème du pointage électronique et fait l'objet du chapitre 5. Les principes généraux des réseaux d'antennes sont brièvement introduits. Il est ainsi rappelé que l'orientation du faisceau principal de rayonnement est obtenue en imposant un gradient de phase au niveau de chacune des antennes élémentaires constitutives du réseau. Ce gradient a pour objectif de compenser le retard de phase géométrique imposé par la délocalisation spatiale des différentes antennes. En s'appuyant sur ce résultat, et dans un souci de validation de ce principe dans le cas du réseau d'antennes à résonateurs partagés, un gradient de phase statique est réalisé par l'introduction d'une asymétrie de phase à chaque étage du réseau de distribution précédemment validé. Il a ainsi pu être montré qu'un autre intérêt de la technique des résonateurs partagés résidait dans un dépointage plus important du faisceau principal pour un gradient de phase donné. Ce résultat est démontré par les mesures réalisées, dans un premier temps, sur un réseau 1×4 éléments, pour lequel le même gradient de phase est appliqué aux deux polarisations. Un dépointage de l'ordre de 15° est observé sur la polarisation pour laquelle les résonateurs partagés sont contributifs pour seulement 5° pour la seconde. Afin d'étayer cette constatation, le même réseau de distribution présentant un gradient de phase dans une seule direction est réalisé pour les deux polarisations

d'un réseau 4×4 éléments. Cette fois-ci, pour les deux polarisations, un dépointage de l'ordre de 15° est observé en mesure prouvant tout l'intérêt de cette configuration. La technique de partage des résonateurs permet non seulement de réduire la distance inter-éléments, mais aussi de réduire la dynamique de phase à appliquer au réseau pour un dépointage du faisceau principal donné.

Quelques études préliminaires concernant la problématique du pointage électronique sont présentées. Nous avons ainsi envisagé deux solutions de déphaseurs commandables électriquement qui reposent sur un ou plusieurs varactors. Une analyse théorique basée sur les performances attendues de ces déphaseurs a montré qu'il était tout à fait possible d'obtenir un pointage électronique continu en utilisant le réseau d'antennes à résonateurs couplés partagés, ce qui devrait permettre à terme de réaliser les fonctions de recherche et de pointage automatique vers les satellites de programmes télévisuels. De même, nous avons montré, en appliquant un gradient de puissance entre les éléments centraux du réseau et les éléments périphériques, qu'il était possible de réduire de manière significative le niveau des lobes secondaires sur une large dynamique de dépointage du faisceau principal. En contrepartie, une légère diminution du gain et une augmentation de l'ouverture à 3dB du faisceau principal sont observées.

Pour atteindre les objectifs en terme de gain, le nombre d'antennes élémentaires à mettre en réseau, et par voie de conséquence le nombre de déphaseurs associé, augmente de manière importante. La complexité du système de commande s'en trouve alors largement impactée. L'un des problèmes majeurs réside dans le nombre important de sources de tension à générer et à contrôler pour piloter chaque déphaseur. De plus, commander tous les déphaseurs simultanément est un challenge à part entière. Durant ce travail, nous avons aussi identifié et introduit un circuit mixte radio-fréquence/numérique capable de répondre à ces problèmes. Ce circuit utilise un ensemble de potentiomètres numériques. Une seule source DC est alors suffisante et sera distribuée de manière pondérée au travers des potentiomètres. Un microprocesseur est intégré au circuit pour piloter les différents potentiomètres et communiquer avec l'utilisateur afin d'obtenir le dépointage souhaité. Enfin, un circuit permettant la transmission sur le même câble coaxial de l'alimentation DC, du signal reçu en bande intermédiaire et des signaux de commande est aussi introduit. Le détail de ce travail est disponible dans les annexes du manuscrit.

Nous avons démontré l'intérêt et la faisabilité d'un réseau d'antennes à résonateurs partagés pour répondre aux objectifs de ce projet. La conception et la réalisation d'un réseau de plus grande taille, exploitant les résultats démontrés dans ce travail, est l'une des perspectives. Pour un gain attendu de 26dBi, un réseau de 256 éléments (réseau 16×16 éléments) devrait théoriquement être suffisant. Ce réseau, dont les dimensions n'excèdent pas 30cm×30cm pour une épaisseur de

4,7mm, associé à un LNB et un démodulateur, devrait permettre la mise en œuvre d'une chaîne complète et la validation de la réception correcte des signaux satellites. Une autre perspective est la réalisation et la validation pratique d'un réseau à pointage électronique. Enfin, des études complémentaires doivent être menées sur l'intégration des déphaseurs, sur l'introduction d'amplificateurs à gain contrôlé ou encore de diviseurs de puissance large bande non équilibrés afin de proposer un système antennaire intégré. Quoiqu'il en soit, ces topologies d'antennes réseaux sont des alternatives intéressantes aux antennes paraboliques actuellement utilisées pour la réception des signaux TV des systèmes DBS.

Contents

List of Tables

List of Figures

1

Introduction

In 1977, the International Telecommunication Union (ITU) adopted an international BSS plan under which each country was allocated specific frequencies at specific orbital locations of Broadcasting Satellite Service (BSS). BSS standard is generally organized and managed by ITU. The frequency bands in ITU region 1 (Europe, Russia and Africa) is 10.7-12.75 GHz, in region 2 (North and South America) is 12.2-12.7GHz and in region 3 (Asia and Australia) is 11.7-12.2GHz. Over the years, this plan has been modified to, for example, accommodate new countries, increase coverage areas, and reflect digital (rather than analog) technology. At present, numerous countries have brought into use BSS plan allocations [14]. BSS is also known as Direct-Broadcast from Satellite (DBS) system which serves billions of people all around the world with plentiful TV programs. Comparing with earth based radio relay TV broadcasting (in UHF and VHF band) and close-circuit TV broadcasting (with coaxial cable), BSS/DBS system has obvious advantages like low-cost, ultra wide coverage (especially convenient for suburban and remote districts), very less maintenance and higher capacity of channels.

BSS/DBS system is composed of 3 main parts, as depicted in Fig. 1.1, which are maintenance center, geostationary satellites and user reception devices. Maintenance center located on earth is mainly used to upload TV programs. In addition, it monitors satellite status including orbit altitude and location, angle of inclination and etc. The uplink frequency band from maintenance center to geostationary satellite is 17.3-18.1GHz (some countries also use the frequency band from 14.0 to 14.5 GHz). To achieve stable communication with satellites, maintenance centers are commonly located at suburban area with clear opening sky. There are also some

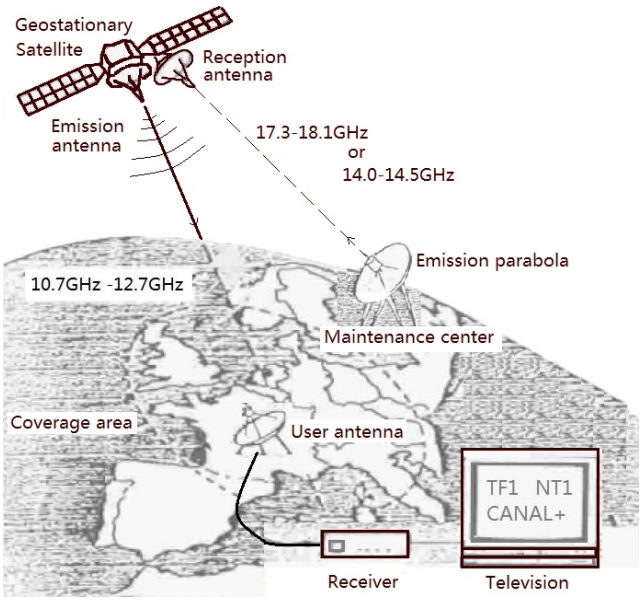

Figure 1.1: Diagram of DBS system [2]

mobile nodes equipped with high power emitter and collapsible parabola antenna carried by car which appear at sport matches provide rapid uploading and real-time broadcasting.

Geostationary satellites in the outer space play an important part in DBS system as relay stations and repeaters. All of these Geo-satellites are located in the stationary orbit of our earth which is 35,786 Kilometers high. As the period of revolution of geo-satellite is exactly equal to the rotation period of earth (23h 56min 4s) [15], each satellite appears relatively stationary to a reference point on the surface of the earth. This advantage makes communication between satellites and earth-based devices more convenient because there is no need to steer antenna to track satellite.

As Geo-satellite acts as relay station, its reception antenna for uplink and emitting antenna for downlink operate in different bands to avoid electro-magnetic interferences. Normally, the downlink is allocated with a band lower than uplink band and it ranges from 10.7 - 12.7 GHz. Usually, Geo-satellite is able to broadcast a list of TV program channels and each channel in downlink is located in a central frequency specified carrier and assigned with enough sub-band. In addition, different polarizations are often used to decrease interactions between adjacent channels.

Satellites in outer space are equipped with solar cells which supply sufficient power for satellites themselves and high-power microwave repeaters, most of satellites are able to service continuously more than 20 years. Until 2010, the total number of geostationary satellites is reported to be more than 379 [16] which means more than one geostationary satellites per-degree on average around our earth. Some of these geo-satellites are especially dedicated for television broadcasting, for example ASTRA at 19.2°E and Hotbird at 13°E in European and African

airspace. In addition numerous geo-satellites provide multiple services including telephone, data transmission and television broadcasting, for example Eutelsat at 3.1°E, 7°E, 9°E, 10°E and 21.5°E. Figure 1.2 illustrates a diagram of geo-satellites distribution (a small part) in the stationary Orbit. Abound satellite resource applies us possibility to voluntarily choose satellite to receive.

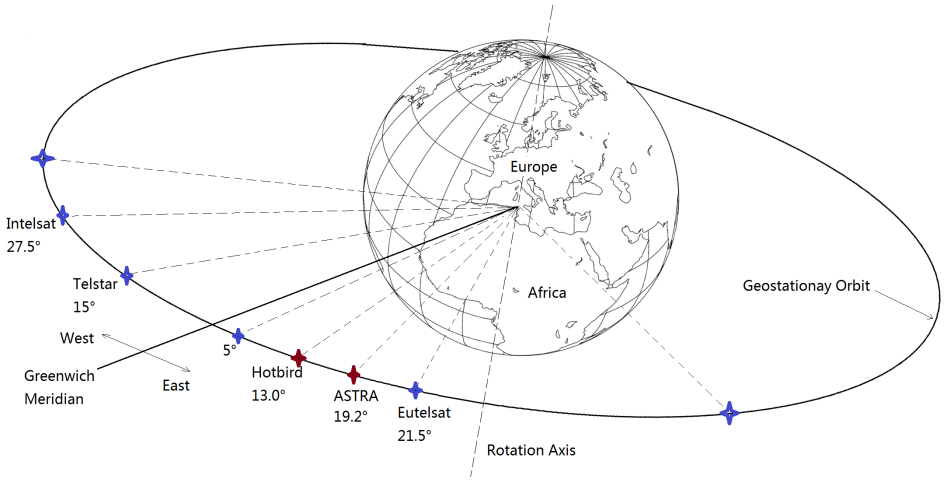

Figure 1.2: Illustration of Geostationary satellite distribution [2]

Comparing to L band (1-2GHz), S band (2-4GHz) and C band (4-8GHz) satellite telecommunications which use parabolic reception antennas bigger than 1.8m in diameter, DBS reception antenna has much lower profile as it operates in the higher frequency band which is from 10.7GHz to 12.7GHz. The key parameter to choose the exact size of reception antenna in different regions is the Effective Isotropically Radiated Power (EIRP) of satellite. Figure 1.3 and Figure 1.4 illustrate the EIRP distribution maps of DBS satellites ASTRA and Hotbird. It can be found that, most of European countries are covered in the radiation districts of both ASTRA and Hotbird with EIRP higher than 50dBW. Table I gives the recommended diameter of reception antenna corresponds to EIRP values. Generally speaking, a parabola reception antenna with the diameter 60cm is sufficient to receive satellite-broadcasting programs from ASTRA and Hotbird in Europe according to Fig. 1.4 and Table 1.1. Recent years, with the developments of space-borne high power Ku-band repeater and antenna, DBS satellites are able to cover much wider districts and provide higher level EIRP, the dimensions of reception antenna can be further decreased.

The third part of DBS system is user reception device, including reception antenna, Low-Noise Block (LNB) and decoder. Generally, offset-fed parabola antenna is used as reception antenna. Its metallic and parabolic reflector has very good reflecting and focusing functions to microwave. Signal from satellite could be gathered at the focus of parabola antenna where the LNB is located and then be captured

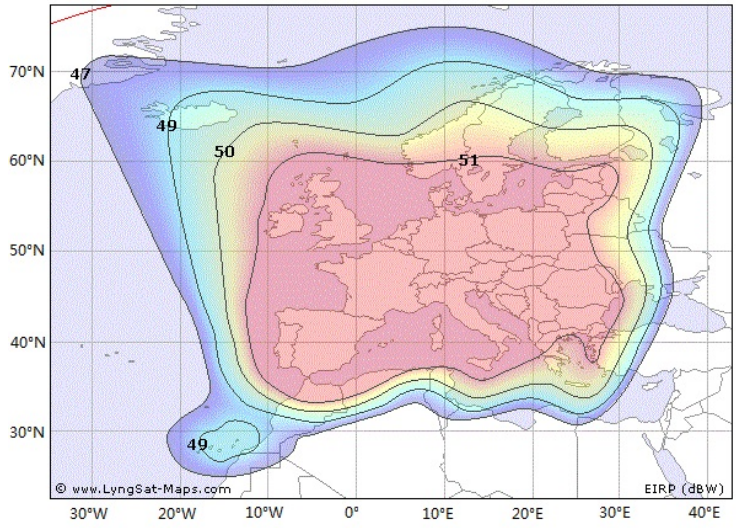

Figure 1.3: EIRP map of ASTRA Geo-satellite [3]

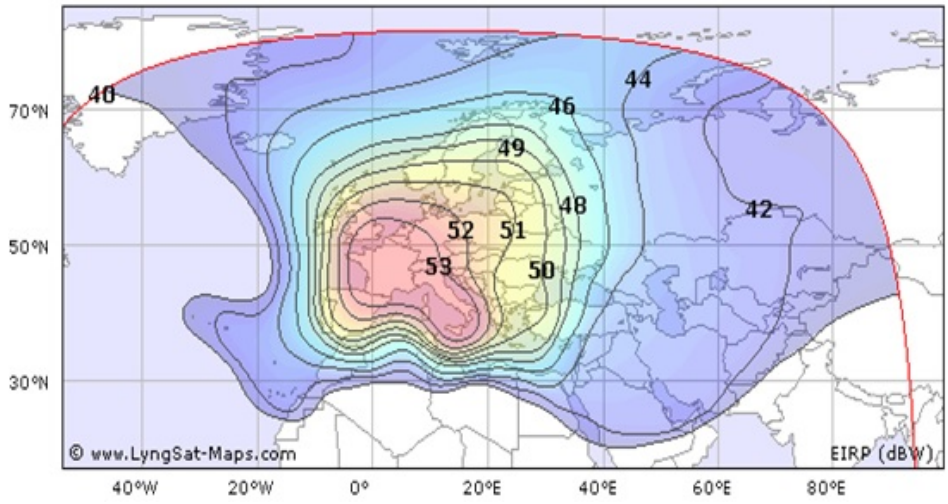

Figure 1.4: EIRP map of hotbird Geo-satellite [4]

by probes in the waveguide of LNB. Figure 1.5 shows a photograph of parabola antenna with LNB, the reflecting and focusing principle of parabolic reflector and the internal schematic diagram of LNB. The Low-Noise Block is a complex high frequency circuit covered by closed metal box remains a microwave port to connect cable. Generally, there are two probes inside the input waveguide of LNB, respectively for receiving horizontal polarized signal and vertical polarized signal. However, only one polarized signal will be amplified and chosen to pass to the rear part at one time. This function is realized by the voltage detector in LNB which switches vertical polarization at DC 13 volts and switches horizontal polarization at DC 18 volts. From Fig. 1.5, we can see that the pre-amplified signal passes a BPF and then mixes with local oscillating frequency. It is worth while noting that there are two local dielectric oscillators which resonate at 9.75GHz and 10.6GHz

Table 1.1: EIRP and corresponding diameter of parabola reception antenna

EIRP (dBW)	Diameter (cm)	EIRP (dBW)	Diameter (cm)
>50	50	50	50-60
49	55-65	48	60-75
47	65-85	46	75-95
45	85-105	44	95-120
43	105-135	42	120-150
41	135-170	≤ 40	170-200

respectively under the control of a 22 KHz signal loaded on coaxial cable. As the receiver can be installed in house, the cable used between the antenna part and the receiver might be very long. To decrease losses, the output signal is then transposed to Intermediate Frequency (IF) band which is from 950MHz to 2150MHz thus the losses in long coaxial cable will be less compare with Radio Frequency (RF). The frequency band of output signal is obtained with equation 1.1.

$$\boldsymbol{f_{out}} = \boldsymbol{f_{in}} - \boldsymbol{f_{osc}} \tag{1.1}$$

When $\boldsymbol{f_{in}} \in (10.7GHz, 11.7GHz)$, $\boldsymbol{f_{osc}} = 9.75GHz$, yields

$$\boldsymbol{f_{out}} \in (0.95GHz, 1.95GHz)$$

When $\boldsymbol{f_{in}} \in (11.7GHz, 12.7GHz)$, $\boldsymbol{f_{osc}} = 10.6GHz$, yields

$$\boldsymbol{f_{out}} \in (1.1GHz, 2.15GHz)$$

To sum up,

$$\boldsymbol{f_{out}} \in (0.95GHz, 2.15GHz)$$

Parabola antenna has been very widely used all around the world as DBS reception antenna due to its simple structure, stable gain, ease of fabrication and low-cost. Parabola antenna can be installed on the roof of house or at the balcony of apartment, once it is installed its beam is fixed to point to one satellite therefore users can only receive television programs from the chosen satellite. As it is difficult to find the accurate elevation and azimuth angles of satellite in the sky, sometimes parabola antenna should be installed by some trained people. Beam fix, non-planar and weak wind resistance ability are the main disadvantages of parabola antenna. Furthermore, it is also unpleasant to the eyes when installed on the roof of house.

In recent years, there is an increasing demand of new antennas which could

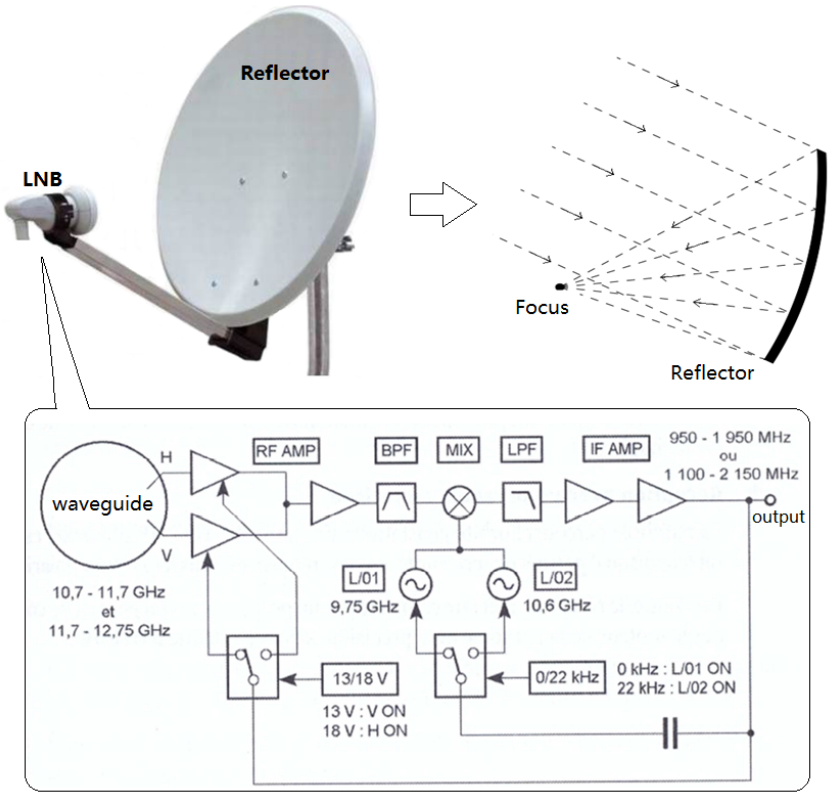

Figure 1.5: Principle of parabola antenna and topology of Low-Noise Block

replace parabola antenna with exceptional performances such as flatness and automatically steerable beam. Many researchers have done a lot of studies and some new products and new technologies emerge which are reported to have very outstanding performances. Table 1.2 lists three kinds of most recent products which stand for the state of arts of DBS reception antenna.

The antenna SNIPE SEDEA works in a wide band which covers the entire downlink frequency band of DBS system. Its antenna part is able to turn in three-dimensional by step motors so as to search satellites automatically. Comparing to parabola antenna, SNIPE has lower dimensions while its gain remains still very high. SNIPE antenna is applied for district where EIRP is higher than 50dBW, as depicted in the last section, it is suitable for almost all the European countries. Nevertheless, the satellite-searching process with mechanical structure is slow, and its non-planar design is not drastically improved because of motors and their control modules. Meanwhile its price has raised more than ten times compare to parabola antenna. It is therefore not a credible alternative to parabola antenna.

StealthRay 3000/40 is presented by RAS Company in Israel. StealthRay is composed of several antenna array panels to integrate a bigger array while the entire thickness is not significantly increased. As the most up to date phased array technology is adopted, StealthRay is able to search satellite automatically just by tuning

Table 1.2: Up-to-date DBS reception antennas

			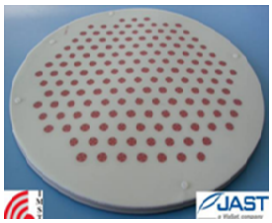
Product Name	SNIPE SEDEA (France)	StealthRay3000/40 (Israel)	NATANIA (Germany)
Working Band	10.7-12.75GHz	10.95-11.7GHz or 11.7-12.75GHz	10.7-12.75GHz
Polarization	Linear Polarization	Circular Polarization	Circular Polarization
Weight	17Kg	35Kg	–
Dimensions	45L*32W*19H	115L*90W*19H	Ø20
Beam adjusting (elevation angle)	Mechanically 15°-90° continuously	Electronically 20°-80° continuously	Electronically 20°-60° 4 steps
Gain	33.7dBi@12.7GHz	29.5dBi	–
Support EIRP	$\geq$ 50dBW	$\geq$ 50dBW	–
Price	800 Euros	$\geq$ 4000 Euros	1000 Euros

its main beam electronically with internal integrated phase shifters. StealthRay is reported to have the ability of steering its main beam between 20° to 80° in less than one second in elevation angle. With the assistance of step motor, the whole array is steerable in azimuth angle 360°. It is then able to position all the direct-broadcasting satellites. The main disadvantage of StealthRay is that its working band should be reserved in two options, not able to cover the entire band of DBS system. Moreover, StealthRay antenna is quite heavy and its very high price might be a great shock to one's credit card.

Another example of TV reception antenna is present by NATANIA project from Germany. This antenna has flat structure and very small profile especially suitable for cars and camping cars. Antenna array and integrated phase shifter technologies are adopted in this antenna according to their publications. Each element in the antenna array is driven by dedicated GaAs-MMIC phase shifter and Low-Noise Amplifier (LNA), therefore its main beam is steerable from 20° to 60° in elevation angle, but its cost is hard to decrease as hundreds of phase shifters and amplifiers

are used.

According to the current technologies, phased array antenna with flat structure is the most practicable solution for satisfying the new demands of DBS reception antenna. In our project, we would like to follow this way but to find a more economical substitute antenna with high performances. For the sake of completeness, we summarize the main specifications to be satisfied in our project in Table 1.3.

Table 1.3: Requirements

Operating frequency: 10.7GHz -12.7GHz
High gain, gain $\geq$25dBi
Flat, thickness less than 5cm
Polarization: dual linear and orthogonal, horizontal and vertical
Polarization isolation, better than 20dB
Beam continuously steerable rang $\geq 40°$
Half-Power Beam-Width $\leq 6°$
Low cost

Our project has been divided into two main parts, which are the beam steerable antenna array part and the corresponding RF to IF transposition circuit with phase shifter controllers. In this thesis, we are engaged to realize the antenna part. The entire thesis is consisted of 6 chapters. Introduction of the TV reception system, the state of the art and the requirements of our project are already given in chapter 1. In the second chapter, the reason of choosing microstrip patch antenna to begin our conception and the theory of microstrip antenna will be presented. Some up-to-date technologies to improve microstrip antenna bandwidth, polarization and gain are then introduced. According to the new technologies, two kinds of microstrip patch antennas are then discussed which are the CPW-fed antenna and the cross-type antenna. Their dimensions and design processes including parameter optimization will be illustrated with figures. Simulated and measured results and discussions will also be given. In chapter 3 and chapter 4, antenna arrays constructed with the proposed two kinds of microstrip patch antennas will be presented separately. To realize such arrays, different kinds of array arrangement methods and feeding networks including power distribution methods will be discussed. Simulated and measured results are presented to show the performances of proposed antenna arrays. As cross-type antenna array indicates more attractive performances, continuous studies are then carried out in chapter 5. To obtain beam steering function, firstly the fixed phase shifting networks are applied on cross-type antenna arrays. The advantage of using patch sharing technique which can not only decrease inter-element distance

but also increase beam steering angle will be introduced with diagrams and figures. Furthermore, to achieve beam continuously steerable array, varactor diode based and voltage controlled phase shifters will also be introduced in this chapter. With the help of phase shifter, the main beam of cross-type antenna array is able to steer electronically and automatically. Finally in chapter 6, conclusion and perspectives of the future work are given.

2

Single element antenna design

As proposed in chapter 1, phased array antenna with flat structure is the most practicable solution to satisfy the new demands of DBS reception antenna. According to the state of arts, microstrip patch antenna and reflect array antenna (as well as transmit-array) [17–19] are excellent candidates. Reflect array antenna which includes a feed horn and a flat array of radiation elements is proposed and developed quickly in recent years. Such antenna adopts the best features of parabola antenna and printed phased array antenna. It is very easy for fabrication and circuitry integration. The reflecting surface is often a planar array where power accepted by each element is re-radiated with a prescribed phase. Element phases can be fixed to produce a fixed beam or tunable to scan or reconfigure a beam [20]. As radiating elements are individual and no feed lines used, power loss in the feeding part of reflect array antenna remains very low and can be, most of the time, ignored. However as a horn antenna is placed at a distance away from reflecting surface, reflect array antenna is thus not a flat structure. In addition, to realize beam steering ability, quantity of phase shifters should be used which raises the complexity and cost of entire system. Comparing with reflect array antenna, microstrip patch antenna has strictly flat structure because both the antenna part and feeding part could be fabricated on very thin substrate with printed circuit technology. With the developments of antenna technologies, some new kinds of microstrip patch antennas with outstanding performances emerge in recent years. This leads us to finally adopt microstrip patch antenna as the solution of our project due to its flat conception and low cost, low weight advantages.

In this chapter, we will first introduce the basic microstrip patch antenna based

on rectangular shape microstrip antenna. Then we will focus on some of the existing techniques available to achieve the required performances. And finally, we would like to propose two different ways to design a patch antenna with suitable behaviors.

2.1 Microstrip Patch antenna theory

In this section, we would like to start with the introduction of the basic microstrip patch antenna conception and its standard performances. For simplifying reason, this introduction is based on simple shape resonating antenna. This antenna is approached from circuit point of view as well as radiation one. This part allows to better understand the key point of our project defining the limitation of such a technology.

2.1.1 Basic patch antenna model

Microstrip antenna is one of the most useful antennas at microwave frequency (f>1GHz), it consists of a metal patch on top of a grounded dielectric substrate, as shown in Figure 2.1. The shapes of microstrip antenna could be rectangular (square), circular, elliptical, triangular or any other continuous shapes. Rectangular patch is the most commonly employed. The rectangular patch antenna is approximately a half wavelength long section of microstrip transmission line. Its size is directly tied to the resonance frequency.

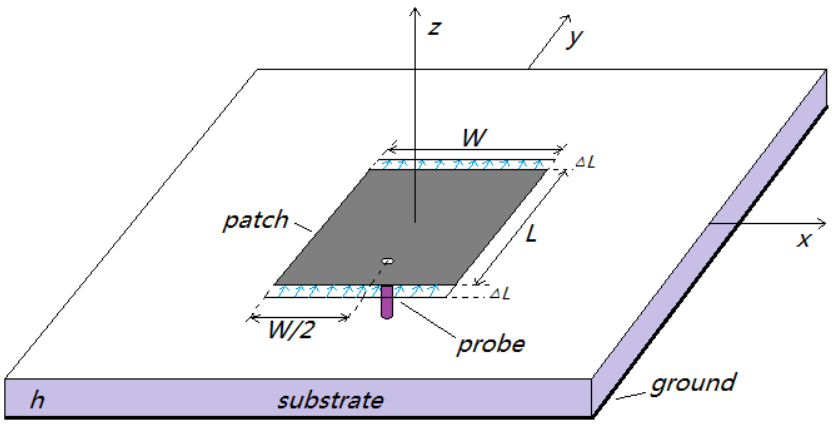

Figure 2.1: Microstrip patch antenna

Due to the fringing fields along the radiating edges of the antenna, a line extension ΔL associated with the patch has to be inserted into each radiation edges, the electrical patch dimension will then be bigger than its physical dimensions. We can add fringing length extension ΔL to each edge of the patch to get an effective length L_e. As depicted below:

$$\boldsymbol{L_e = L + 2\Delta L} \tag{2.1}$$

The line extension ΔL is given by formula [21]:

$$\frac{\Delta L}{\boldsymbol{h}} = 0.412 \left[\frac{\boldsymbol{\varepsilon_{eff}} + 0.3}{\boldsymbol{\varepsilon_{eff}} - 0.258}\right] \left[\frac{\boldsymbol{W/h} + 0.264}{\boldsymbol{W/h} + 0.258}\right] \tag{2.2}$$

Here, ε_{eff} is the effective dielectric constant and is given by [21]:

$$\boldsymbol{\varepsilon_{eff}} = \frac{\varepsilon_r + 1}{2} + \frac{\varepsilon_r - 1}{2}\left(1 + \frac{10\boldsymbol{h}}{\boldsymbol{W}}\right)^{-1/2} \tag{2.3}$$

ε_r and W/h should be limited in the ranges of [22]:

$$1 \leq \varepsilon_r \leq 128 \qquad and \qquad 0.01 \leq W/h \leq 100$$

2.1.2 Resonance frequency

Patch antenna is a distributed resonator and inherently exhibits several modes of resonance, but only a few modes are potentially useful [5]. Depending on wanted performances, the most useful modes are TM_{10}, TM_{01}, TM_{11}, and TM_{20}. For a given rectangular patch with a dimension LxW, the resonance frequencies could be expressed as follows [23]:

$$\boldsymbol{f_{mn}} = \frac{c}{2\pi\sqrt{\boldsymbol{\varepsilon_{eff}}}}\sqrt{\left(\frac{\boldsymbol{m\pi}}{\boldsymbol{L_e}}\right)^2 + \left(\frac{\boldsymbol{n\pi}}{\boldsymbol{W_e}}\right)^2} \tag{2.4}$$

Where $c = 1/\sqrt{\mu_0\epsilon_0}$, which is the light speed in vacuum.

The dominant mode of single patch antenna is TM_{10}. It is usually used because the radiation pattern has a broadside beam. In this mode, patch antenna acts as a wide microstrip line (width W) that has a resonant length of approximately half guided wavelength ($\lambda_g/2$). The resonance frequency of TM_{10} mode could be yielded from equation 2.4 when $m = 1$ and $n = 0$, which is

$$\boldsymbol{f_{10}} = \frac{c}{2\sqrt{\boldsymbol{\varepsilon_{eff}}}}\left(\frac{\boldsymbol{1}}{\boldsymbol{L_e}}\right) \tag{2.5}$$

2.1.3 Impedance matching

Patch antenna is usually fed along the center line which is orthogonal to the radiating edge (W) to maintain symmetry, minimize excitation of undesirable cross modes and then achieve good polarization. There are quantities of methods to feed patch antenna, for example, end feed, insert feed, coaxial cable feed, aperture feed

and coupled feed [24]. For each feeding method, the input impedance should be matched thus the patch antenna could absorb more input power and reflect less. The key point is to know the impedance distribution along the patch. According to the voltage and current, impedance distribution on a rectangular patch antenna at the resonance frequency can be plotted as shown in Figure 2.2. It can be seen that the electric field is zero at the center of the patch, maximum (positive at one side) and minimum (negative) on the opposite side. The current is just opposite with voltage which is zero at the edge and maximum at the center. Impedance is the ratio of voltage over current. Therefore the impedance of patch antenna is zero at the center and maximum at the edge. The typical edge impedance ($R_{edge} = \boldsymbol{F}(w, h, \varepsilon_r, f)$) of microstrip antenna depends strongly on the substrate permittivity and the width over height and it ranges typically from 150 ohm to 300 ohm [21, 25].

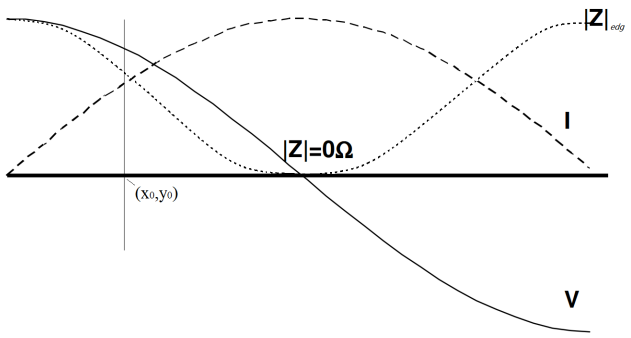

Figure 2.2: Voltage, current and impedance distribution of patch antenna [5].

For a given patch fed with coaxial cable (probe fed), as shown in Figure 2.3, the outer conductor of the coaxial cable is connected to the ground plane and the inner conductor is extended up to the patch antenna. When the feed point is shifting along the center line ($y_0 = W/2$) from one edge ($x = 0$) to the other edge ($x = L$), the impedance varies as the following expression depicts [23]:

$$\boldsymbol{R_{in} = R_{edge} cos^2 \left(\frac{\pi x_0}{L} \right)} \tag{2.6}$$

Generally, the coaxial cable used here follows the industrial standard of 50 ohm. From Fig. 2.2 and equation 2.6 it can be seen that there must exist two points on the patch, at which the impedance of feeding point matches well with the impedance of coaxial cable. As mentioned before, more power could be transmitted to antenna and very less power reflected to input port. The antenna can then radiate more power that increases the radiation efficiency of the antenna. Matching condition is maintained only for the resonance frequency while not for surrounding frequencies, which is the main factor which limits the bandwidth of the antenna.

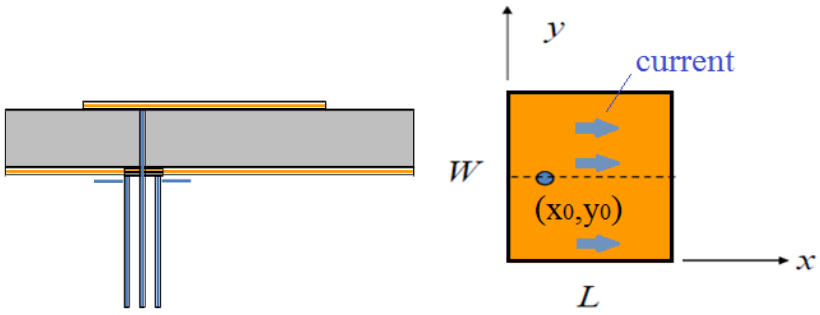

Figure 2.3: Geometry of coaxial cable fed patch antenna (left) and current flowing direction on patch (right).

2.1.4 Bandwidth

Bandwidth is another fundamental antenna parameter. Bandwidth describes the range of frequencies over which the antenna can properly radiate or receive energy. The bandwidth is often specified in terms of Fractional Bandwidth (FBW) which is the ratio of the frequency range (highest frequency minus lowest frequency) divided by the center frequency [26].

$$FBW = \frac{f_{max} - f_{min}}{f_0} \tag{2.7}$$

The bandwidth can also be specified in terms of return loss (reflection coefficient, S parameter: $|S_{11}|$) or a voltage standing-wave ratio (VSWR). Furthermore, the bandwidth of antenna is related to the antenna Q factor, as given by [8]

$$BW = \frac{VSWR - 1}{Q\sqrt{VSWR}} \tag{2.8}$$

Where Q is also known as quality factor, which is defined as the quotient between the power stored in the reactive field and the losses [27–30], as depicted in Equ. 2.9.

$$Q = \frac{E_{store}}{2\pi E_{loss}} \tag{2.9}$$

Where E_{store} indicates the power stored in antenna structure and E_{loss} includes the power radiated to free space and exhausted in substrate and etc.. As we all know that the single patch microstrip antenna is inherently narrow band (less than 10% FBW) as less energy is radiated and more energy stored in the patch capacitance and inductance due to strong influence between patch and ground plane. From Equ. 2.8, it can be seen an efficient way of expand antenna bandwidth is to lower the Q. For a resonator, the lower Q can be cause by either lower stored energy or larger losses [8]. The applications of expanding patch antenna bandwidth by lowering the

Q factor will be introduced in the coming sections in detail.

2.1.5 Radiation

Antenna is a radiator as it transforms high frequency current into microwave in emitting mode and transforms microwave into current in receiving mode. Surrounding an antenna, two main area can be defined: near field and far field. Far field is the most useful area for an antenna, as in the area, antenna's radiation pattern is defined. The radiation pattern defines the variation of the power density radiated by an antenna as a function of the direction away from the antenna. It indicates the directional dependence of the strength of the radio waves from antenna [26]. Generally, the radiation pattern of an antenna is the same with its receiving pattern.

For a given rectangular patch antenna as depicted in Fig.2.1. The dimension L is usually taken to represent the long dimension, which causes resonance at the frequency given by Equ.2.5. The radiating edges are at the ends of the L-dimension of the rectangle, which set up the single polarization. Radiation occurs at the ends of the W-dimension is far less and is referred to as the cross-polarization. The Fig.2.4 left is a side view which shows the snapshot of the E-field under the patch. Note that the fields under the L-edges are of opposite polarity (due to the half-wave nature of the patch) and when the field lines curve out and finally propagate out into the direction to the substrate they are now in the same direction (both facing left), rectangular antenna can then be assume as a two radiating slots (right) separated by L. In the far field perpendicular to the substrate, the radiation from the two sides adds up because the fields are in phase, thus we get the patch antenna radiation [31].

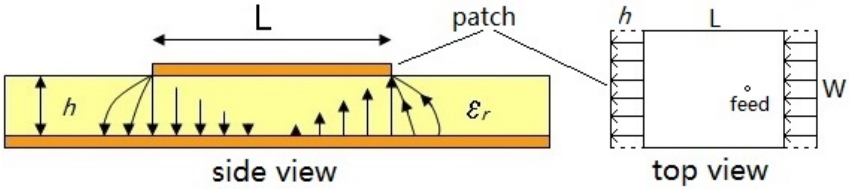

Figure 2.4: Side view of the E-field of microstrip patch antenna (only in substrate)

The microstrip patch antenna with finite ground plane as depicted in Fig. 2.1 is known to have a symmetric and a quite omni-directional radiation pattern in the front side, with wide beam-width and wide angle HPBW (Half-Power Beam Width), as depicted in Fig. 2.5.

2.1.6 Polarization

The polarization of an antenna is the polarization of the radiated fields produced by an antenna, evaluated in the far field area. Antennas are often classified

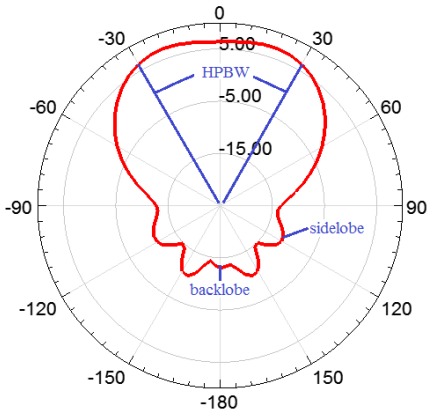

Figure 2.5: Radiation pattern of microstrip patch antenna

as "Linearly Polarized" or "Circularly Polarized", which means the E-field of microwave radiated by antenna varies linearly or circularly along its transmission direction. Horizontal polarization and vertical polarization are the two mostly often used Linear polarizations. And for circular polarization, it includes Left-Hand and Right-Hand Circular Polarizations (LHCP & RHCP). Due to the reciprocity theorem, antennas transmit and receive in exactly the same manner. Hence, a vertically polarized antenna transmits and receives vertically polarized fields. Consequently, if a horizontally polarized antenna is trying to communicate with a vertically polarized antenna, there will be no reception [26].

As the plane in which the electric field varies is also known as the polarization plane. The basic rectangular patch antenna depicted in Fig.2.1 is linearly polarized since the electric field varies only along y-axis (the feed point is along the center line). Thus the polarization plane in this structure is the yoz-plane. Whereas it can also be Circularly polarized if two opposite corners on patch are cut [32, 33] or with dual orthogonal feeds with a power divider network [33–35].

2.1.7 Microstrip antenna summary

In the previous sections, the basic configuration of microstrip patch antenna has been briefly introduced, as well as the relationship between radiator size and resonance frequencies and the voltage-current-resistance distribution on a probe fed patch. These proposed characteristics of microstrip patch antenna are very helpful when designing a new type of antenna with specified performances. In fact, microstrip patch antenna has been acquainted by designers since a long time and quantities of studies have been done to learn more about it. We would like to briefly sum up some of microstrip patch antenna characteristics and list in Table 2.1. This table permits to fix the main drawbacks and limitations which must be solved to achieve our requirements.

Table 2.1: Comparison

Advantages	Disadvantages
• Light weight, low volume and Low profile • Planar configuration. • Low fabrication cost • Supports linear and circular polarization • Can be easily integrated with microwave integrated circuits (MICs). • Capable of dual and multiple frequency operations. • Mechanically robust when mounted on rigid surfaces.	• Narrow bandwidth • Low efficiency • Low Gain • Extraneous radiation from feeds and junctions. • Low power handling capacity ($\approx 100W$). • Surface wave excitation.

2.2 State of the art of microstrip patch antenna

According to the summary given in Table 2.1, it can be seen that microstrip patch antenna is very attractive due to its small size, light weight, low cost, planar structure, ease of fabrication and integration. With these advantages, microstrip patch antenna has been widely used in many domains. As researches never stopped, a lot of solutions have been reported to simplify antenna design processes and solve the disadvantages of microstrip patch antenna. Here in this section, solutions on expanding bandwidth and achieving dual polarizations and high gain will be introduced.

2.2.1 Techniques for broadband

As mentioned previously, microstrip patch antenna suffers of relatively narrow bandwidth. A crucial issue is to broaden its bandwidth. A variety of broadband techniques have been developed using the three approaches categorized in Table 2.2. It is known that the factors affecting the bandwidth of a microstrip patch antenna are primarily the shape of the radiator, the feeding scheme, the substrate and the arrangements of radiating and parasitic elements. Essentially, the broad bandwidth of a microstrip patch antenna can be attributed to its low Q value and simultaneously well excited multiple resonances. If the antenna is considered as high Q resonator, lowering the Q by either reducing the reactive energy around the radiator or increasing losses broadens the bandwidth around its resonance. Alternatively, by inserting

a broadband impedance matching network between the antenna and feeder, good matching over a broad frequency range can be attained. If two or more adjacent modes are well excited simultaneously, the bandwidth can be twice or more than that for the single resonance [1].

In the following subsections, we would like to introduce some up-to-date techniques reported by antenna designers to broaden patch antenna bandwidth. It is worth while noting that, most of the time, several techniques are simultaneously used to broaden an antenna bandwidth.

Table 2.2: Broadband techniques for microstrip patch antennas [1].

Approach	Techniques
Lower the Q	Select the radiator shape
	Thicken the substrate
	Lower the dielectric constant
	Increase the losses
Use impedance matching	Insert a matching network
	Add tuning elements
	Use slotting and notching patches
Introduce multiple resonances	Use parasitic (stacked or co-planar) elements
	Use slotting patches, insert impedance networks
	Use an aperture, proximity coupling

Use thick substrate to Lower the Q

To lower the Q so as to broaden bandwidth, researchers have tried to use thick substrate with low dielectric constant which is good for improving the impedance bandwidth of antenna [6, 36–44], as shown in Fig. 2.6. However, investigations have shown that the impedance bandwidth monotonically increases with the substrate thickness while radiation efficiency rapidly decreases [36] and the achievable bandwidth will decrease when the thickness exceeds a certain value [1].

Use slotting patches to match impedance

U-slot antenna which is best known for its wideband characteristics is firstly introduced in 1995 by Huynh and Lee [45] as a single-layer, single patch linearly polarized and wideband antenna. A number of studies indicate that the U-slot patch antenna can provide impedance bandwidths in excess of 30% for air-substrate and

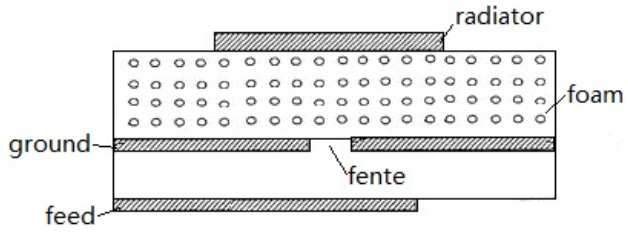

Figure 2.6: Geometry of patch antenna with thick foam substrate (from [6]).

in excess of 20% for material substrates [46]. It is an antenna simple in structure, but versatile in applications [7]. The basic geometry of the U-slot antenna is shown in Fig. 2.7. The U-slot introduces a capacitance, allowing the use of a thick substrate, and induces a second resonance near the dominant resonance of the patch, producing a wideband frequency response. In addition, a single patch antenna with U-slot is reported to have an average gain of 7dBi and good pattern characteristics quite omnidirectional on the broadside [47], which are also very attractive.

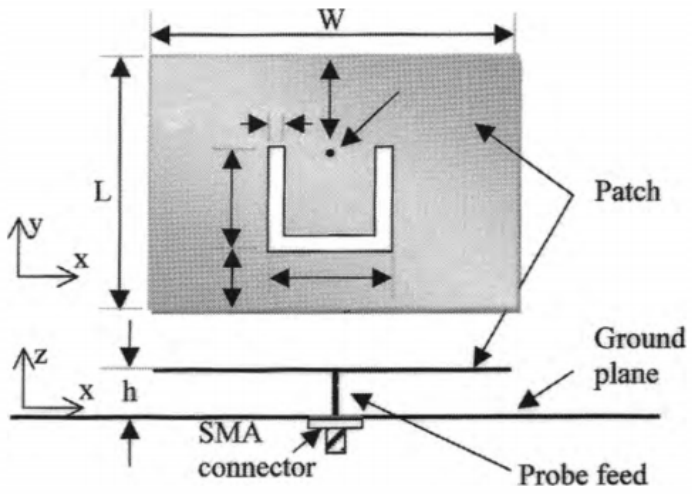

Figure 2.7: Geometry of the U-slot patch antenna (from [7]).

Use parasitic patches to introduce multiple resonances

Another approach is to introduce multiple resonances. The most direct way is to introduce additional radiating patches located close to the main radiator. These parasitic patches are excited by means of the electromagnetic coupling between them and the main patch. The parasitic patches can be located in the same plane, or stacked above the main patch [8]. Fig. 2.8 shows some methods to arrange parasitic patches, whereby one or more parasitic elements are located around the driven element. The small gaps allow the parasitic elements to be strongly coupled to the driven element. The elements have almost the same size. The well-excited

resonances are adjacent to one another such that a broader well-matched bandwidth is achieved, which is usually a few times broader than that of the single radiating element. Fig. 2.9 shows arrangements whereby parasitic elements are placed above the main patch. By dint of the coupling between stacked elements and the driven one, the impedance bandwidth can be greatly increased. Usually, the bandwidth can reach 10-20%, particularly when the medium between the upper and bottom patches is air or material with low permittivity. However, the main shortcoming of co-planar and stacked arrangements is the significant increase in the lateral size and thickness.

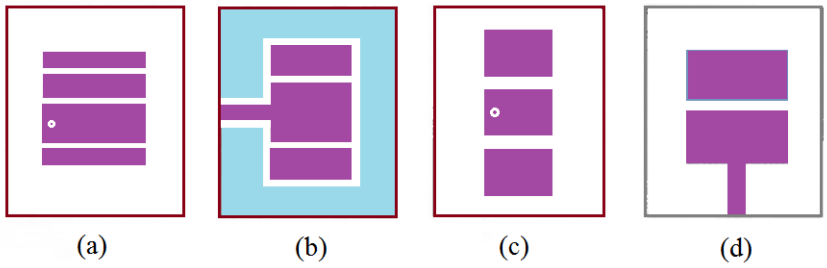

Figure 2.8: Co-planar arrangement (from[8]).

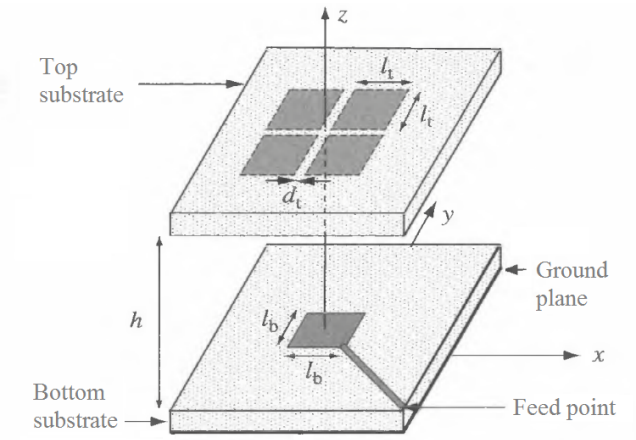

Figure 2.9: Stacked arrangement (from [8]).

2.2.2 Techniques for Ultra-wideband

In the previous section, techniques for broadening antenna bandwidth a few times (or 10-20%) than a single patch antenna have been introduced. However, there exists some other ultra-wideband techniques which could significantly expand the bandwidth over 100%. Meanwhile the antenna types are not anymore limited in the basic structure of microstrip patch antenna.

Coplanar waveguide (CPW) feed printed monopole antenna have received much attention due to its advantages of ultra-wide bandwidth and easy integration with

monolithic microwave circuits. Many researchers from academic and industrial have shown their interest for this kind of antenna. A lot of new antennas with various conceptions are reported. In [9], a CPW-fed square slot antenna with a widened tuning stub is reported to have large bandwidth of 60% obtained, shown in 2.10. In [48], Denidni et al. have proposed an ultra wideband antenna which is composed of a circular slot fed with a 50 ohm CPW line through a circular patch. The proposed configuration offers a large bandwidth from 2.3 to 13.9GHz in other words more than 143% respect to the central frequency. In another article [49], a planar hexagonal antenna fed by a coplanar waveguide has been studied by Santanu et al., which yields -10 dB return loss ranges from 1.24 to 20 GHz (177%). The ultra-wideband features make this kind of antenna a good candidate for ultra-wideband wireless applications. There exists some common ground in [9, 48, 49] that their radiators are all monopole antennas which are assumed to have wideband features [50–55]. Meanwhile these radiators are integrated in various shape slots on coplanar ground plane, the gaps between radiators and ground plane is continuously increased from very thin gap to wide slot. In addition, as ground plane under antenna part are totally deleted, the stored energy is less confined and radiated to free space, Thus the Q factor is reasonably decreased. According to the Equ. 2.8 as mentioned in section 2.1.4, the bandwidth is thus increased as Q factor decreases. With CPW-fed monopole conception the bandwidth of such antenna could be several times larger than a simple monopole antenna. It is worth noting that the CPW-fed technique is also attractive and good for integration with microwave circuits.

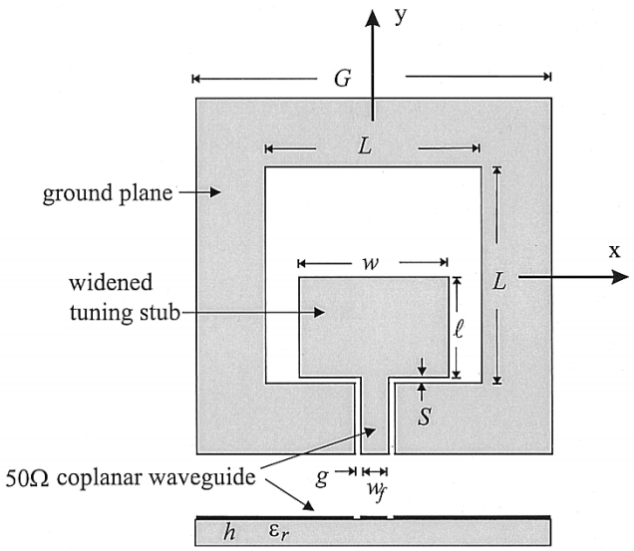

Figure 2.10: Geometry of CPW-fed slot antenna with a widened tuning stub [9].

A compact CPW-fed antenna with ultra-wideband is introduced in [10] and [56], which covers a band from 3.1 to 10.6 GHz (band dedicated to Ultra-wideband applications) with $S_{11} < -10dB$, as shown in 2.11. It can be seen that the proposed

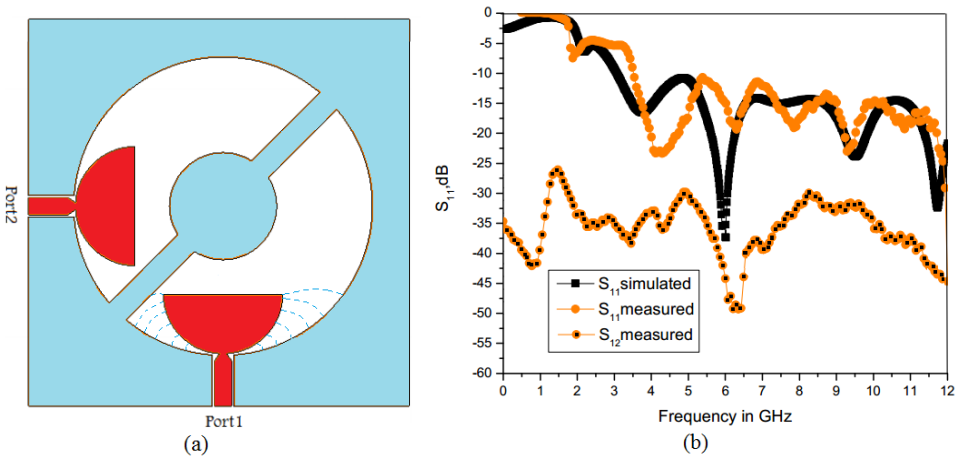

Figure 2.11: Geometry of CPW-fed ultra-wideband antenna (a) and simulated and measured S_{11}(b) [10].

antenna is a circular slot fed by tapered CPW line ending by a semi-circular disc. Dotted curves in Fig.2.11 indicate electric field distributions between monopole radiator and ground plane. As the width of slots varies continuously, a large range of frequencies could be resonating here. Therefore this proposed antenna has an ultra wideband behavior.

2.2.3 Techniques for dual-polarization

Dual-polarization performance enables an antenna to radiate and to receive signals which their E-fields vary in two orthogonal ways. The compact-CPW fed antenna depicted in Fig. 2.11 also gives us a manner of how to obtain dual polarizations in the same conception. It can be seen that the two radiators are arranged orthogonally and fed separately with port 1 and port 2, the current directions on the two patches are totally orthogonal to each other thus both horizontal and vertical polarization are obtained. It is worth noting that the isolation between the antenna ports is a tremendous requirement in the polarization diversity systems. The measured isolation of the CPW-fed monopole antenna is reported to be better than 25dB across all the operating band (by looking at Fig.2.11), which confirms that the two ports are quite isolated from each other [10].

Aperture-coupled microstrip antennas have been reported in [57–59] that dual-polarization is easy to obtain by cutting two offset orthogonal apertures in the feed-line ground plane, each aperture is able to excite antenna patch in a single direction. The isolation achieved in [57] is 18dB, 20dB in [58] and 27dB in [59]. In [60], Gao et al present an aperture-coupled stacked patch antenna with corner feeding and H-shaped aperture, shown in Fig. 2.12, in which about 30dB isolation is achieved. Dual-polarized aperture-coupled antennas with better isolation can be obtained by

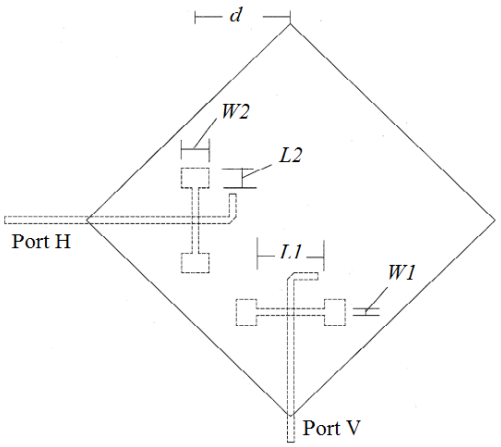

Figure 2.12: H-shaped aperture coupled dual-polarized antenna

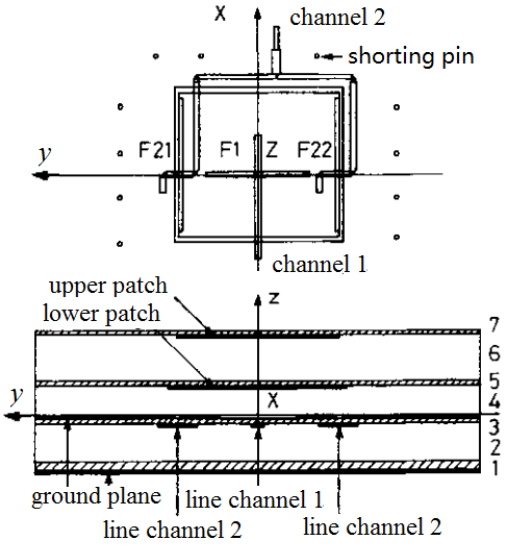

Figure 2.13: Multiple aperture coupled dual-polarized antenna

using multiple coupling apertures, as the multifeed technique is capable of suppressing higher-order modes. One such an antenna is reported by Brachat et al. in[61], where a dual-polarized aperture-coupled stacked patch antenna with multiple apertures is presented, as shown in Fig. 2.13. One centered aperture fed by the microstrip feed line is used for channel 1, and two apertures fed uniformly in amplitude and phase and positioned symmetrically with respect to the center of the patch, are used for channel 2. This antenna achieves an isolation better than 35dB over the bandwidth.

Generally speaking, dual-polarization could be achieved by introducing two orthogonal excitations in antenna conception, and polarization isolation is able to be enhanced by distributing feed lines in separate layers.

2.2.4 Techniques for high gain

For antennas, a common reference unit is dBi, which states the gain of an antenna as referenced to an Isotropic source (point source, perfect omnidirectional radiator). High gain is usually pursued by antenna designers, as the gain indicates the performance of antenna radiation and reception, and wireless communication will be further and more stable with high gain antennas. In our project, to stably receive satellite broadcast signal which the EIRP is about 50dBW on ground, the required antenna gain should be higher than 29dBi (Tab. 1.3) if taking into concern of the space losses and receiver sensitivity. Nevertheless, it is known that a single patch antenna provides a maximum directive gain of around 6-9 dBi [62], which is generally low. The proposed microstrip antenna with U-slot on the patch as shown in Fig. 2.7 is reported to have a gain of only 7dBi and the multiple aperture coupled

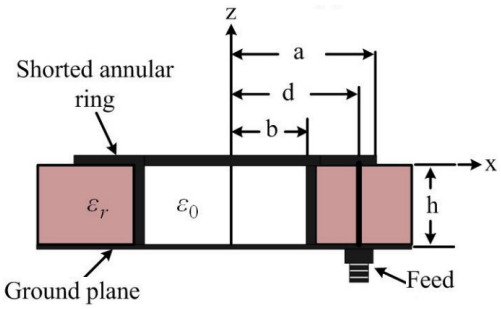

Figure 2.14: The Shorted Annular Patch antenna [11].

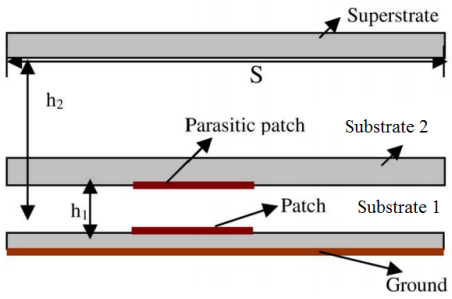

Figure 2.15: Stacked parasitic patch antenna with superstrate [12].

dual-polarized antenna as shown in Fig. 2.13 has a gain of only 7.4 dBi over its operation band.

The gain of patch antenna can be increased by reducing the surface wave which can create ripples in the radiation pattern. Several methods have been proposed to reduce the effects of surface waves [63–66]. One approach suggested is the synthesized substrate that lowers the effective dielectric constant of the substrate by using closely spaced holes [43] or directly delete the substrate under the patch [11], see Figure 2.14. In [11], the proposed antenna consists of the Shorted Annular Patch structure which inhibits the surface-wave is reported to have a 10.5 dBi maximum gain. Other approaches are to use parasitic elements or to use superstrate. In [12], a single antenna with superstate, as shown in Figure 2.15, has achieved a maximum measured gain of 14.6dBi, which confirm that the superstrate will result in a significant effect on the antenna performances.

Using multiple patches to connect to an array is another very useful approach to increase antenna gain. As antenna quantity increases, the number of radiators increases too. Radiated power by each antenna unit will contribute to the entire radiation of antenna array.

Imaging such an antenna array that consists of N units with the same conception, which is shown in Fig.2.16. At the observation point $P(r, \theta, \varphi)$ in the far field area of the antenna array, the integrated electric fields should be the superposition of electric field of each antenna unit along the specified direction (θ, ϕ), as expressed in equation 2.10.

$$\vec{\boldsymbol{E}}(\theta, \phi) = \sum_{i=1}^{N} \vec{\boldsymbol{E}}_{\boldsymbol{i}}(\theta, \phi) \tag{2.10}$$

Where $\vec{\boldsymbol{E}}_{\boldsymbol{i}}$ is the far field of the ith antenna given by [67]:

$$\vec{\boldsymbol{E}}_{\boldsymbol{i}} = \left[\vec{e}_\theta E_{\theta i}(\theta, \phi) + \vec{e}_\phi E_{\phi i}(\theta, \phi)\right] w_i K_i e^{-jkr_i} \tag{2.11}$$

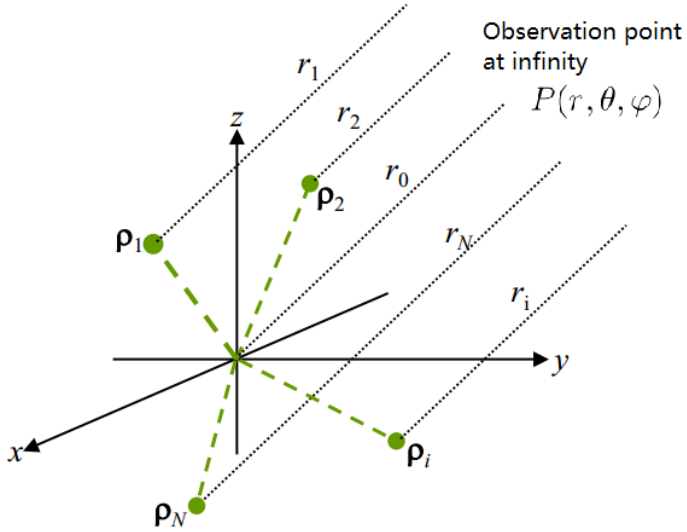

ρ_1,ρ_2,$\cdots$,ρ_i,$\cdots$,ρ_N are the position vectors of antenna elements
r_1,r_2,$\cdots$,r_i,$\cdots$,r_N are the distances of the antenna elements from P
r_0 is the distance of the origin from the observation point

Figure 2.16: Integration of array E-fields.

$E_{\theta i}(\theta,\phi)$ and $E_{\phi i}(\theta,\phi)$ are the θ and ϕ component of the radiation pattern separately, which are obtained with the ith antenna element located at the origin.

w_i is the weighting factor of the excitation source (complex number).

K_i is a constant accounting for the path loss.

To simplify the calculation of Equ. 2.10, we suppose each antenna unit has the same orientation and presents a gain of G_0 along the considered direction and is fed in phase and with the same power. As the reference point P is very far from antenna array, the electric fields at P which are generated by antenna units can be assume having the same direction. The integrated electric field is thus N times of a single antenna unit and the total power received at P is also N times of the received power generated by one antenna unit. In this case, according to power division of antenna array feeding, the gain increment is N times, as expressed in Equ. 2.12.

$$G(N) = 10\log N \tag{2.12}$$

It can be seen from Equ. 2.12 that, when the quantity of antenna array unit increases, antenna gain will be significantly enlarged. For instance, if antenna unit number is doubled, the integrated gain will be increased as much as 3dB ($10\log 2$). As a single antenna unit has a gain of G_0, theoretically, the total gain of an array with N units refers to isotropic source should be:

$$G_T(N) = G(N) + G_0 \tag{2.13}$$

(units: dBi)

Meanwhile, the required antenna units number is able to obtain if the total gain and the gain of single antenna unit are given, with this following equation yielded from Equ. 2.12 and 2.13.

$$N = \lceil 10^{\frac{G_T - G_0}{10}} \rceil \tag{2.14}$$

($\lceil x \rceil$ means ceil(x), to round x upward, returning the smallest integral value that is not less than x).

Conclusion

In this section, several techniques for improving microstrip patch antenna performances are introduced to solve problems in terms of wideband, dual-polarization and high gain. To broaden patch antenna bandwidth, some up-to-date approaches are proposed such as using thick and low dielectric constant substrate to lower the Q factor, using coplanar and stacked parasitic patches to introduce other resonances and using kinds of slots and CPW-fed monopole patch. To realize dual-polarization, the main approach is to excite individually two currents on patch(s) which are in orthogonal directions, by using two separate ports and aperture coupling technique. To enlarge antenna gain, the most efficient method is to connect units to an array. 3dB more gain could be obtained in theory if the quantity of antenna unit is doubled, and for a required gain the number of antenna unit could be predicted if single antenna gain is given, assuming no loss in the feed part. These approaches proposed here provide us very good choices for designing our antenna. In the coming sections, we would like to introduce the process of how to design a cross-type microstrip patch antenna and a CPW-fed monopole antenna both with wideband and dual-polarization behavior. The way of arrange the two proposed antenna elements into arrays will be introduced in next chapters.

2.3 Cross-type microstrip patch antenna design

In the previous sections, the characteristics of microstrip patch antenna and some up-to-date techniques of improving antenna performances have been introduced, which provides us plenty of ideas of designing our own antenna with required performances. In this section, we would like to introduce the process of designing a cross-type microstrip antenna. The steps of achieving required performances with previously mentioned techniques will be presented with figures and diagrams. For a rectangular patch with given dimensions L and W, one can obtain the basic TM_{10} mode resonance frequency from the equation proposed in section I which is rewrote here.

$$\boldsymbol{f_{10}} = \frac{c}{2\sqrt{\varepsilon_{eff}}}\left(\frac{\mathbf{1}}{\boldsymbol{L_e}}\right)$$

This equation could be transformed to obtain an approximate value of the antenna length operating at the frequency f_r, which is

$$\boldsymbol{L_e} = \frac{c}{2\boldsymbol{f_r}\sqrt{\varepsilon_{eff}}}$$

As mentioned before, there exists some fringing field at the end part of the antenna, the antenna effective length L_e is thus longer than the geometrical one (L). As expressed in the following equation:

$$\boldsymbol{L_e} = \boldsymbol{L} + 2\boldsymbol{\Delta L}$$

Therefore, the true length of patch could be depicted as:

$$\boldsymbol{L} = \frac{c}{2\boldsymbol{f_r}\sqrt{\varepsilon_{eff}}} - 2\boldsymbol{\Delta L} \tag{2.15}$$

Equation 2.15 indicates that, the length of patch radiator could be easily obtained when the basic model resonance frequency is given in the case the extension length is known.

Generally, the line extension could be simplified as:

$$\boldsymbol{\Delta L} \approx \mathbf{0.5}\boldsymbol{h}$$

which is a good rule of thumb [23].

Recall that the bandwidth requirement of the expected antenna is from 10.7GHz to 12.7GHz with the central frequency 11.7GHz. We can use the central frequency as f_r in equation 2.15 to obtain the size of patch antenna. It is worth noting that the substrate we adopted is TEFLON with the thickness of $h = 1.524mm$ and dielectric permittivity as reported to be $\varepsilon_r = 2.55$ when the working frequency is lower than 10GHz. However, our antenna works at the frequency band higher than 10GHz, thus the relative permittivity of given substrate is then measured using the method presented in [68] and briefly introduced in Annex A. The measured relative permittivity of given Teflon substrate at 11.7GHz is 2.62. The effective length is thus achieved about 8.3mm and the real length of patch is then evaluated as 6.8mm according to Equ. 2.15.

2.3.1 Single element microstrip patch antenna

A model of single patch microstrip antenna is constructed in HFSS, as shown in Fig. 2.17. The patch at the center of substrate is square with length 6.5mm and fed with probe (black point on patch). To obtain better impedance matching, the location of probe is adjustable by setting a variable in HFSS. Therefore we can choose the best feeding point according to the tuning results generated by parametric optimizing function. Fig. 2.18 gives a group of simulated S-parameters when tuning the offset of feeding point on a single patch microstrip antenna with a step of 0.2mm. It can be observed that as feeding point shifts from 1.2mm to 1.6mm, the resonance intensity is enhanced significantly, the center resonance frequency is also moved to higher frequency meanwhile the bandwidth becomes wider. At the feeding point which is 1.6mm offset to the center of patch, the antenna resonates very well at the center frequency 11.6GHz where the simulated reflection coefficient is as low as -33dB, that means more than 99.9% of RF power is accepted and not return back to input port. The -10dB bandwidth achieved is from 11.2GHz to 12.1GHz in other words about 7.7% relative bandwidth respect to the center frequency which is far insufficient compare to the required bandwidth. Furthermore, only one polarization is obtained with such a conception.

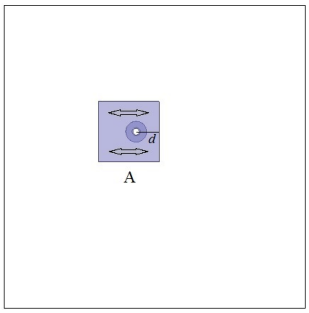

Figure 2.17: Single patch antenna

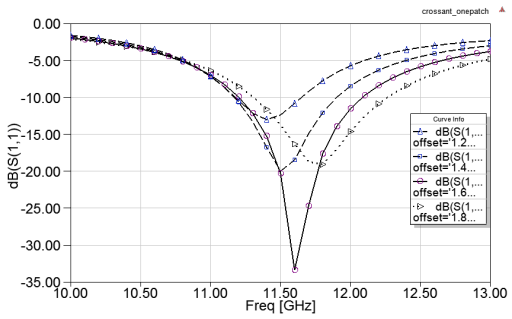

Figure 2.18: Tune feed point

2.3.2 To realize dual polarization

Figure 2.17 also illustrates the current flowing direction when patch A is excited by probe at the horizontal center line. In this case, the patch works in TM_{10} mode and acts as a wide truncated microstrip line. The basic patch is linearly polarized since the electric field only varies in one direction. To obtain dual orthogonal polarizations performance, another patch (B) with the same dimension is placed beside patch A but rotated 90 degree. The second feeding point is at the vertical center line of patch B. From Fig. 2.19, we can see that the current directions on patch A and patch B are totally orthogonal to each other, therefore the two patches radiate microwaves in two orthogonal directions, dual linear polarization is expected to obtain

(power coupling is not considered here but it will be discussed later). Simulated results shown in Fig. 2.20 indicate that patch B resonates at the same frequency with patch A due to the same conceptions.

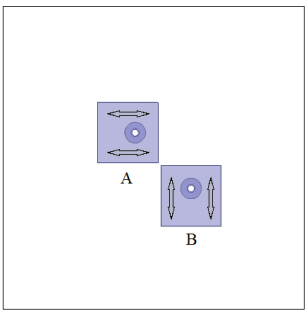

Figure 2.19: Orthogonal arranged dual-patch

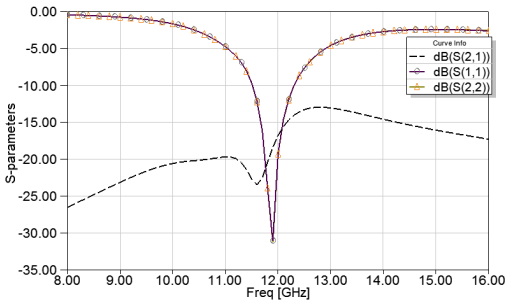

Figure 2.20: Simulated S-parameters of dual-patch

As proposed before that dual-polarization could also be obtained with only one patch. However, as our antenna works in the frequency band higher than 10 GHz, the patch is very small. Simulations indicate that the isolation becomes very bad if a single patch is fed with dual ports. More over, the two ports should be far enough to install SMA connectors when antenna is realized. Therefore, it is more reasonable to apply two separate patches to achieve dual-polarization.

In this section, even if dual-polarization is achieved by using two orthogonally placed patches, the bandwidth remains too low. In the coming sections, several techniques to enhance bandwidth will be introduced.

2.3.3 To broaden bandwidth

Recall that in section 2.2.1 several solutions of expanding patch antenna bandwidth are introduced. Considering such a conception as shown in Figure 2.19, the method of using parasitic patches is thought to be the best choice. In this manner, several parasitic patches are arranged beside the two driven patches to expand the bandwidth and very thin gaps between patches are adopted for power coupling, as illustrated in Figure 2.21. The entire antenna seems like a cross but with unequal-length arms, so we call it cross-type patch antenna in the following text. The cross shape is especially suitable for dual polarization because its two arms are orthogonal. RF power from the horizontal and vertical feeding points will not only excite the driven patches but also pass to the parasitic patches and make them resonating. The cross-type patch antenna model is thus simulated in HFSS, the width of gaps are optimized as well as the dimensions of patches are tuned to avoid frequency shift. The simulated S-parameters of cross-type antenna is shown in Figure 2.22. It can be found that the achieved -10dB bandwidth is from 10.6GHz to 12.8GHz which cov-

ers our required bandwidth. The relative bandwidth of cross-type antenna is more than 19%, about 11% increased compare to the single patch shown in Fig. 2.17. Thus it can be concluded that the method of using parasitic patches to expand bandwidth is truly effective as expected. The transmission coefficient (dB(S21)) is also given in Figure 2.22 which indicates the isolation between the two ports. It seems that the horizontal and vertical ports are well isolated outside the working band but the curve increases rapidly as resonance goes deeper. The minimum isolation is only about 14dB at 11.7GHz where the two ports are not assumed well isolated. An effect to enhance isolation without degrading the other parameters should be done. The approaches are presented in the coming section. It is worth noting that the return loss of vertical port is alike the horizontal port as they have almost the same conceptions thus it is not illustrated in the figure.

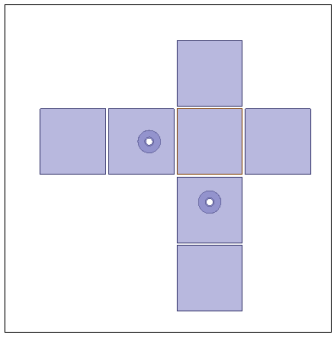

Figure 2.21: Cross-type antenna

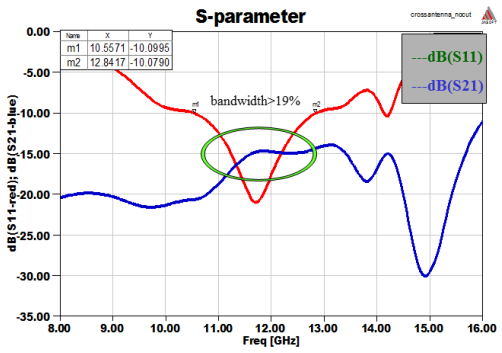

Figure 2.22: S parameters

2.3.4 To enhance isolation

Isolation is a crucial issue in our application to avoid crosstalk. According to the solutions proposed in section 2.2.3, two efficient methods to enhance the isolation between the two ports are applied. At first several angles are cut at the interaction district which is around the center patch, because these angles are supposed to be the main paths which RF power from each port can easily pass by. Fig. 2.23 shows the model after angles are cut and Fig. 2.24 illustrates the corresponding simulated S-parameters. Obvious improvements can be seen, especially the isolation is optimized several dB compare to the previous conception. The isolation becomes better than 18dB in our required band and it is as good as 21dB at the center frequency. Meanwhile the bandwidth is also increased a little, which is about 22% respect to the center frequency.

Continuous study on increasing the isolation is carried out. As the central patch is shared by the two arms of cross-type antenna, it supplies available paths for electromagnetic interaction. Therefore 4 square holes are cut on the central patch to

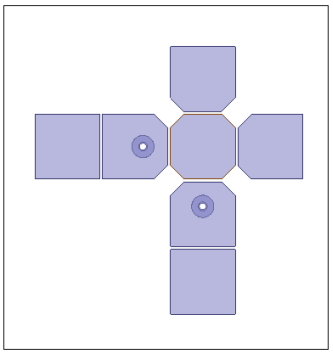

Figure 2.23: Topology of angles cut

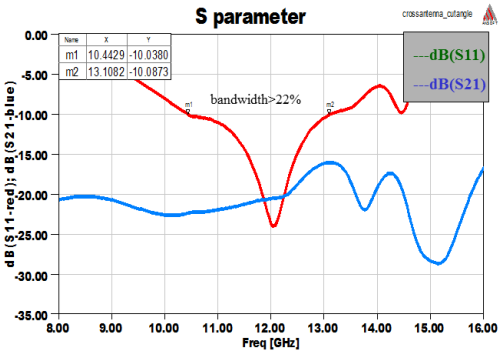

Figure 2.24: S parameters

destroy the interaction fields but maintain the current flowing traces. Simulated results indicate that the port isolation is enhanced more than 1dB at the center frequency and the frequency band is also continually broadened more than 3%, as seen in Fig. 2.25 and Fig. 2.26.

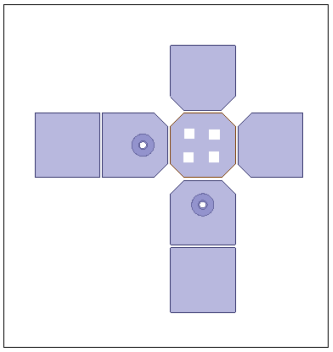

Figure 2.25: Topology of holes cut

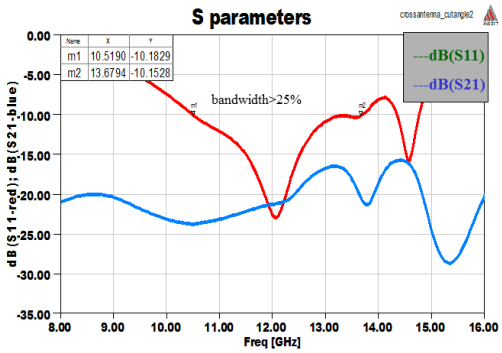

Figure 2.26: S parameters

2.3.5 To insert U-type slots

The cross-type patch antenna with corners and square holes cut matches well with our required performances which are wideband, dual polarized and flat structure. However the achieved band seems quite sharp and difficult to maintain if fabrication tolerance is taken into account. In this case, U-type slot is adopted here to enhance resonating and enlarge the bandwidth again as its structure and advantages are proposed in section 2.2.1. Two U-type slots are therefore etched on the two driven patches separately. The dimensions and locations of U-type slots are optimized in simulation, as well as the location of feeding points are matched again because the input impedance shifted while U-slot technique is applied. The construction of developed cross-type antenna is depicted in Figure 2.27. Simulated S-parameters represented in Figure 2.28 indicate deep resonances obtained in our required band and the entire bandwidth is again broadened as U-type slots applied.

As can be seen that another resonance (at 10.9GHz) near the main resonance (be shifted to 12GHz) of the patch is induced, the -10dB relative bandwidth is more than 26.6%. However one can also notice that the S21 curve increases, interactions between ports are enhanced as resonance become deeper. Although quantities of methods on changing the structure of cross antenna are applied, the relative high transmission coefficient is hard to decrease any more. The main problem is due to the coexistence of dual feeding network at the same surface. In the third chapter of this thesis, we would like to introduce a strip line feeding network designed with multilayer construction which could effectively enhance the ports isolation.

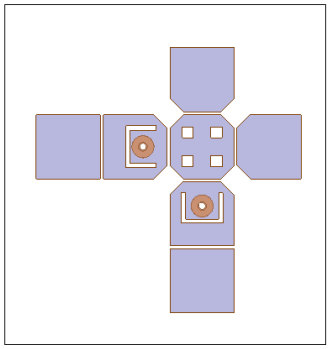

Figure 2.27: Antenna topology when U-slot is used

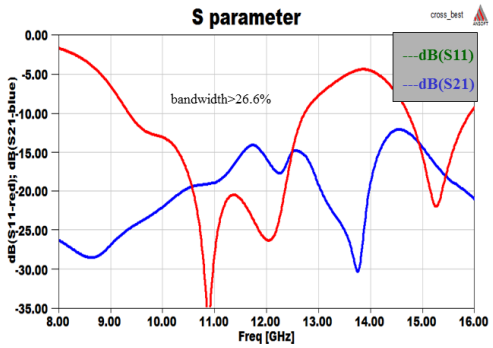

Figure 2.28: Simulated S-parameters

As can be seen from Figure 2.27 that the bandwidth achieved in simulation is from 9.3GHz to 12.7GHz, which is very close to the right edge of the required bandwidth (10.7-12.7GHz). To obtain better resonance and avoid affections caused by fabrication tolerance, the operating band should be shifted a little higher. The most direct way to shift the entire band of patch antenna is to decrease the dimensions of each patch. Figure 2.29 represents the final conception and dimensions of cross-type patch antenna fed with microstrip line. It can be seen that the width of each patch has been decreased from 6.5mm to 5.8mm. The other parameters including the location of feed point, location of U-type slot are also optimized again to satisfy the modification of patch width. At the bottom layer, two orthogonal placed microstrip lines are used to transmit power between input ports and antenna. The widths of microstrip lines are calculated with Linecalc tools licensed by Agilent Advanced Design System by inserting the relative permittivity, thickness and losses of substrate. The impedance of microstrip lines and feeding point are all maintained 50 ohms to match the impedance of input ports where SMA connectors are commonly used. Figure 2.30 shows the photograph of a realized cross-type patch antenna in our laboratory.

The S parameters of cross-type patch antenna is simulated in HFSS and then realized and measured with Agilent Vector Network Analyzer E8364B, the compari-

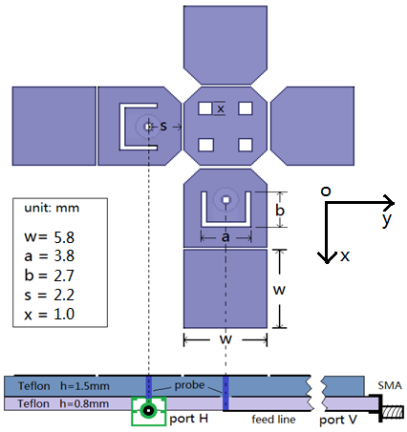

Figure 2.29: Final dimension of cross-type antenna

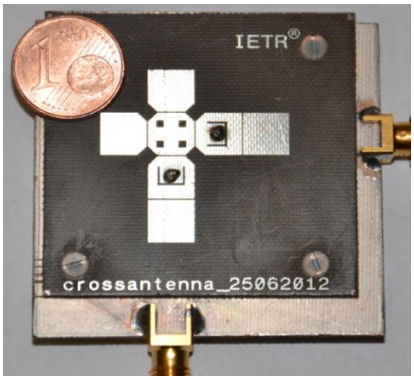

Figure 2.30: Photograph of realized antenna

son is given in Figure 2.31. As U-type slot is introduced into cross-type antenna and the dimensions of patches are decreased to shift the entire band, the final achieved bandwidth is significantly improved. Both simulation and measurement indicate very good resonances of cross-type antenna, -10dB bandwidth could be obtained from 10 GHz to 14.7 GHz in other words 38% relative bandwidth respects to the center frequency. In addition, dual resonance frequency points could be obviously found at 10.6GHz and 11.7GHz, one of which must be contributed by the U-type slot. As can be seen from Fig. 2.31 that the measured curve (solid) matches very well with simulation (dotted) at the lower band but a few dB differences could be observed at the higher frequency band, which is mainly due to variation of permittivity of substrate as frequency goes higher. It is worth noting that the exceptionally obtained band from 14 GHz to 14.5 GHz might be very interesting because it corresponds to the uplink band of DBS system (see Chapter 1). This outstanding characteristic makes cross-type patch antenna a good candidate for satellite reception antenna integrated with downlink and uplink band, which is suitable for bidirectional communications such as internet access from satellites.

Figure 2.32 illustrates the simulated E-fields when vertical and horizontal ports are excited separately. It can be seen that there exists very strong electrical field near the gaps and U-type slot on each arm of cross-type antenna when the corresponding port is excited. At the same time, the other arm can hardly get energy from the port so the patches refuse to resonate. As expected, the cross-type patch antenna is dual-polarized and the two polarizations are well isolated.

Figure 2.33 plots the radiation patterns simulated at two principal planes when port 1 is excited at 11.6 GHz. Good cross polarization levels (about 25dB) is observed and the maximum directivity is 9.4dBi obtained at -35 ° of theta which indicates that the main beam has been shifted from the normal direction. Figure

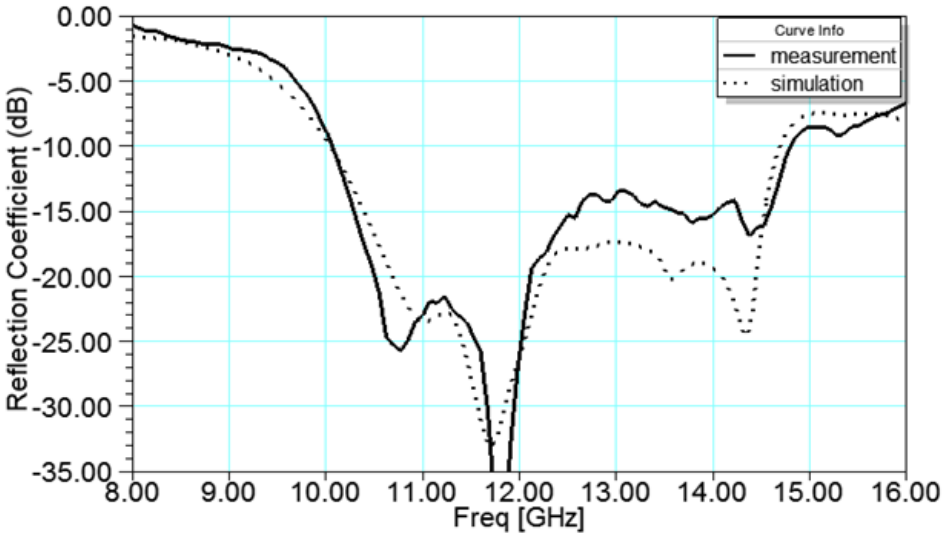

Figure 2.31: Comparison of simulation and measurement of cross-type antenna

2.34 gives the simulated antenna gain versus frequency, in which it can be seen that the maximum gain is about 9.65 dBi obtained at 11.3 GHz and the average gain maintains higher than 8 dBi in most part of the required band. Obviously we can see that the gain of cross-type antenna is much higher than a single patch antenna whose gain is only about 2 - 4 dBi, mainly due to using several parasitic patches which act as additional resonators and contribute to the total gain of entire antenna. The relative high gain of cross-type antenna is also very attractive and pleasing.

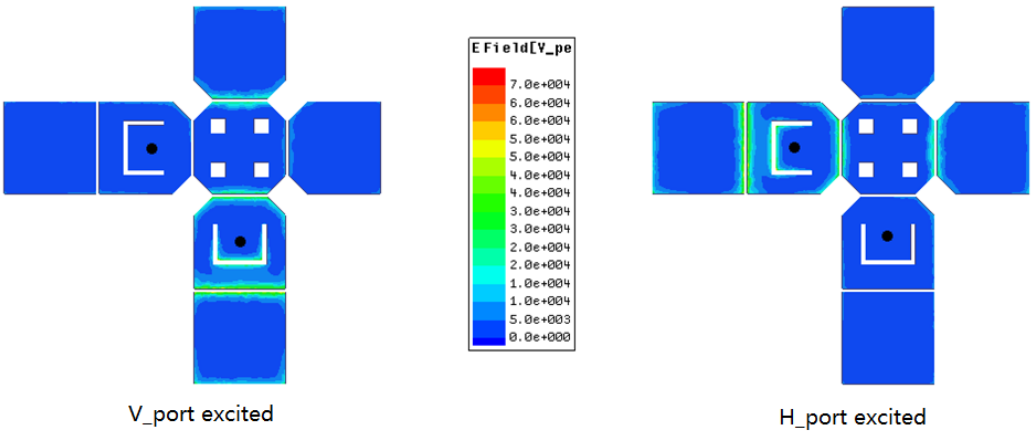

Figure 2.32: Simulated electrical field of cross-type antenna

Nevertheless, quite omnidirectional and symmetric pattern is not achieved due to the asymmetric conception of proposed cross-type antenna. As can be seen from the E-plane radiation of Fig. 2.33, there exists a nearly null gain at around 30° at 11.6GHz. This problem has to be solved and is introduced in the next section.

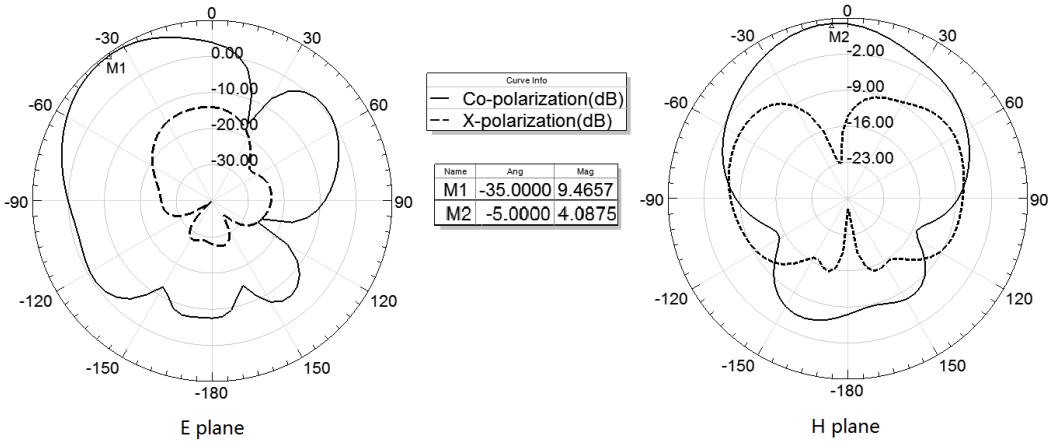

Figure 2.33: Simulated radiation patterns of cross-type antenna at 11.6GHz
E plane: plane containing the electric field vector and the direction of maximum radiation, eg. xoz plane in Fig.2.29 when vertical port is excited.
H plane: plane containing the magnetic field vector and the direction of maximum radiation, eg. yoz plane in Fig.2.29 when vertical port is excited.

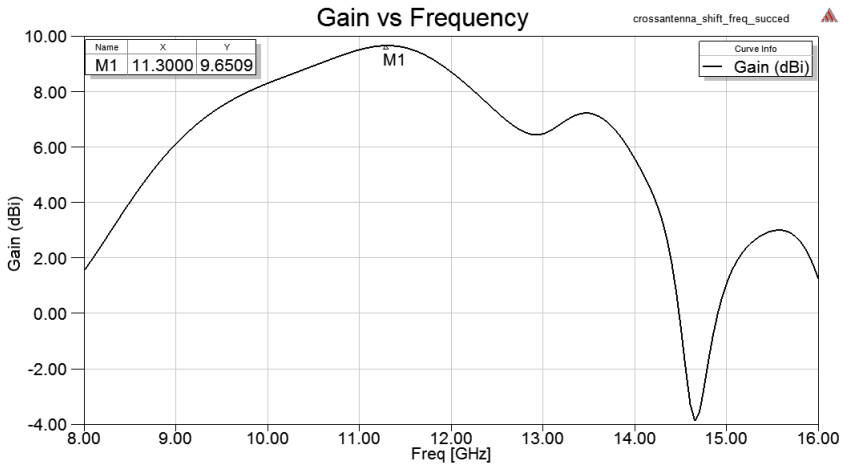

Figure 2.34: Gain versus frequency

2.3.6 To adjust directivity and suppress side-lobe level

According to the radiation patterns shown in Fig. 2.33, the cross antenna has a disturbed omnidirectional pattern in the front side and its main beam is also steered due to the unsymmetrical structure. As an omnidirectional and stable radiation in front side is expected over all the bandwidth, a solution to correct these disturbances is required. The idea of using meta-material to improve antenna directivity has been proposed in [69–71]. In [69] Turpin et al. have constructed a meta-lens for crossed-dipole feed antenna and the measured directivity was reported to have increased more than 6dB. In [70, 71], two types of meta-material structures composed of copper grids with lattices are introduced for patch antenna; not only directivity but also the front-to-back ratio is greatly increased as reported in their studies. But according to their methods, the meta-lens is a non-planar structure which looks like a wall. Furthermore the copper grids methods are not suitable for broadband applications

due to the relative narrow band of meta-material structure. Reference [72] provides us a single element antenna which uses free formed cylindrical woodpile cavity; very good SLL (side-lobe level), narrow beam, and good directivity are achieved. But the non-planar design by using extrusion free-forming technique depicted in [73] and [74] makes fabrication much more complex.

As we all know that, in patch antenna architecture, the most part of input power is radiated by antenna but some power is leaked to substrate from the feed line and the edge of fringing field. This part of power transmits to the edge of substrate, then radiates due to discontinuousness of boundary conditions (dashed curves in Figure 2.35), and finally contributes to a relatively high sidelobe level in radiation pattern. One solution to solve side radiation is to use quarter-wavelength transmission line ($\lambda_g/4$ Transmission Line, obtained with the center frequency). As a transmission line with the length of a quarter guided wavelength is employed, according to the principle of $\lambda_g/4$ TL, the left fringe of the TL performs as open circuit to RF power while the right fringe performs as short circuit (solid line in Figure 2.35, assume that antenna and feeding line are placed at the left side). RF power can hardly pass through the $\lambda_g/4$ length TL and then be attenuated or reflected, so the side radiation from the boundary of substrate is weakened.

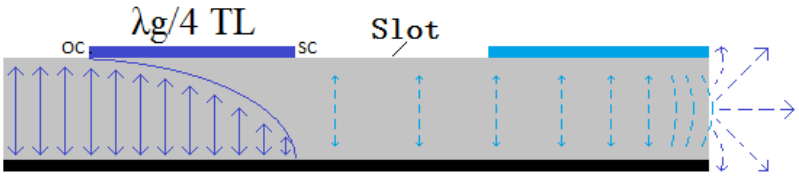

Figure 2.35: Illustration of side radiation (dashed) and RF power suppression (solid).

An experimental structure with cross-type patch antenna as radiating part and a circular conductor ring with the width of $\lambda_g/4$ are designed to verify the function of the proposed side radiation suppression method, as depicted in Figure 2.36. As cross-type antenna is fed by coaxial cable, the inner conductor passes through the substrate and some RF power is leaked into the substrate. Therefore the relatively high sidelobe level could be found in Fig. 2.33 mainly due to side radiation from boundary. By using $\lambda_g/4$ TL side radiation suppression method, around cross-type antenna and at a distance l, a conductor ring and a circular slot both with the width of a quarter guided wavelength of the central frequency are placed on the top layer, as shown in Figure 2.36. It can be seen that the cross-type antenna is located in a dashed circle with radius r; the center of cross-type antenna is 3mm offset from the center of circle due to its unsymmetrical conception. From the side view of Figure 2.36, we can also find that the field irised out by dashed rectangle corresponds to the

model as depicted in Figure 2.35. It is worth noting that the conductor ring should be placed at one guided wavelength away where the other performances of antenna are not impacted except the side radiation. The width of circular slot is also set to be $\lambda_g/4$ to maintain good electromagnetic isolation between conductor ring and outer conductor. To see more details about how to obtain the width of conductor ring and slot and the distance between antenna and conductor ring, please refer to [75].

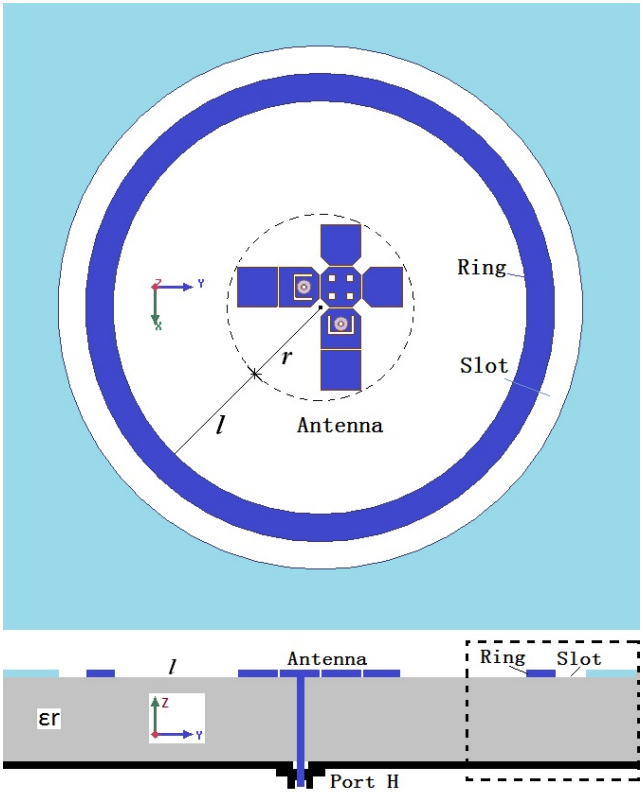

Figure 2.36: Cross-type antenna with sidelobe suppression structure

The experimental structure is fabricated and measured in our laboratory. Figure 2.37 shows some radiation patterns measured at 5 different frequencies over the bandwidth before and after the radiation stabilization structure is carried out. Solid curves in Figure 2.37 illustrate the measured directivity patterns of the proposed cross-type patch antenna without conductor ring and circular slot. As shown in Figure 2.37, there exists some spurious sidelobe with levels relatively high with respect to main lobes. Moreover main lobe steering can be found at each frequency point and is shifted from the broadside direction. The pattern measured at 12 GHz presents a null direction at about -30°, where the main lobe is thus drastically disturbed. The calculated half-power beamwidth (HPBW) at 12.96 GHz is only about 35° which is much less than that of other frequencies.

As radiation stabilization structure is employed, the measured radiation patterns are illustrated with dashed curves in Figure 2.37 in comparison to these measurements of individual cross-type antenna. It can be seen that these stabilized patterns

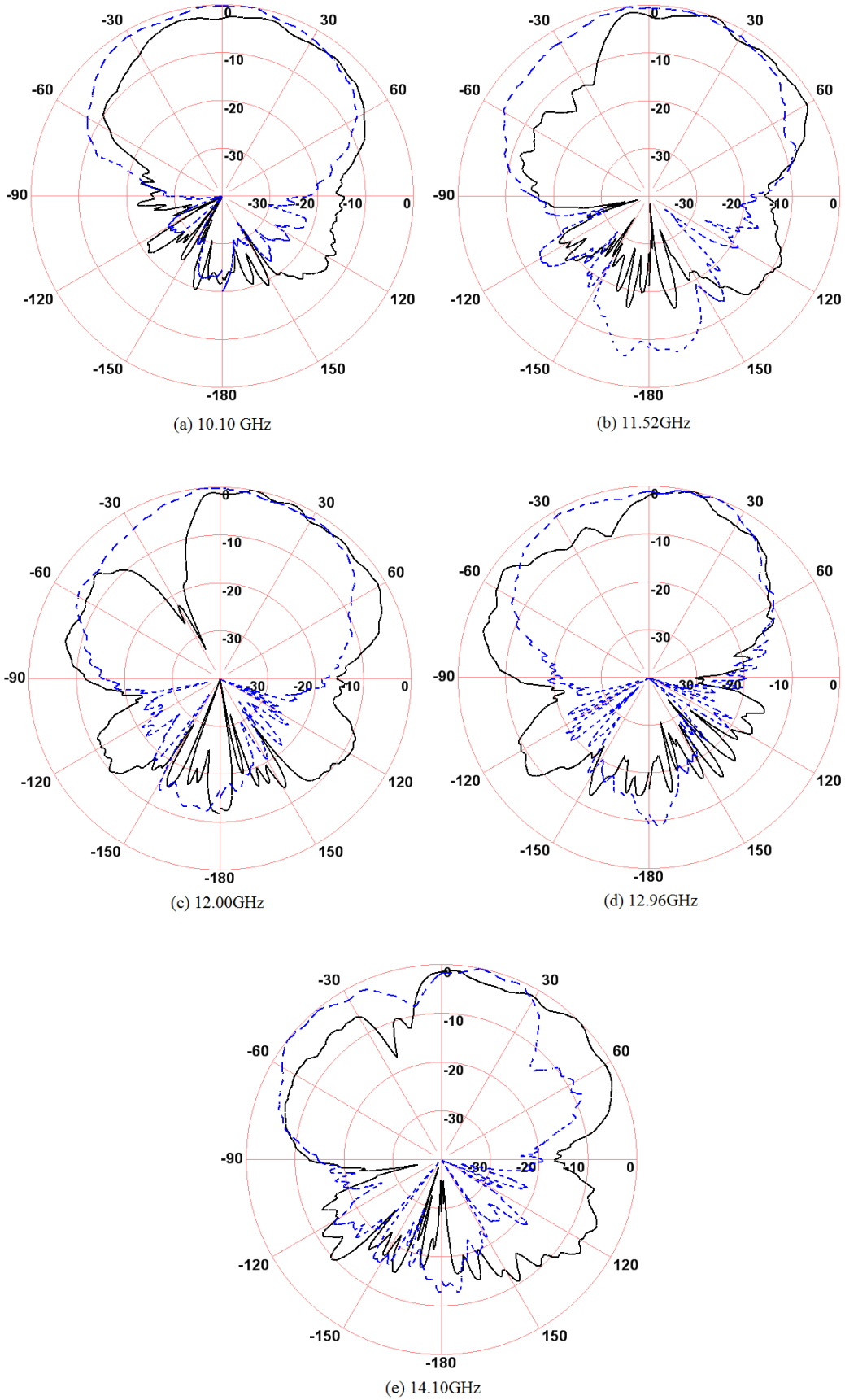

(a) 10.10 GHz

(b) 11.52GHz

(c) 12.00GHz

(d) 12.96GHz

(e) 14.10GHz

Figure 2.37: Measured directivity patterns at 5 frequency points before (solid) and after (dashed) radiation stabilization structure is employed.

are compact and smooth over the working bandwidth. Sidelobe levels have been decreased several dB. The maximum directivities are also achieved at the broadside direction of antenna plane. The case where the pattern is drastically disturbed at 12 GHz is also eliminated. As the influence of side radiation is decreased by conductor ring and circular slot, antenna radiation is thus stable and symmetric. The optimal HPBWs reach up to 70° at each measured frequency point, which makes cross patch antenna a very good candidate of large-angle-beam-steering array. Tables 2.3 and 2.4 list the comparisons of HPBW and direction of main beam before and after radiation stabilization structure is employed. These tables sum up the strong interest of this approach to stabilize the radiation patter over the whole working band.

Table 2.3: Half-power bandwidth (HPBW).

	GHz				
	10.1	11.52	12.00	12.96	14.10
Without ring	70°	75°	75°	39°	75°
With ring	80°	80°	72°	80°	90°

Table 2.4: Direction.

	GHz				
	10.1	11.52	12.00	12.96	14.10
Without ring	25°	22°	25°	12.5°	32.5°
With ring	2°	5°	0°	0°	-10°

Conclusion

Till now, we have successfully achieved a single element microstrip patch antenna named cross-type antenna which is wideband, dual polarized and relatively high gain compare with single patch antenna. The cross-type antenna part is printed on a 1.524mm thickness Teflon substrate and the feed part is on a 0.8mm thickness Teflon substrate, hence the entire structure is flat and very thin. As we all know that the applied Teflon substrate is cheap and easy to find, therefore the cost and fabrication complexity of cross-type antenna are both very low. It can be seen from the proposed characteristics that the cross-type antenna is a good candidate to constitute a big array which could satisfy the requirements of satellite communication antenna. In the fourth chapter of this thesis, we would like to introduce the approach of designing an array consisted of the cross-type antenna unit according to a valuable approach of shared parasitic element..

2.4 Coplanar waveguide feed monopole antenna

As mentioned previously in section 2.2.2 that by using monopole patch antenna, ultra wideband is able to obtain. In [10], the proposed CPW-fed monopole antenna which operates in a wideband ranges from 3.1GHz to 10.6GHz provides us a very good candidate for satellite communication applications. Based on the geometry presented by R.YAHYA et al. [10] as depicted in Fig.2.11, another single element antenna which is fed by Grounded Co-planar Waveguide Transmission Line (CPWG-TL) is designed and hereby introduced.

2.4.1 Antenna conception

Figure 2.38 illustrates the geometry of the proposed CPW-fed monopole antenna designed according to the requirements of our project (Table 1.3). It can be seen that the antenna is consisted of a half-circle patch with diameter of L as the main radiator and a small half-ellipse patch as a parasitic patch. The whole antenna part is located in a big circle with top and bottom conductor etched but remains a cross-shaped ground. The entire structure is printed on a $h = 1.524mm$ EPOXY substrate with dielectric constant $\varepsilon_r = 4.4$ and with dual-layer conductors. This kind of substrate is relatively cheap and propitious to decrease the cost of entire antenna system. Quantities of metallica via holes are applied to link top and bottom conductors to maintain good electric connections and consistency of ground plane.

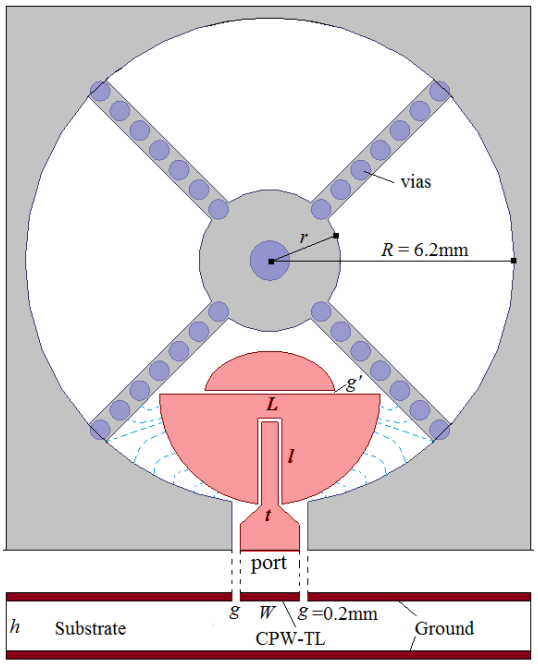

Figure 2.38: Geometry of CPW-fed monopole antenna

To obtain wideband

It can be seen from Fig. 2.38 that there are three techniques used for broadening the bandwidth. Firstly, the radiator applies monopole antenna with bottom ground etched, which has inherently broadband performance. Secondly the continuously increasing slots between main radiator and outer circular ground plane works as a bandpass filter which allows only the chosen frequencies resonate around the slots. As the required bandwidth is only 2GHz and not for broadband applications like proposed in [10], therefore the minimum and maximum width of slots and the length of slots can be optimized in the given band to lower the size of antenna unit. The optimized diameter R of circular ground is 6.2mm and the diameter of the half-circle radiator L is only 2.8mm. Compare with the proposed cross-type antenna which has a dimension of 23.95mm in square, the CPW-fed monopole antenna is much smaller. The third technique used here to master bandwidth is the half-ellipse parasitic patch which obtain power by coupling from the main radiator and acts as another resonator which contributes to the total bandwidth. The gap g′ between the main patch and the parasitic patch is only 0.1mm which has been optimized for RF power coupling in the required band.

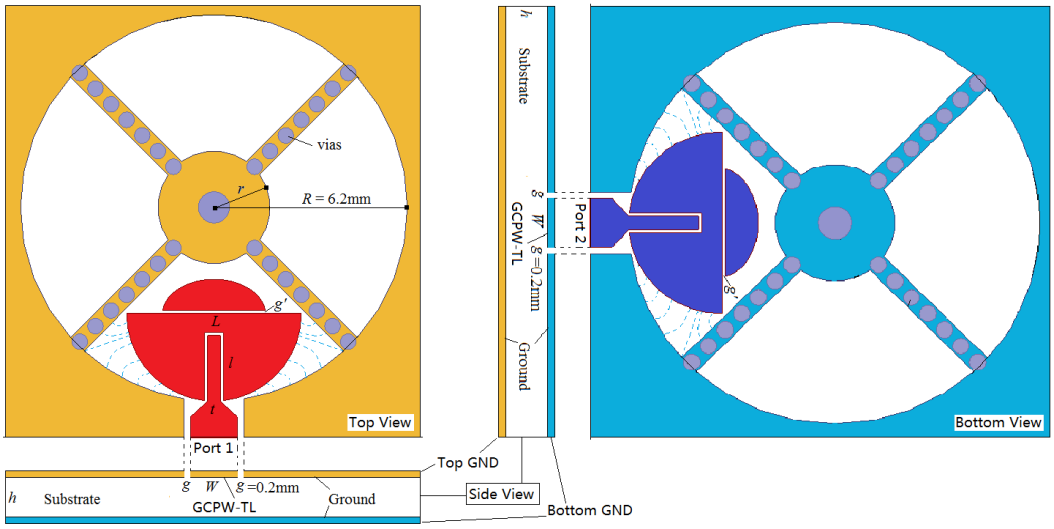

Figure 2.39: Geometry of dual-polarized CPW-fed monopole antenna

Impedance matching

To feed such a monopole antenna and to maintain good impedance matching, insert feed [5] method is used in the conception. As can be seen that the feed line is inserted to the center of the main patch with the depth of l and the thin gap enables RF power coupling between main patch and feed line. The other terminal of the feed line is connected with CPW line and a trapezoid line acted as a impedance

converter is used here to match the impedances of inserted line and CPW line. With insert feed, the monopole antenna is able to obtain a 50 ohm impedance at the input port.

Dual-polarization

To realize dual-polarization performance of the proposed CPW-fed monopole antenna, another group of patches and feed line are placed at the orthogonal direction of the vertical antenna unit, as depicted in Fig. 2.39. Different from the arrangement method proposed in [10], the horizontal antenna unit in our conception is placed at the bottom layer and ground plane exists at the bottom layer of CPW-fed line (called GCPW-TL). In other words, the top and bottom conductor plane are not only the co-planar ground plane for correspond antenna unit, but also back ground planes of feed lines for the other side antenna unit. Several via holes on the cross arms are used to obtain good isolation between the dual polarized antenna units. These via holes act as an electric wall which inhibits radiated field to travel from an antenna to the other.

Mono-directional radiation

In the geometry of dual-polarized CPW-fed antenna, the two monopole antenna units radiate microwaves both in forward and backward directions as monopole antenna has inherently omnidirectional directivity. Nevertheless, only the forward radiation is useful in our case of receiving satellite signal. [60] introduce an approach to enhance front radiation and improve front-to-back ratio by putting a second ground plane below the antenna structure.

A metallic reflector (eg. 1mm thick aluminum board, one half wavelength wider than antenna board) is thus placed at the bottom of antenna board with a distance adjustable by screw. This metallic board acts as a reflector and limits the rear-lobe when the distance is tuned to the best location ($2.5h$, h is the thickness of substrate). In addition, antenna resonance frequency could also be slightly shifted by adjusting the distance between antenna board and reflector.

Even if a metallic reflector is used in the antenna conception to adjust radiation direction, the entire structure remains still flat as the thickness just increases a few millimeters.

2.4.2 To feed with GCPW line

Classic CPW is formed from a conductor separated from a pair of ground planes all on the same plane and atop a dielectric medium. A ground plane could provided

on the opposite side of the dielectric, in this case, the technology is called Grounded Co-Planar Waveguide (GCPW). GCPW can propagate extremely high frequency response since connecting GCPW does not entail any parasitic discontinuities in the ground plane. The impedance of GCPW fed line is mainly depended on the width of feed line and the width of the both side gaps and certainly the dielectric constant of substrate. For a given line characteristic impedance, there is an infinite number of solutions for the geometry of a GCPW line. One can make a 50 ohm line 10 microns wide, or 50 microns wide, by adjusting the gap dimension. In practice, feed line size and the line loss should be tradeoff because skinny lines can become quite lossy [76].

The proposed dual-polarized monopole antenna is fed with GCPW technique by considering its co-planar structure. To test the transmission coefficient of GCPW line, a model is constructed in HFSS. A stand 50 ohm GCPW line with 20 cm long is realized on a EPOXY substrate with the optimized width of 1.5mm while the both gaps are set to 0.2mm taking account of fabrication ease. It can be seen from Fig. 2.41 that the CPWG line could transmit RF signal very well at low frequency and the transmission coefficient decrease rapidly as frequency goes higher. At the frequency 12.5 GHz the received power at the terminal port is only half (-3dB) of the emitted power.

To maintain good transmission coefficient along long transmission line, GCPW feed line accompanied with via holes at both sides is then simulated in HFSS, as depicted in Fig. 2.40. The solid line with circle symbol in Fig. 2.41 indicates that more than -25dB return loss could be obtained when frequency is lower than 15GHz, which is 5 - 7 dB optimized than the return loss of GCPW line without via holes. Even more, along the entire simulated frequency band the transmission coefficient is always higher than -1 dB. Via holes along transmission line have efficiently limited the power leaked to the substrate. In addition, Simulated results indicate that metallic via hole does not impact on CPWG line impedance.

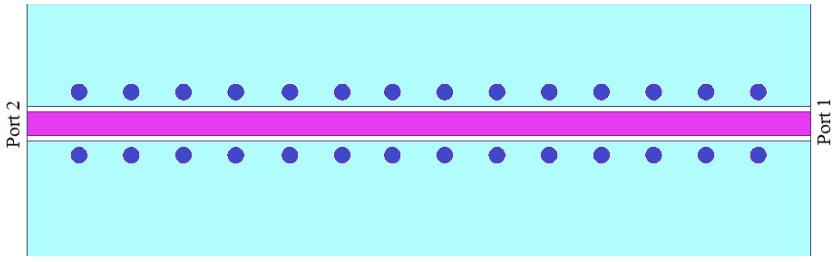

Figure 2.40: Geometry of co-planar waveguide feed line accompanied with metallic via holes

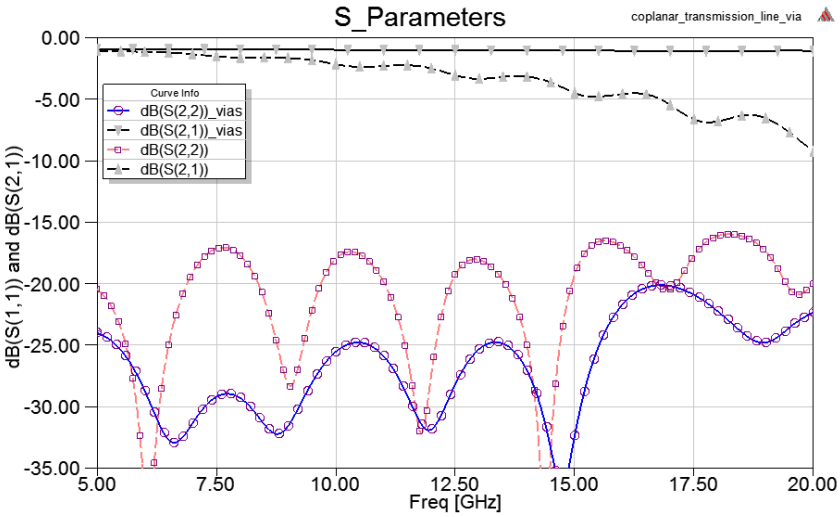

Figure 2.41: Comparison of S-parameters with or without via holes

2.4.3 Simulation and measurement

The single element CPW-fed monopole antenna has been simulated using HFSS and then realized in our laboratory. Fig. 2.42 shows the impedance bandwidths when tuning the insert feed depth $feed\_match$ from 2 to 2.4mm by a step of 0.2 mm. It can be seen that the impedance bandwidth as well as the resonance intensity varies a lot when the feed depth changed. At last, the $feed\_match = 2.2mm$ is applied when tradeoff the bandwidth and resonance.

The comparison between simulation and measurement of CPW-fed antenna return loss is depicted in Fig. 2.43. Good agreement on bandwidth could be observed, both simulation and measurement indicate that the proposed single element antenna resonate very well at the required band which is from 10.7 to 12.7GHz. The importance of reflector can also be observed from the figure. If no reflector exist, the resonance becomes weaker.

Fig. 2.44 depicts the radiation pattern of dual antenna units in the same conception. The solid curve illustrates the radiation of the antenna unit placed at the top layer while the dashed curve illustrates the bottom layer antenna radiation. It can be seen that both antennas have obvious main beams at the front side. Due to the influence of metallic reflector, bottom antenna radiation seems enhanced and more symmetric compare to top antenna unit. In the next chapter, we would like to focus on CPW-fed antenna array, the method of optimizing the radiation of CPW-fed antenna will be introduced.

2.4.4 Sum up CPW-fed monopole antenna

In this section, a wideband , dual polarized and low profile planar structure antenna is introduced. This antenna has inherently wide bandwidth as a monopole

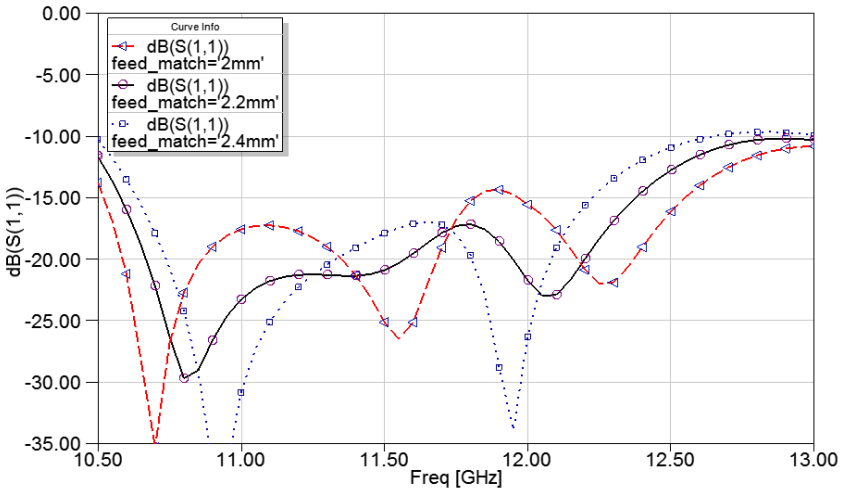

Figure 2.42: Simulated S11 when tuning insert feed length

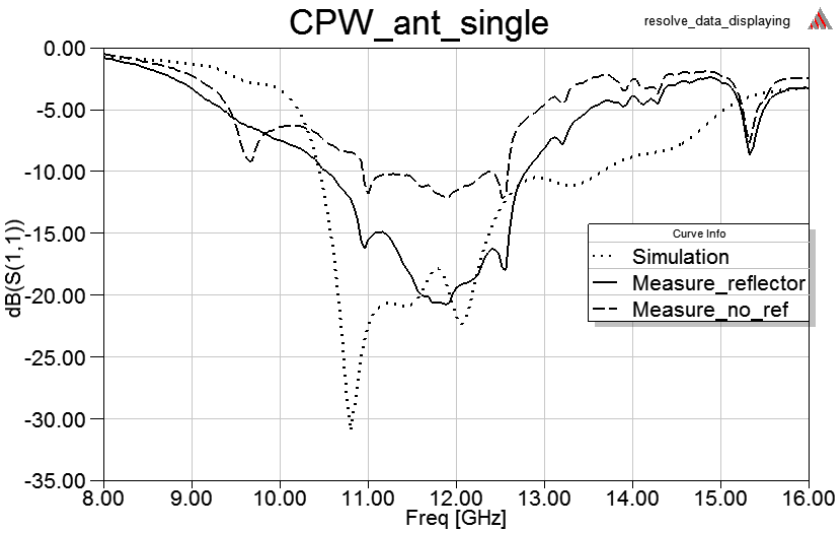

Figure 2.43: Comparison of simulation and measurement of single element CPW-fed monopole antenna

antenna, even more parasitic patch and arc slot are used to maintain bandwidth. Therefore in a low profile as small as 6.2 mm in diameter, the CPW-fed antenna achieves sufficient bandwidth. Dual-polarization is obtained by duplicating the monopole structure and rotating it 90 degree. To enhance isolation, the two structure are placed at different layers separated by thick substrate and via holes. To realize mono-direction, a metallic reflector is placed at the right bottom to limit rear lobe and reflect back radiation to forward direction. To sum up, the CPW-fed monopole antenna has very good performances and it is also a good candidate to construct a big array for KU-band satellite communication.

Fig. 2.45 shows the photo of realized single element CPW-fed monopole antenna.

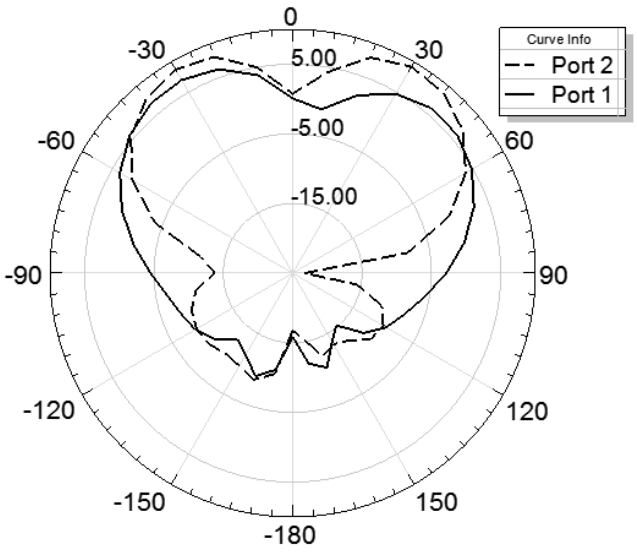

Figure 2.44: Radiation patterns of top layer (solid) and bottom layer (dashed) antenna units

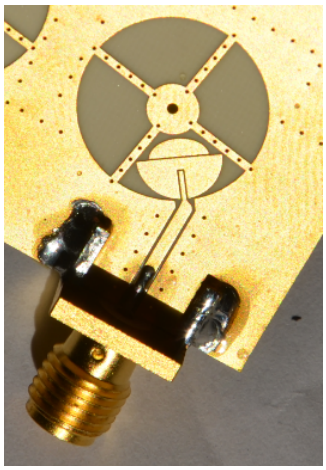

Figure 2.45: Photograph of realized CPW-fed monopole antenna (the other unit on the bottom layer is not presented in this figure).

2.5 Conclusion

In this chapter, two types of patch antenna designed with different techniques are introduced. Both of the antennas are optimized under the required performances. Simulations and measurements are given to show the achieved wide bandwidth, dual-polarization and flat structure. In summary, Cross-type antenna and CPW-fed monopole antenna are both good single antenna elements. In comparison, Cross-type antenna has higher gain than CPW-fed monopole antenna as it is consisted of several parasitic patches, but CPW-fed antenna has much lower profile than Cross-type antenna which is suitable for compact structure use. Table 2.5 gives more comparisons between the two antennas.

Table 2.5: Comparison between Cross-type antenna and CPW-fed monopole antenna.

	Cross-type antenna	CPW-fed monopole antenna
Bandwidth	10.0 - 14.7GHz	10.5 - 12.8GHz
Polarization	dual	dual
Profile	$0.9\lambda_0$	$0.25\lambda_0$
Thickness	2.3mm	6mm
Gain	9.6dBi	6dBi
Radiating efficiency	$\star\star\star\star\star$	$\star\star\star$
Cost	$\star\star$	$\star$
Fabricate ease	$\star\star\star$	$\star\star\star\star\star$
Accuracy required	$m_{in} = 0.25mm$	$m_{in} = 0.1mm$

3

Co-planar waveguide fed antenna array

The single element CPW-fed monopole antenna has been introduced in the last chapter, simulation and measurement indicate that the proposed antenna has very good performances such as wideband, dual-polarization, ultra-compact profile and flat structure. However, the gain of a single CPW-fed antenna is low, attempts to enlarge single element antenna gain can not satisfy the requirement. As mentioned previously in section 2.2.4, an effective solution to enlarge antenna gain is to arrange quantity of such antennas into an array.

In this chapter, we would like to introduce firstly a dipole-liked sub-array which consists of 2 opposite placed CPW-fed monopole antenna units in the same conception. The sub-array is then assumed as the basic element of big array therefore a linearly arranged CPW-fed monopole antenna array is then realized and introduced. The corresponding feeding network designed according to Dolph-Chebyshev current distribution theory will also be presented. In the third section of this chapter, an even bigger 2-Dimensional arranged array which consists of several columns of linearly arranged array will be introduced, measured results will also be given. The fourth section will give conclusions.

3.1 CPW-fed monopole antenna Sub-array

In this section, the process of designing the proposed CPW-fed monopole antenna sub-array will be introduced in detail. The sub-array conception, as well as

its simulated and measured performances will also be given.

3.1.1 Sub-array conception

It can be seen from Fig. 2.38 that the single element CPW-fed monopole antenna consists of a monopole antenna unit and a circular aperture which is separated to four sectors by a cross-type arm connected to the ground plane. The monopole antenna unit is located in one of the four sectors. An idea of duplicating the antenna unit and put into the opposite sector has been carried out. With this method, the number of antenna unit is doubled while the entire dimension remains the same. According to the equation mentioned in section 2.2.4, the integrated gain should increase 3dB in theory. The structure consists of two opposite arranged CPW-fed antenna units is assumed as a sub-array compare with the arrays which will be introduced later in this chapter. The geometry of such a sub-array is illustrated in Fig. 3.1. However, such sub-array is mono-polarized.

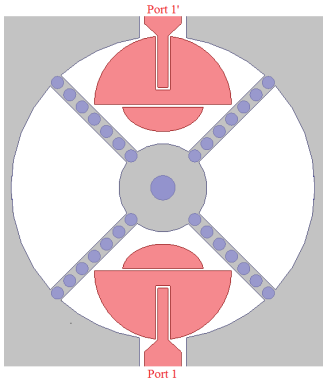

Figure 3.1: Sub-array of CPW-fed monopole antenna

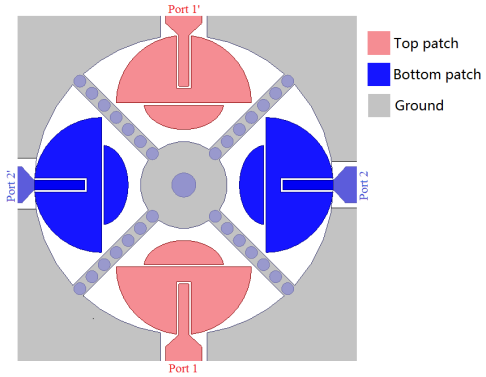

Figure 3.2: Dual-polarized sub-array

3.1.2 Dual-polarized sub-array

Recall that the single element CPW-fed monopole antenna is dual-polarized as the other antenna unit is placed at the bottom layer and is orthogonal with the top unit. Now that the top layer antenna unit is duplicated and arranged as sub-array, the bottom unit can also be reconfigured in the same manner. Till now, the four sectors separated by cross-arms are all respectively assigned to one antenna unit. As the two sub-arrays are located in different layers and they are still orthogonal to each other, therefore the sub-array element is also able to realize dual-polarization. The geometry of such a dual-polarized sub-array is shown in Fig. 3.2.

It can be seen from Fig. 3.2 that all the four sectors of circular aperture have been filled by four antenna units and the opposite sectors are used for the same

polarization. The cross-type arms act as extended ground plane and some via holes are placed on them to connect top and bottom ground plane. The via holes which act as metallic walls play an important role in enhancing the polarization isolation.

3.1.3 To feed the sub-array

As in the sub-array the two antenna units on the same layer are placed oppositely while they are attempted to resonate in the same polarization, therefore the current direction and electric field direction of the two units should also be opposite. To maintain co-resonance at the same situation and the co-radiation in the same direction, the sub-array should be fed with the same magnitude power and with phase difference of 180°. In this case, the sub-array seems like a dipole antenna.

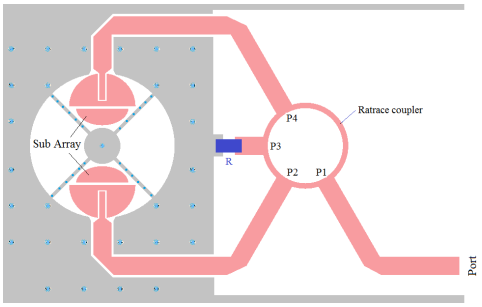

Figure 3.3: Sub-array feed with Ratrace coupler

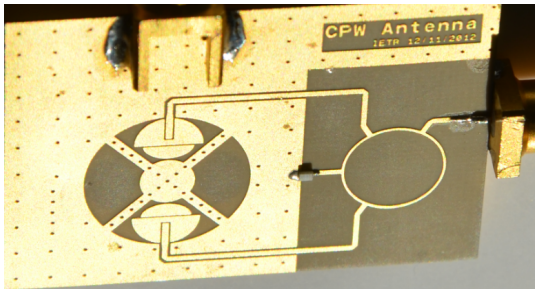

Figure 3.4: Realized sub-array antenna

To satisfy the feed condition of sub-array, a Rat-race coupler is thus used in the conception as shown in Fig. 3.3. Rat-trace coupler is a lossless reciprocal four-port network. It comprises three 90 ° branches and one 270° branch. The characteristic impedance of the ring is $\sqrt{2}$ times the characteristic impedance of the port terminations with the purpose of impedance matching [77–81]. In the case that sub-array operates as emitting antenna, the Rat-trace coupler is used as out-of-phase power divider. The signal injected into port 1 divides evenly in ports 2 and 4 with 180° phase difference, and port 3 is isolated. When sub-array operates as reception antenna, signals received from the two opposite placed antenna units are injected into port 2 and 4 and they have a 180 ° phase difference. The sum of the signals is formed at port 1 while the difference is formed at port 3. It can be seen that both in emitting and receiving modes, port 3 obtains less power from other ports and usually, it is connected to ground via a resistor to avoid inserting interferences to the circuit. The resistor should have a resistance corresponding to the impedance of port 3.

Fig. 3.4 shows the photograph of a realized Rat-race coupler feeding sub-array in PCB factory.

3.1.4 Sub-array performances

The insertion of Rat-race coupler applies possibility to feed two opposite units with the same magnitude power and with required 180° phase difference, while it does not modify any parameter of CPW-fed monopole antenna unit. Therefore the sub-array has almost the same return loss as single unit which is illustrated in Fig. 2.43.

However, as the two opposite placed units are located in a space less than $0.25\lambda_0$, their radiations will surely interact. Thus the integrated radiation must be the vectorial sum of each antenna radiation, taking into account their locations relative to each other. Fig. 3.5 illustrates the simulated radiation patterns of sub-array in E-plane and H-plane at 11.9GHz. Obviously it can be seen that at either plane, the co-polarization is 45dB higher than the cross polarization, which means the sub-array antenna is perfectly a linear polarized antenna and the polarization isolation is quite high. In addition, as there exists a metallic reflector, the main radiation is enhanced at the forward direction and the front-to-back ratio (FBR) is higher than 28dB. More over, as the quantity of antenna unit is increased and each unit radiates toward the broadside direction, the maximum directivity is increased more than 2dB compare to single element CPW-fed monopole antenna (Fig. 2.44).

As mentioned previously in section 2.4.3 that the top unit of single element antenna radiates microwaves toward two angles (Fig. 2.44). Nevertheless, By looking at Fig. 3.5 that, the radiations are found symmetric and the maximum directivity is at the broadside direction. In our opinions, the inter-element distance between the two antenna units in sub-array is quite close (about $\lambda_0/10$), interaction between two units is very strong, the array factor will compensate single unit radiation and integrate a larger radiation in the broadside direction. To sum up, we can say that the method of arranging CPW-fed monopole antenna unit as sub-array improves the entire radiation.

Even though the proposed sub-array arrangement has taken advantage of more sectors to place antenna units, which has increased the antenna gain more than 2dB. But the achieved gain is only 8.3 dBi and is still very low compare to the required 29dBi gain. Thus a bigger array which consists of more antenna units is required. In the next section, an array which is constructed with the proposed sub-array as element is introduced, the linear arrangement method and the outstanding power distribution network will also be presented.

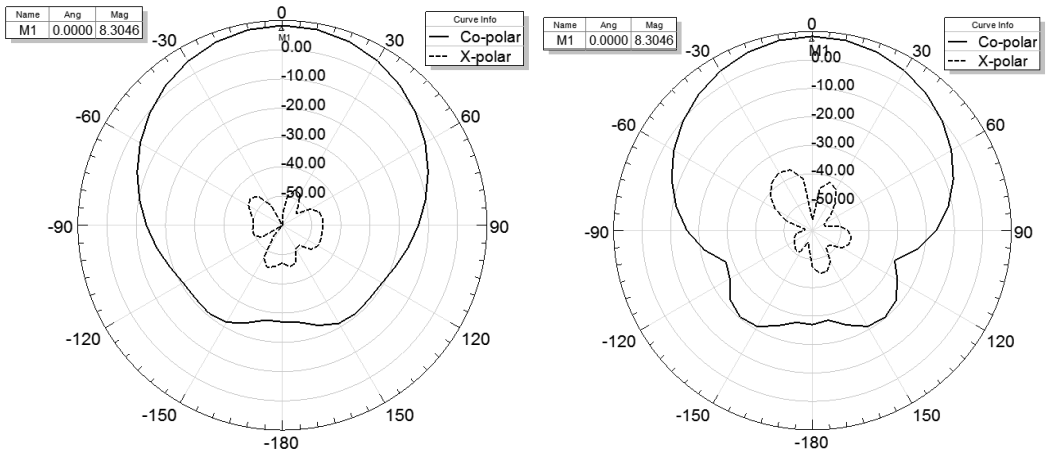

E-plane H-plane

Figure 3.5: Radiation patterns simulated at 11.9GHz

3.2 Linearly arranged CPW-fed monopole antenna array

To effectively increase antenna gain, in this section, a linearly arranged array which is composed of sub-array CPW-fed monopole antenna as element will be introduced.

3.2.1 linear array conception

The proposed linearly arranged CPW-fed monopole antenna array is depicted in Fig. 3.6. This array comprises 4 sub-array thus in fact 8 CPW-fed monopole antenna units at the top layer (light color) and another 8 units at the bottom layer (deep color). The inter-element distance d is set to one guided wavelength (λ_g) which is about 16mm with respect to 11.7 GHz, in the substrate with dielectric constant 4.4 and thickness 1.524mm. In addition, to avoid overlapping of bottom antenna ports, each element is entirely turned 36° compare to the single element position. In this case, the inter-space between adjacent antenna ports on bottom layer is 8mm ($d' = \lambda_g/2$). This distance is sufficient for placing feed network. It is worth noting that even if elements in array have been steered, sub-arrays in corresponding layers are still in parallel and with the same polarization.

In this array, the inter-element distance $d = 16mm$ and it operates in a band with 11.7 GHz as the centering frequency. Thus the ratio of inter-element distance over wavelength in free space could be yielded from the following equation:

$$\delta = \frac{d}{\lambda_0} = \frac{d \cdot c_0}{f_r} \tag{3.1}$$

Generally, the inter-element distance should be less than wavelength in air to avoid grating lobes but more than half-wavelength to decrease correlation coefficient [82]. From Equ. 3.1, the achieved inter-element spacing is about $0.62\lambda_0$, which is thus moderate in such a linear array.

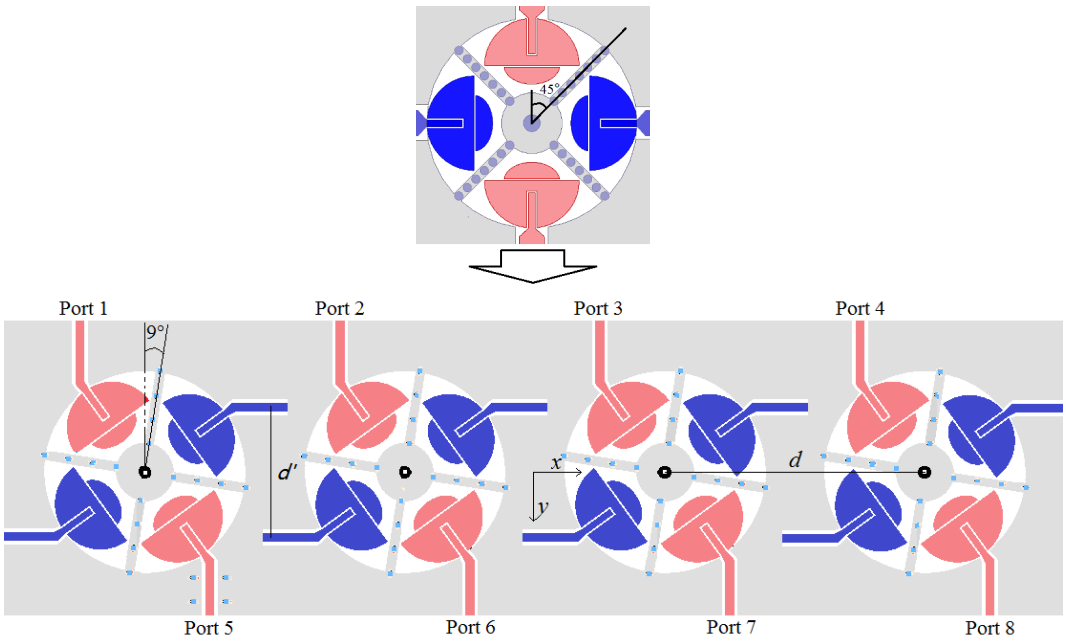

Figure 3.6: Linearly arranged 1x4 array

As this arrangement seems to provide interesting behaviors, we have now to focus on how these elements being excited. This is the aim of the next section.

3.2.2 To feed the linear array

Since we have constituted a linearly arranged array in the last section, the elements are placed separately and it is very difficult to feed simultaneously all these ports. In addition, by considering the monopole antenna element is fed with grounded co-planar waveguide line, we have to find a corresponding feed network with the same technology to integrate feed network and antenna part. Many attempts are carried out and finally the method using serial and in-phase feeding with Dolph-Chebyshev magnitude distribution is adopted.

Chebyshev current distribution

In array processing, a highly directive radiation pattern can be generated by means of appropriate choice of the antenna excitations. The Dolph-Chebyshev method for beam pattern design provides a minimum null-to-null beamwidth for a given equal sidelobe level. This distribution has direct control over the main-lobe width and maximum sidelobe level. The relationship between the beamwidth

and side-lobe level is that for a given side-lobe level the beamwidth is the smallest, and, conversely, for a specified beamwidth the side-lobe level is the lowest. Consequently, beamwidth and side-lobe level requirements can be met with the minimum number of elements if the array is of Chebyshev type [83–86].

Bresler has provided a new algorithm for calculating the current distribution of Dolph-Chebyshev array in [87]. That is, in a equally spaced Chebyshev array, the array weights (or current distribution) could be obtained if the number of element is known (either even or odd), and the required sidelobe level is given. This algorithm has been transformed to Matlab language for fast calculating which is given in Annex 2. By using the proposed program, we plan to achieve an linear array with 10 elements and sidelobe level less than 26dB, the normalized current ratio is achieved as follows:

$$I_1 : I_2 : I_3 : I_4 : I_5 : I_6 : I_7 : I_8 : I_9 : I_{10} = \\ 0.357 : 0.485 : 0.706 : 0.890 : 1 : 1 : 0.890 : 0.706 : 0.485 : 0.357 \tag{3.2}$$

Feeding network simulation

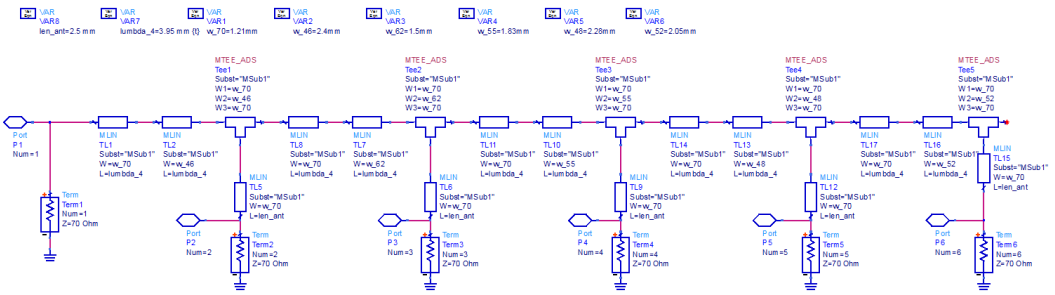

Figure 3.7: Schematic of Chebyshev amplitude distribution feed network

As the current distribution ratio is achieved for a linear array with 10 elements and this kind of array is central symmetric, to simplify the model and save time in simulation process, only one side of the feed network is simulated with the software Advanced Design System (ADS). Fig. 3.7 shows the schematic of proposed feed network. To satisfy the Chebyshev current distribution ratio, a few quarter-wavelength transmission lines ($\lambda_g/4\ TL$) are used at the nodes of antenna units to control the current division. The impedance of each quarter-wavelength TL is obtained according to the current ratio as expressed in Equ. 3.2 and multiplied by 70 ohm The 70 ohm is the impedance of the main TL, which is preferred to 50 ohm as the 70 ohm line is narrower and the achieved $\lambda_g/4\ TLs$ are also relatively narrower

in consideration of the limited space between adjacent antenna elements. In this case, to match the impedance of main TL, the impedance of CPW-fed monopole antenna unit is also optimized to 70 ohm.

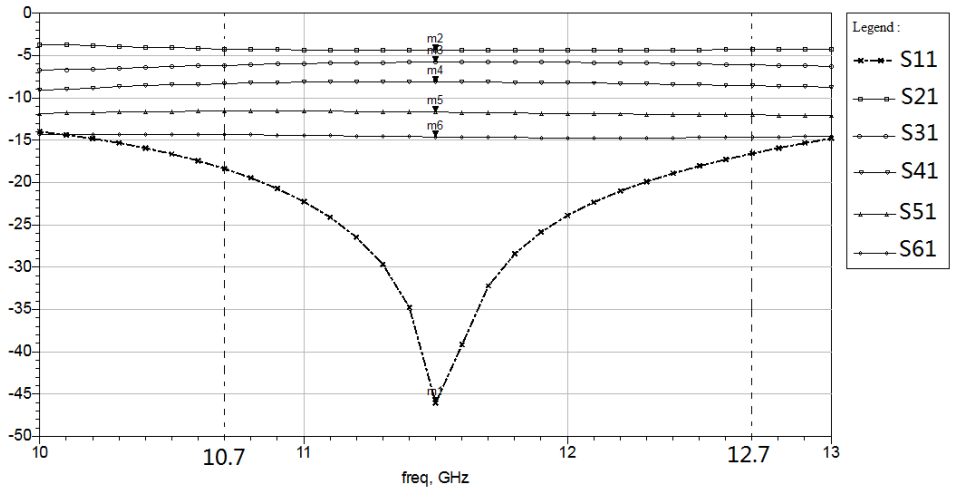

Figure 3.8: Simulated S parameters of feed network

Simulated results given by ADS is shown in Fig. 3.8. From this figure we can see that the feed network is well matched along the band from 10.7-12.7 GHz where $S_{11} \leq -15dB$ is obtained, especially at 11.5 GHz where the return loss is as low as -45dB. More over, as a few $\lambda_g/4$ TLs are used at each nodes, antenna elements in such linearly arranged array are allocated with unbalanced power. From the diagram we can find at the center frequency that:

$$S_{21} = -4.41dB$$
$$S_{31} = -5.77dB$$
$$S_{41} = -8.12dB$$
$$S_{51} = -11.7dB$$
$$S_{61} = -14.6dB$$

Suppose that the input power at port 1 is 1W, according to simulated results, the power distributed to the other five ports should be:

$$P_2 = 10^{S_{21}/10} = 0.362W$$
$$P_3 = 0.265W$$
$$P_4 = 0.154W$$
$$P_5 = 0.068W$$
$$P_6 = 0.035W$$

thus the power ratio is:

$$P_2 : P_3 : P_4 : P_5 : P_6 = 1 : 0.732 : 0.425 : 0.188 : 0.1 \tag{3.3}$$

From Equ. 3.2 and refer to the schematic of feed network, the current distribution in theory is:

$$I_2 : I_3 : I_4 : I_5 : I_6 = 1 : 0.890 : 0.706 : 0.485 : 0.357 \tag{3.4}$$

and we all know that $P = I^2R$, therefore the current squared ratio is:

$$I_2^2 : I_3^2 : I_4^2 : I_5^2 : I_6^2 = 1 : 0.792 : 0.498 : 0.235 : 0.123 \tag{3.5}$$

Comparing Equ.3.5 with Equ.3.3 we can find that, the ratio of current squared is quite close to the ratio of power distributed to each port. The very slight differences might be caused by substrate losses and insertion loss. In addition, as two quarter wavelength TLs are used between adjacent ports, the ports in serial have equal different phase different of 180°. To sum up, we can say that the feed network illustrated in Fig.3.7 has successfully achieved the required Dolph-Chebyshev amplitude distribution.

Feeding network layout

In the last subsection, the schematic of serial feed network is simulated using ADS and found useful in distributing power to each antenna element in the linear array according to the required ratio. By considering the geometry of CPW-fed monopole antenna element, we have designed a layout which integrates antenna elements and feeding network, as shown in Fig.3.9.

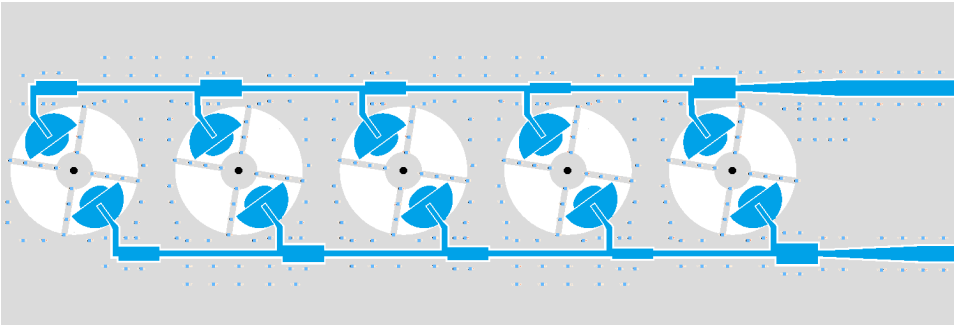

Figure 3.9: Layout of linear array feeding network

Nevertheless, in such an 1-D arranged array, Linear arrangement could not take advantage of space that, only the antenna units on top layer are connected in feed network. In this case the bottom layer units are not able to be fed. Even more, the

quantity of antenna element can not be increased without limitation because the feed line loss will significantly decrease the transmission efficiency. Due to this reason, this kind of linear array has not been actually realized, we directly paid attention to the 2-D arrangement. In the next section, the 2-D arrangement method will be introduced which provide solutions to arrange antenna elements in a planar surface so as to increase elements effectively.

3.3 Planar arranged CPW-fed monopole antenna array

In the last section, the linear arrangement with amplitude distribution method can only excite the top layer elements in 1-D array, which could not effectively take advantage of space. Here in this section, we will try to arrange antenna element in a planar array. The 2-D array conception and enhanced feed network will be introduced.

3.3.1 2-D array arrangement

Based on the geometry of 1-D arranged array where antenna elements are placed along x-axis only, we propose a 2-D array in which elements are arranged both along x-axis and y-axis, as shown in Fig. 3.10.

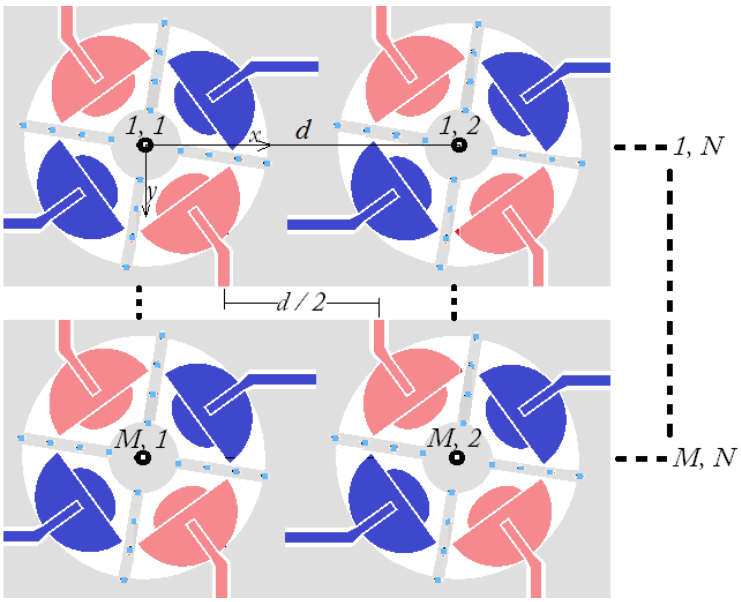

Figure 3.10: Planar arranged CPW-fed monopole antenna array

With such an arrangement method, the array consists of N rows and M columns, therefore the total number of antenna unit is MxN. The inter-element distance d

between antenna units remains λ_g ($0.62\lambda_0$) which is about 16mm in the given substrate. In this case, the distance between adjacent co-planar antenna units is only $\lambda_g/2$ by looking at Fig. 3.10. To feed such a compact array becomes more complex and challenging.

3.3.2 Two sides feeding network

In the last section, the method of feeding linear array using serial network with Dolph-Chebyshev current distribution has been introduced. Power from input port can be distributed to each port corresponds to required ratio. In this manner, we can continue optimizing such a network by increasing the terminal ports and decreasing the inter-port distance. Fig. 3.11 gives such an optimized feed network.

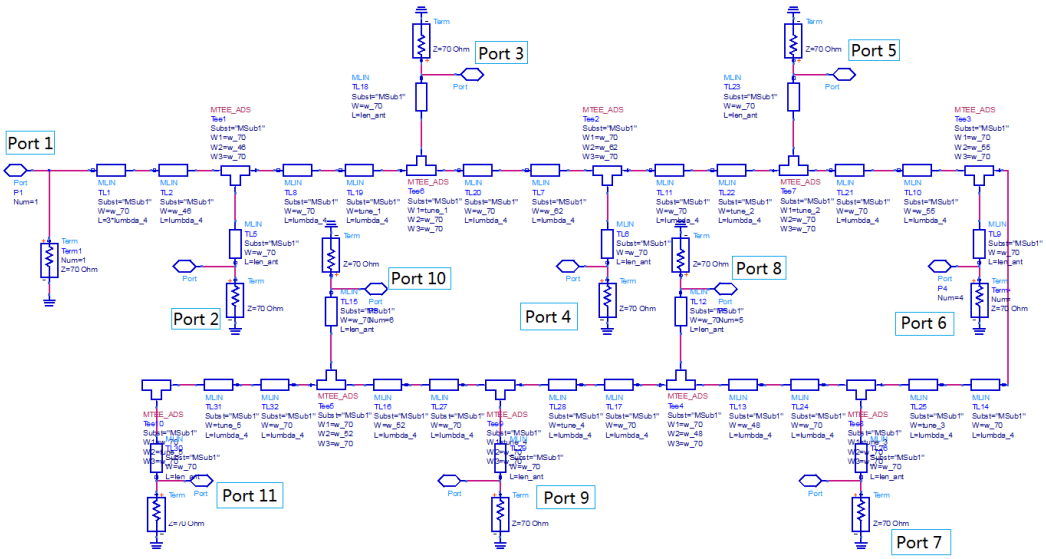

Figure 3.11: Schematic of enhanced serial feed network

From Fig. 3.11 we can see that there are now 10 antenna units connected to the main feed network. Numerous $\lambda_g/4$ TLs are used to adjust power division between antenna units. The schematic is then simulated in ADS and the results are given in Fig. 3.12. It can be seen that the 10 ports obtain power from main feed line mainly in 5 grades which corresponds to the current distribution ratio similar with the previous single side feeding network. The input port is well matched as can be seen that, along the band ranges from 10.5-12.6 GHz the simulated S_{11} is lower than -10dB. The highest transmission coefficient is located at around 11.7 GHz where S_{11} is as low as -26dB and more than 99.9% input power is distributed through feed network.

Fig. 3.13 illustrates the antenna array layout transformed from the schematic diagram, in which it can be seen that the antenna units are distributed on both sides

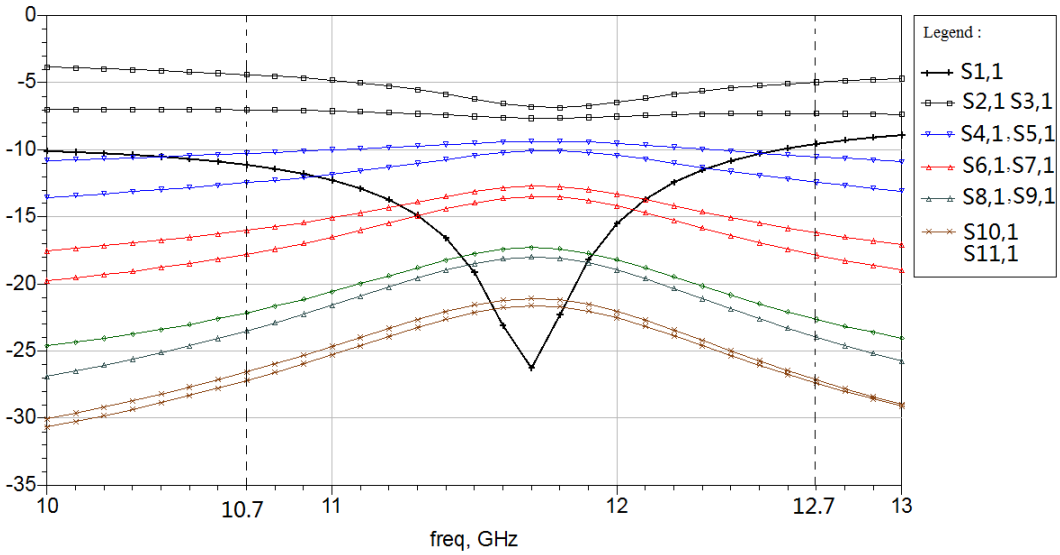

Figure 3.12: Achieved S-parameters of proposed serial feed network

of the main feed line. In this array, even though the inter-element distance is fixed to λ_g but the distance between adjacent monopole antenna units is only $\lambda_g/2$. Antenna units in each row have assigned with almost the same power level, the units in each sub-array have also the same power level. In addition, with such feeding network, units in each element have exactly a phase difference of 180 degree ($\lambda_g/2$), which is the basic requirement for CPW-fed monopole sub-array to obtain broadside radiation.

With two-side arranging method, we are able to increase antenna element not only by arranging more units in each branch (x direction), but also by duplicating branch to get more columns in y direction. However, as column increases, to distribute input power into each branch and maintain reasonable sidelobe level in both x and y directions become a new challenge.

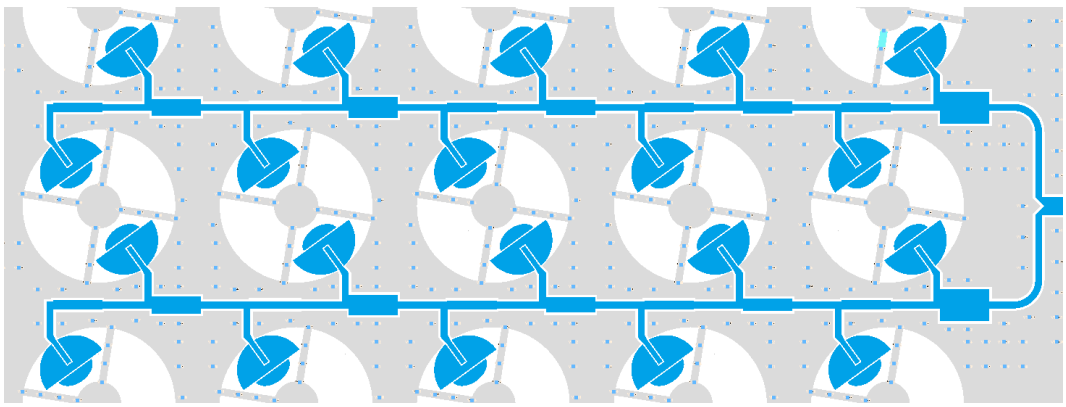

Figure 3.13: Layout of two sides arrangement feeding network

3.3.3 2D arrangement method

To solve the problem of distributing input power into each branch which consists of numerous CPW-fed monopole antenna units to realize a real planar array, in this section, two solutions will be introduced. One is equal-distribution network composed of T-type power dividers, and the other one is unequal- distribution network which applies Dolph-Chebyshev amplitude distribution again in y direction.

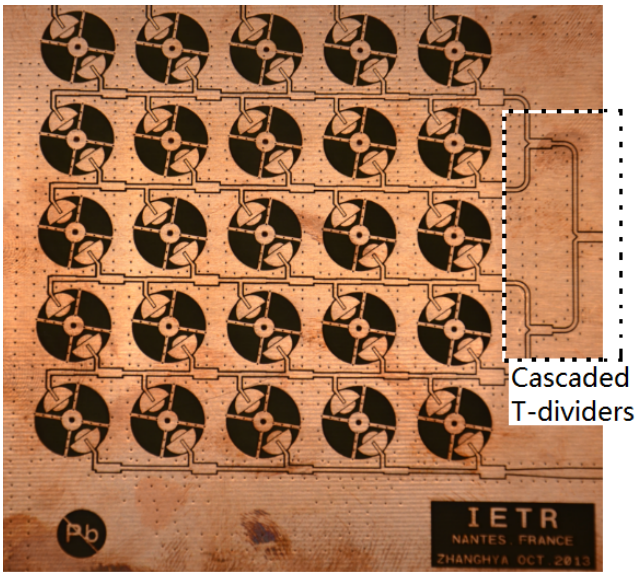

Figure 3.14: Photograph of 5x5 CPW-fed monopole antenna array fabricated in 'KEYUAN' PCB factory of Shenzheng, CHINA

Equal-distribution network fed 5x5 array

As we all know that, by using 3dB T-junction power divider, it is able to obtain balanced and in-phase power at the two output ports [88]. T-junction divider could be cascaded therefore input power can be divided into more portions. In this manner, 4 branches of CPW-fed antenna array should fed with 3 cascaded T-junction dividers. A photo of realized antenna array which consists of 5 columns by 5 rows of CPW-fed monopole sub-arrays is shown in Fig.3.14. In the photo, there are 4 central branches connected individually to the output ports of a 1-to-4 division network, thus all the 25 elements could be excited simultaneously by the unique input port.

However, along y-direction of such an equal-distribution array, RF power are equally assigned to each branches, the achieved sidelobe level over this plane might be exceptionally high (about 11dB less than the main beam). In this case, an unequal-distribution feed network is required.

Unequal-distribution network fed 3x12 array

As mentioned in previous section that, in a Dolph-Chebyshev array the sidelobe level is controllable by adjusting current distribution ratio. In the proposed 5x5 array, this method has already been used in each column where the input power is distributed to 10 units according to achieved current division ratio to obtain a -26dB sidelobe level. In this manner, we can use Dolph-Chebyshev current distribution method again to replace the proposed equal-distribution network so as to pursue sidelobe level reduction in yoz plane. Fig. 3.15 illustrates a part of 3x12 CPW-fed monopole antenna array, in which antenna elements are distributed at the two sides of main feed line. In each branch, the number of antenna element is 12 and expected to obtain a sidelobe level lower than -30dB, current division ratio is easy to obtain with the Matlab program given in annex 2. It can be seen that numerous of $\lambda_g/4$ TL are used to adjust current division at each element node, and their impedances are calculated according to the achieved current division ratio. Meanwhile, in this photo, we can see that the four branches are connected to the central feed line. The four branches can also be attributed as elements in Chebyshev array, and -30dB sidelobe level is also required along the main feed line. At the central part, the main feed line is then connected to a SMA connector, as the total and unique input and output port.

Figure 3.15: Photograph of 3x12 CPW-fed monopole antenna array (part) fabricated in 'PROTECNO GTID' PCB factory of Brest, FRANCE

With 2-D arrangement method, CPW-fed monopole antenna element can be arranged in big planar array which its column and row numbers can both increase to satisfy antenna gain. In this kind of array, Chebyshev current distribution method is applied not only in columns but also in rows. Therefore, sidelobe level is expected to be limited in both E and H planes.

3.4 Results and discussion

As mentioned in previous section that, CPW-fed monopole antenna could be made easily by using Printed Circuit Board technology, but the very high accuracy (0.1mm) is strictly required as it impact on antenna performance significantly. The proposed 5x5 CPW-fed monopole antenna array and 3x12 array are not able to be made in our laboratory due to the difficulty of via hole metalization, therefore they are both fabricated in PCB factories. As shown in Fig. 3.14 and Fig. 3.15.

The S-parameter measurements are carried out in our laboratory with a Vector Network Analyzer Agilent E8364B and radiation measurement are carried out in the anechoic chamber. Fig. 3.16 illustrates the measured S_{11} of 5x5 array and the measured radiation pattern at 10.8GHz is given in Fig. 3.17.

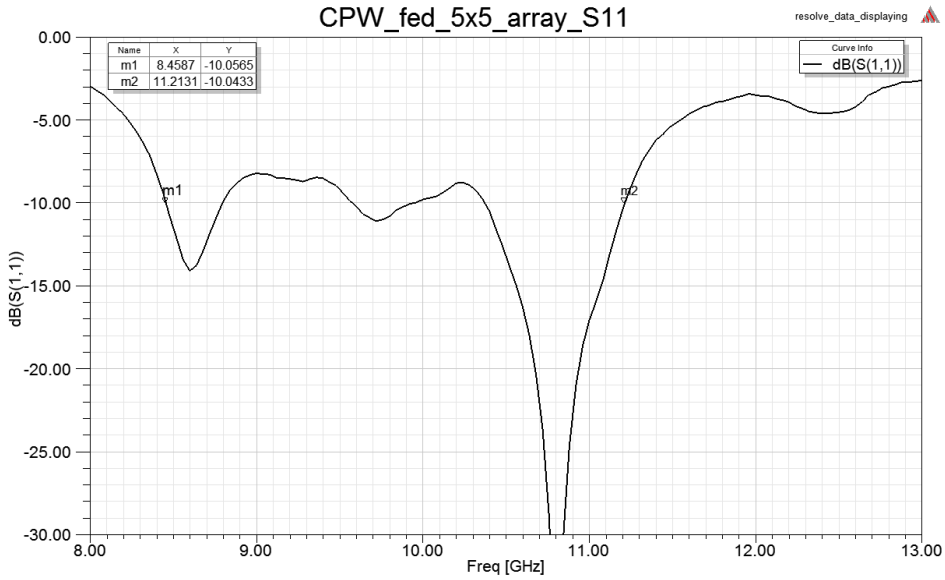

Figure 3.16: Measured reflection coefficient of CPW-fed monopole antenna 5x5 array

The measured return loss indicates that the realized array works in a $VSWR \leq 2.5$ band ranges from 8.5 GHz to 11.4GHz, which is obviously shifted from the required band (10.7 - 12.7GHz). Due to this reason, the central frequency band has not been well matched, where more than 15% RF power is reflected back to the input port. Nevertheless, in the higher band start from 10.4 to 11.2 GHz the antenna resonates well, especially at 10.8 GHz the measured return loss is as low as -34dB. After verifying the design layout and realized antenna board, by looking at Fig. 3.18. It can be seen that the slots and gaps between antenna patch and ground plane are significantly enlarged, which impacts on impedance matching along wide band. Simulations carried out in HFSS with measured dimensions indicates narrow bandwidth and mismatching happens at higher frequency band, as shown in Fig.3.19.

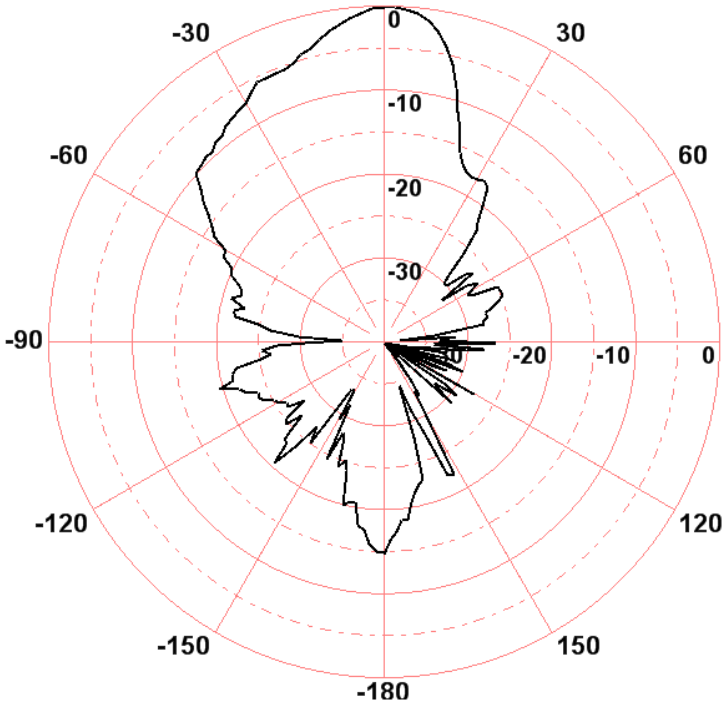

Figure 3.17: Measured radiation pattern of CPW-fed monopole antenna 5x5 array at 10.8 GHz

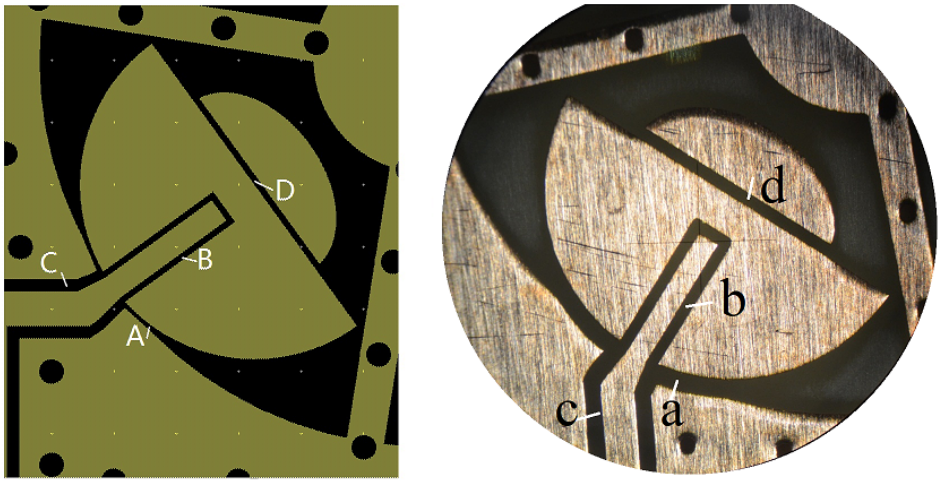

Design layout

A=0.1mm C=0.2mm
B=0.1mm D=0.1mm

Realized antenna

a=0.279mm c=0.292mm
b=0.165mm d=0.161mm

Figure 3.18: Fabricating tolerance between design layout and achieved antenna board

Fig. 3.17 illustrates the measured radiation pattern of 5x5 array at 10.8 GHz as this frequency point has the best resonance. It can be seen that the main beam is not symmetric due to the unsymmetrical structure of antenna array which is shown in Fig .3.14. At the right side of radiation pattern, -25dB sidelobe level is obtained which matches well with the conception value (-26dB) in Dolph-Chebyshev array.

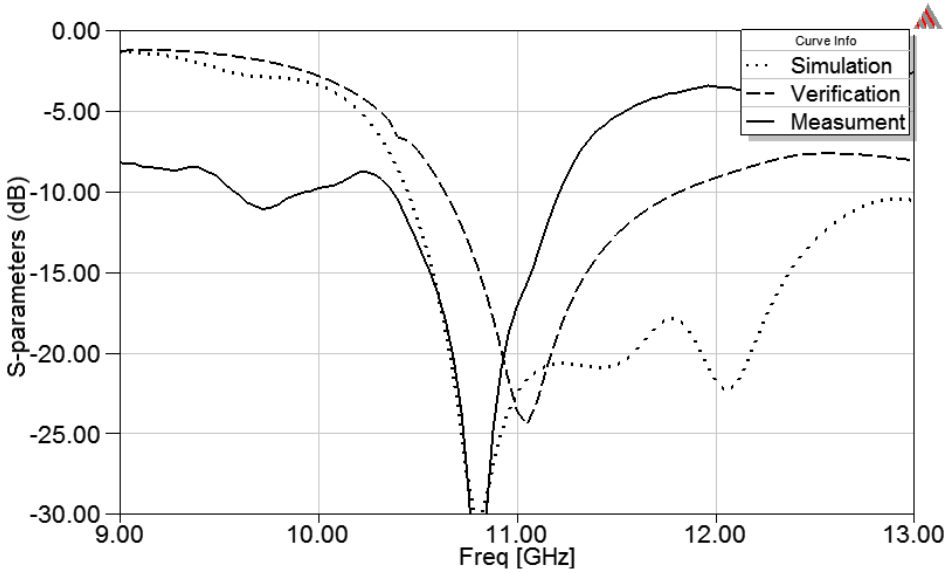

Figure 3.19: comparison among simulation, measurement and simulated result with measured dimensions

But at the left side of the radiation pattern, the main beam is very wide as no corresponding Chebyshev array exists on this side.

The proposed 2-D arranged CPW-fed monopole 3x12 array has also been fabricated in factory, the realized antenna broad is shown in Fig. 3.15. Nevertheless, we have made some serious mistakes in the layout file (unwanted ground planes are inserted), the realized feed line impedance has been unexpectedly changed, therefore the measured results are extremely bad and could not be given here. Most recently, we have already a plan to realize this antenna again to test its performance.

3.5 Conclusion

In this chapter, a series of antenna arrays which apply CPW-fed monopole antenna as element are introduced. Antenna element has firstly been arranged linearly in a 1-D array and fed in serial. Then the planar arrangement method has been used to place antenna element both in x-direction and y-direction. Dolph-Chebyshev current distribution method has been used not only in assigning power to each element, but also in distributing power to each branch, to control sidelobe level both in x and y direction. Measured results indicate the realized sidelobe level could be effectively limited.

However, it is worth while noting that, as CPW-fed monopole antenna array becomes bigger using planar arrangement, more and more quarter-wavelength transmission lines should be used. As we all know that $\lambda_g/4$ TL has narrow band characteristic and it may impact on antenna performance. Nevertheless, if more studies are carried out, the CPW-fed monopole antenna array with Dolph-Chebyshev mag-

nitude distribution feed network is expected to have better performance.

Recall that the cross-type microstrip patch antenna has been introduced previously, its performances are attractive and pleasing. In the next chapter, we will divert the focus on arrays which consists of such antenna element.

4

Cross-type antenna array

Cross-type antenna, as proposed in the second chapter, has some attractive performances such as wide-band (10.0-14.7 GHz), dual-polarization (Horizontal and vertical), high radiating efficiency, flat structure, low cost and low fabrication complexity. The cross-type antenna can also be assumed as a sub-array as it comprises several parasitical radiators thus its gain is relatively higher than single patch microstrip antenna. However, the achieved gain is still much less than the required gain to stably receive satellite broadcasting signal. We have to find solutions to effectively enlarge cross-type antenna gain and also directivity.

As mentioned in chapter I that the most effective method to increase antenna gain is to duplicate antenna element and construct an array. In this chapter, we would like to introduce step by step approaches to conceive cross-type antenna array. The cross-type antenna element is firstly arranged linearly in a 1x4 array and then in a 4x4 array with planar arrangement, which are introduced in section 1 and 2 separately. The corresponding feed networks is also presented in both kinds of array. Meanwhile, a method of decrease cross-type antenna array inter-element space by sharing patches between adjacent elements will be discussed. This method has been applied both in linear and planar arrays. To increase isolation between two feed ports, in the third section, a method of integrating both horizontal and vertical feed network in the same structure but in different layers with the very up-to-date multi-layer technique will be introduced. Finally in the fourth section, conclusion will be given.

4.1 1-D linearly arranged cross-type antenna array

Although the single element cross-type antenna has a relatively high gain, but its profile is as high as $0.94\lambda_0$ (Table. 2.5), which is quite close to the wavelength respect to central frequency of operation band. Thus even if we take no account of interaction between elements and arrange this kind of antenna one by one, the inter-element distance remains still high.

As we all know that the inter-element distance is extremely important as it affects the broadside gain, the sidelobe level, and the cross polarization discrimination [89]. Generally, the inter-element distance should be chosen less than wavelength to avoid grating lobes but more than half wavelength to decrease correlation coefficient [82]. To solve this problem, Shi-Gang et al. have proposed an aperture shared antenna array in [90] and [91]. The proposed array is reported to have overall size and weight reduced by using aperture sharing method. In [92], Kainan et al. have emphasized the element also act as a reflector in a switched parasitic antenna array and achieved inter-element distance reduced.

In the case of using proposed cross-type antenna which comprises several parasitic patches as array element, we propose a method of arranging antenna element one after another and separated by narrow gaps. An experimental array which is composed of 4 cross-type antenna elements and arranged linearly using this technique will be introduced in this section.

4.1.1 1x4 cross-type antenna array conception

Fig. 4.1 illustrates the conception of linearly arranged 1x4 cross-type antenna array. It can be seen that each element in this 1x4 array shares one patch with adjacent element. These patches of deep color in this figure, which are called shared patches, play important roles in connecting contiguous elements. RF power which is provided from coaxial cable and coupled by thin gaps arrives at shared patches with different phase, due to unequal distances from contiguous feeding ports. Therefore the integrated electro-magnetic field on shared patches does not equal to zero. It is worth noting that, all the patches are designed to have the same width calculated according to center frequency of Ku-band. Thus the shared patches can also resonate and emit microwave as the other patches and contribute to wider bandwidth and higher radiation level.

Simulated S-parameters of 1x4 array are depicted in Fig. 4.2 while the four horizontal ports H1 to H4 are fed separately. It can be found that the bandwidths of the four elements in the linear array match very well and they are almost the same with the bandwidth of individual cross-type antenna (Fig. 2.31). The simulated return losses are similar at lower band but vary slightly as the operating frequency

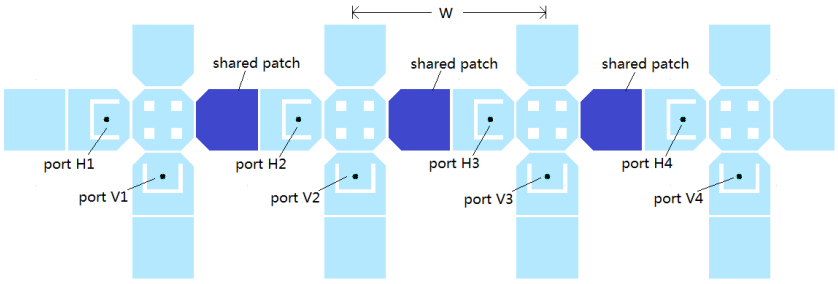

Figure 4.1: Topology of 1D linearly arranged cross-type antenna array

goes higher. This can be explained as the gaps become more sensitive at higher frequency. In such a linear array, only the horizontal arm of each element has patch shared. The vertical arms are separated from each other, therefore simulated return losses of vertical ports are totally similar with single element.

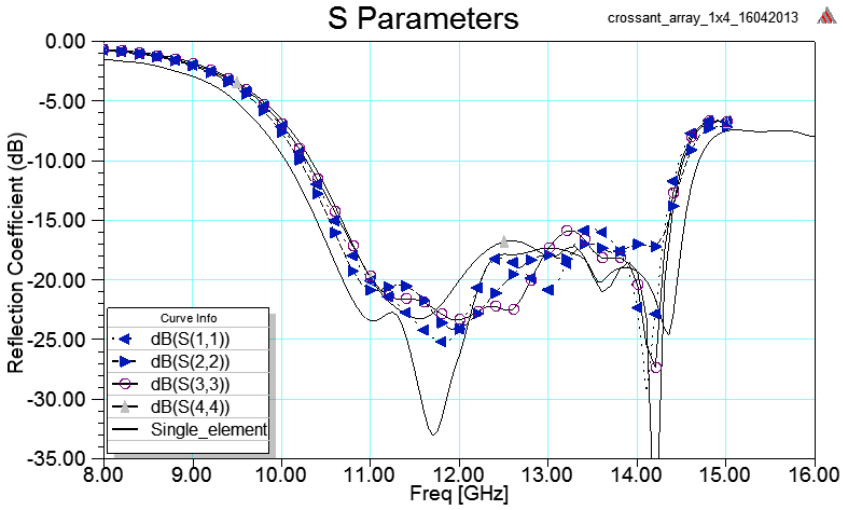

Figure 4.2: Simulated return losses of antenna units in 1x4 array

4.1.2 Patch sharing technique

As can be seen from Fig. 4.1 that, the patches in deep color are now shared by adjacent elements. The equivalent element could then be assumed as the prototype illustrated in Fig. 4.3. The horizontal arm is composed of only 3 patches while the vertical arm does not change. The inter-element distance w in Fig. 4.1 is now quite smaller than the width of a single antenna. In this manner, the linear array could be increased by arranging more equivalent units in the horizontal direction. The method of arranging antenna array by sharing one patch of its element to decrease inter-element distance is called patch sharing technique, and to the best of our knowledge, this technique is the first time proposed in antenna array arrangement and is introduced detailedly in [93].

Patch sharing technique could be applied to the cases of decreasing inter-element distance in antenna array whose element uses parasitic patches to expand antenna band.

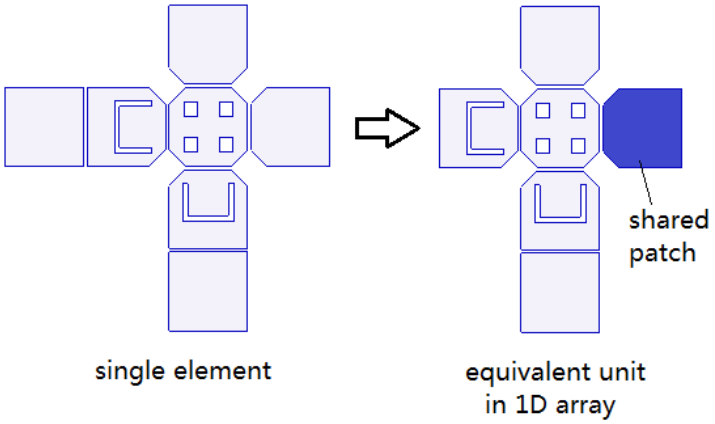

Figure 4.3: Equivalent unit in 1D arranged array

As mentioned previously that the single element cross-type antenna has a profile of $0.94\lambda_0$, as patch sharing technique is used in the linear array, the inter-element distance is as low as $0.7\lambda_0$. As can be seen from simulated S-parameters (Fig. 4.2) that decreasing on inter-element distance does not impact on return loss of each element in the linearly arranged cross-type antenna array.

4.1.3 1x4 array feeding network

The proposed 1x4 linear array has in fact 4 horizontal ports and 4 vertical ports. These ports should be connected into two separate networks so as to maintain dual-polarization performance. Fig. 4.4 presents a simple method to excite the 1x4 array. We firstly consider the horizontal feed network for example. It can be seen that three T-junction dividers are used in this network to equally distribute HF power from port 1 to the 4 terminals whose impedances have already been matched to each antenna input port.

In such a feed network, both trapezoid and quarter-wavelength transmission lines are used for impedance matching at each T-junction dividers. As we all know that, trapezoid line can match a high impedance at the thin terminal to low impedance at the thick terminal in a wide band if its length is long enough. Whereas quarter-wavelength line applies to the same function, its impedance is the square root of impedance product of two terminals and its length is quarter guided wavelength as its name. However it is a kind of narrow band component. As the dedicated space is too narrow to develop trapezoid TL at the second grade, only the first grade applies trapezoid TLs. The second grade dividers apply quarter-wavelength TL, as shown in Fig. 4.4 .

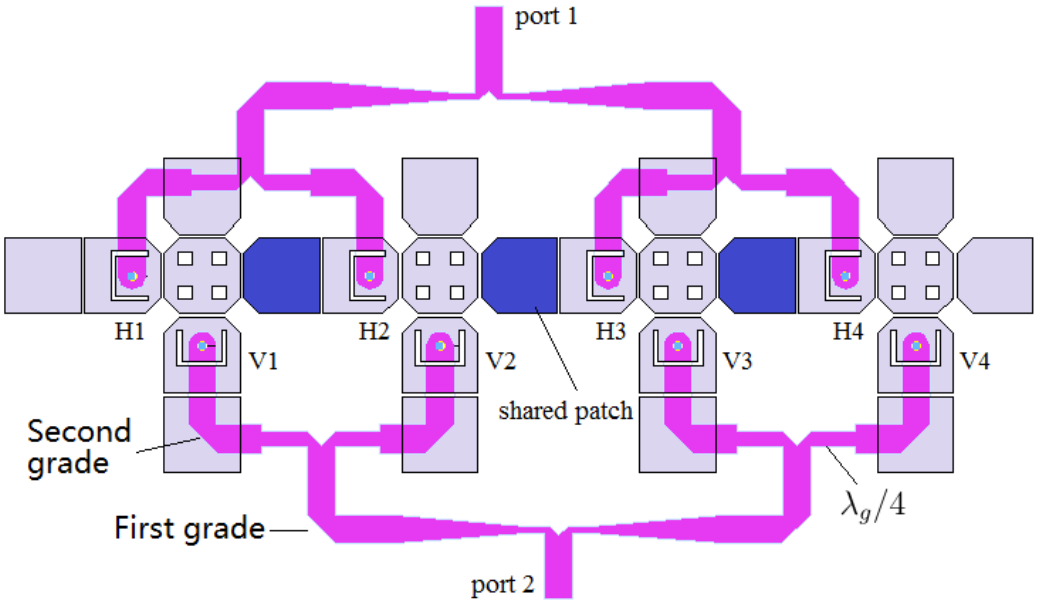

Figure 4.4: Feeding networks for 1x4 array

It is worth noting that, each divider used in this kind of feed network has average power distribution and all the terminals are with the same length. Therefore each antenna element obtains power with the same magnitude and in phase.

4.1.4 Results and discussion

The proposed 1x4 array and feed network are realized in our laboratory. The antenna array is printed on a substrate with dielectric constant 2.55 and thickness 1.524mm while the feed network is printed on the same substrate but with thickness 0.8mm. The feed board is located under antenna board, metallic probes with diameter 0.6mm are used to connect antenna input ports to feed network terminals. Port 1 and port 2 in Fig. 4.4 are finally connected with SMA connectors, measurements are carried out within the two main ports.

Fig. 4.5 illustrates the measured S-parameters of proposed 1x4 array. It can be seen that the impedance bandwidths obtained at port 1 and port 2 cover the required band which ranges from 10.7-12.7 GHz. However, the horizontal arms in the linear array have adopted patch sharing while the vertical arm don't, so the return losses measured at port 1 and port 2 are not similar. The port 1 has a -10dB impedance bandwidth from 10.2GHz to 12.8GHz and at port 2 it is from 10.2GHz to 14.0GHz. The deepest resonance measured at port 2 is at 12.35GHz where the return loss is as low as -37dB. The dotted curve in this figure depicts the transmission coefficient from port 1 to port 2, which indicates the isolation between the two ports maintains better than 20dB at the lower frequency band. As frequency goes higher, the transmission coefficient rises rapidly, thus the isolation becomes

worse than 18dB at the higher frequency band but remains acceptable.

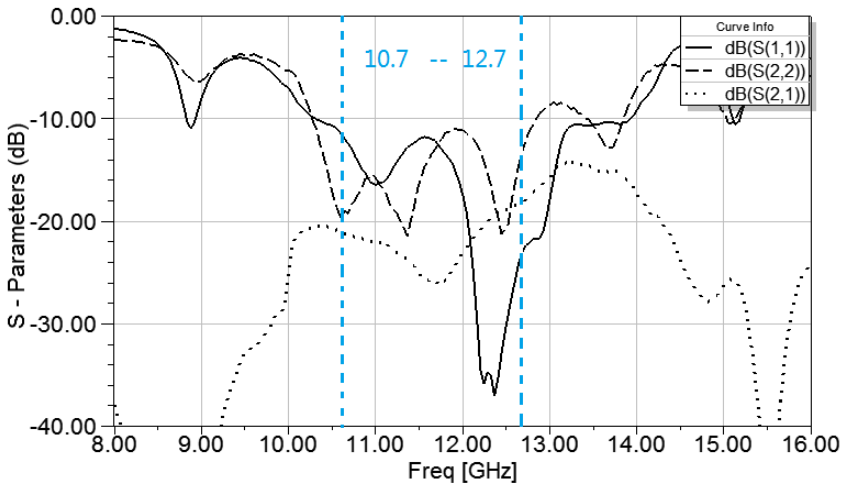

Figure 4.5: Measured S-parameters of 1x4 array

Measured radiation patterns are presented in Fig. 4.6 and 4.7 which are carried out at 10.56GHz and 11.68GHz. Fig. 4.6 illustrates the measured directivity when port 1 is excited and port 2 is connected with a matched load. At each frequency, we can obviously see a main beam at the broadside direction. Meanwhile each main beam has a HPBW about 20°. At 10.56GHz, the measured cross-polarization is about 20dB lower than co-polarization and sidelobe level is 13dB lower than the main beam, while at 11.68GHz the cross-polarization increases a few dB and sidelobe rises at the left side as operating frequency becomes higher. The back radiation level depicted in both patterns can be found very high due to the exposed microstrip feed line at rearward.

When port 2 is excited and port 1 is loaded, the measured directivities are shown in Fig. 4.7. The main lobe can also be seen at each pattern which is close to the broadside direction, but when compared with the measured radiation patterns at port 1, it can be seen obvious sidelobes exist at both sides, even more the cross-polarization increases a few dB.

Fig. 4.8 depicts the measured polarization isolation when the linear array is loaded on a motor which turns in the vertical plane (array turns along angle phi) and port H and port V are excited separately. It can be seen that the cross-type antenna array has very high quality linear polarizations, the two linear polarizations are very well isolated that better than 20dB isolation could be observed.

Conclusion

Till now, we have successfully achieved a linear array which consists of 4 cross-type antenna elements. In the proposed array, the inter-element distance is opti-

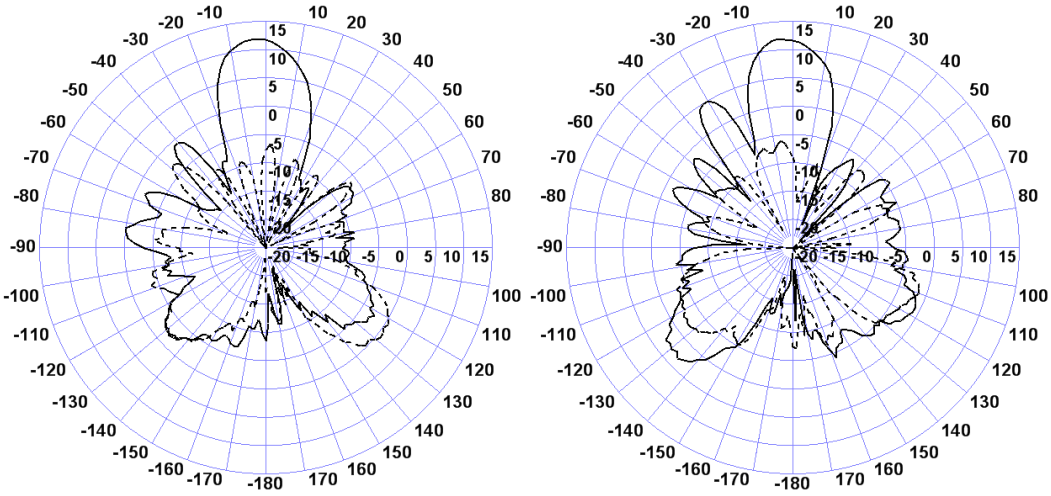

Freq = 10.56 GHz Freq = 11.68 GHz

Figure 4.6: Measured radiation patterns while Horizontal ports are excited

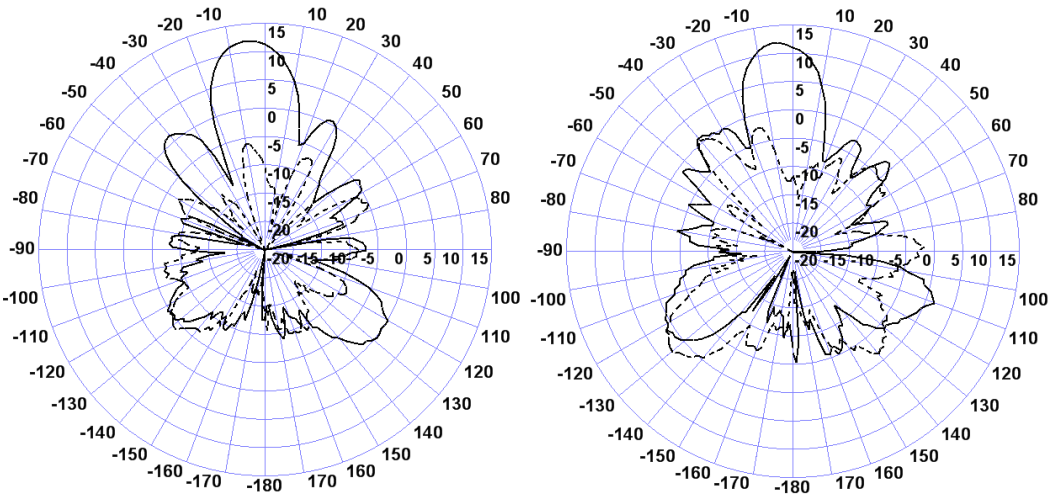

Freq = 10.56 GHz Freq = 11.68 GHz

Figure 4.7: Measured radiation patterns while Vertical ports are excited

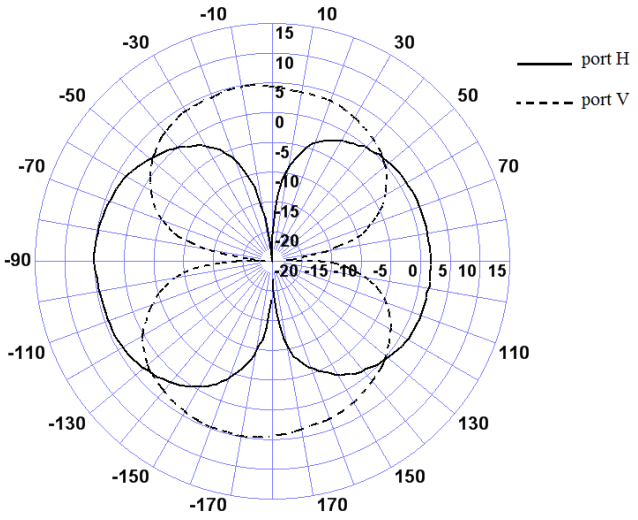

Figure 4.8: Measured polarization isolation

mized to only $0.7\lambda_0$ using patch sharing technique, although a single cross-type antenna has a dimension of $0.94\lambda_0$. Both simulation and measurement indicate that the required band could be obtained with such a linear arrangement method. Measured radiation patterns show that the array has an integrated narrower main lobe compare to single element due to the array factor. Both sidelobe and cross-polarization could be limited below -15dB with only 4 elements in this array. However, simulated result indicates that the gain of such a linear arranged array is only 12.5dBi, which is only about 3dB higher compare to single cross-type antenna even if antenna number increases four times in this array. That's because the total number of radiators has not been increased four times as patch sharing technique is used. To increase cross-type antenna array gain much bigger, we have to find solutions to arrange more antenna elements. The 2-D arrangement method is thus introduced in the coming section.

4.2 2-D planar arranged cross-type antenna array

In the last section, the 1-D linearly arranged cross-type antenna array has provided us higher gain, narrower beam and better directivity performances. By using patch sharing technique, the inter-element distance can be decreased to $0.7\lambda_0$, antenna array becomes smaller and more compact. In this section, the 1-D arrangement method is extended to planar application to realize a 2-D array. Experimental antenna array structure, feed network and measured results are given.

4.2.1 Topology of 2-D array

In the linear array as shown in Fig. 4.1, the horizontal arms are connected one by one and the patch in deep color is shared by two adjacent elements therefore the inter-element distance could be decreased effectively. In this manner, we can extend this method to a 2-D arranged array, in which antenna element are placed along both x-axis and y-axis (like the planar CPW-fed monopole antenna array).

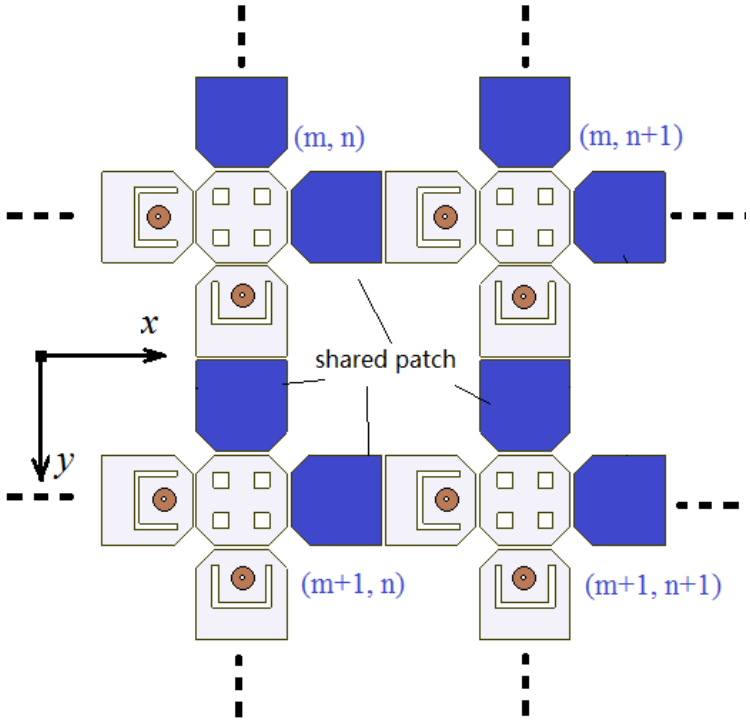

Figure 4.9: Topology of 2-D arranged cross-type antenna array

Fig. 4.9 gives the topology of 2-D arranged array. In such an array one can see that cross-type antenna element is placed not only along its horizontal arm but also along the vertical arm, and patch sharing technique is then used in both directions. It can be found shared patches in deep color on x and y axis. In this case, the inter-element distance in such a planar array can maintain $0.7\lambda_0$ with respect to the central operating frequency. Probably we can say that the equivalent unit in such 2-D arranged array is alike the simplified shape as depicted in Fig. 4.10. In this manner, using 2-D arrangement method, cross-type antenna array is able to be extended to big array which consists of large quantity of elements, so as to obtain higher gain. Here we present an experimental planar array which is composed of 16 cross-type antenna elements and is arranged in the form of 4x4, by looking at Fig. 4.11.

The realized 2-D arranged planar array shown in Fig.4.11 is composed of 16 elements, and each element is dual-polarized. Therefore, the total number of feeding port is 32, and located in a small area of 78.4mm in square. The complexity of

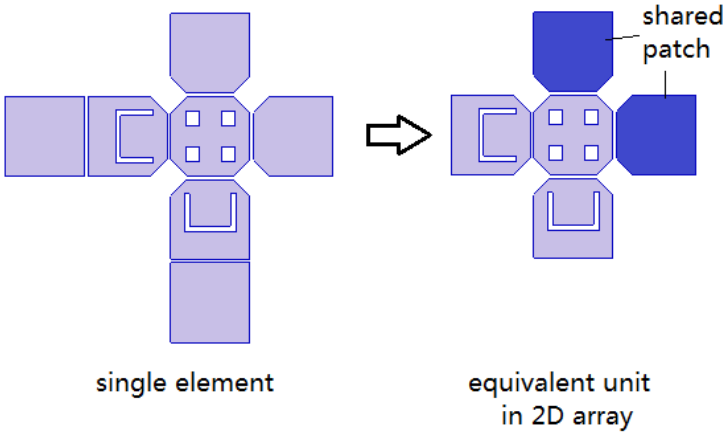

Figure 4.10: Equivalent unit in 2-D arranged array.

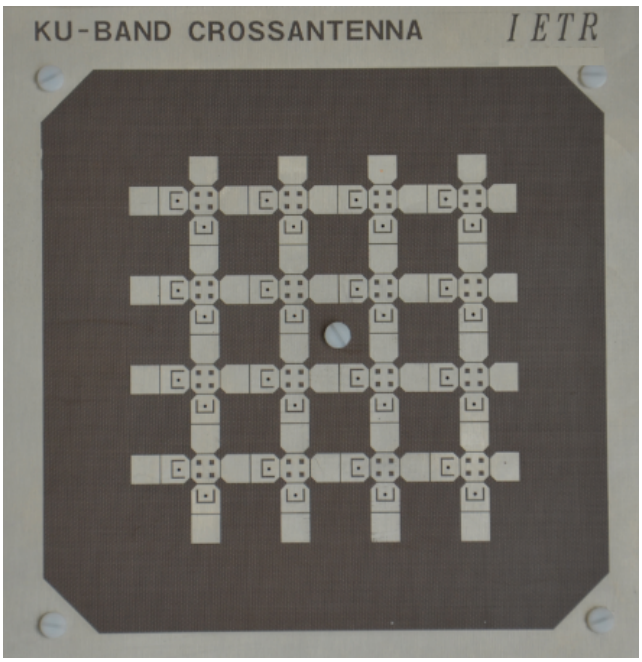

Figure 4.11: Realized 4x4 cross-type antenna array using 2-D arrangement

feeding such an array is really a great challenge. Due to this reason, we would like to firstly realize a single polarization excitation and then extend to the dual polarizations. The method of isolation enhancement will also be discussed in the coming sections.

4.2.2 Circuit configuration of 4x4 array feed network using T-junction divider

As mentioned before in section 4.1.3 that the linearly arranged 1x4 array network is realized with microstrip transmission line, in which quarter guided wavelength TL and trapezoid TL are used to match impedance at each T-junction. With such a parallel feed network, elements in the array are assigned with equal-magnitude

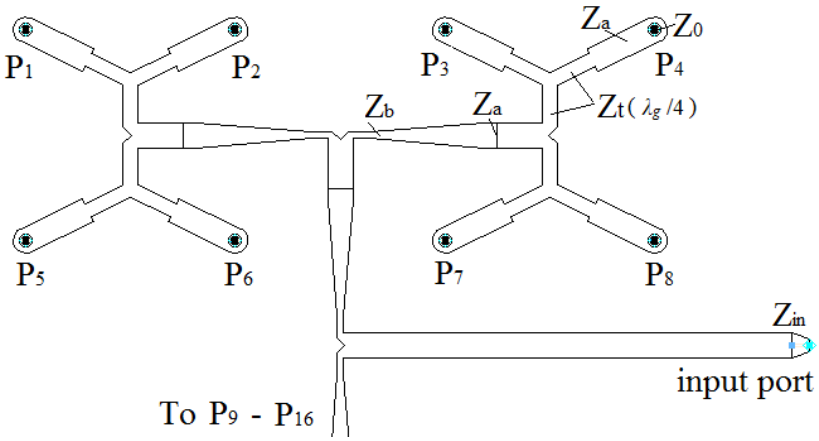

Figure 4.12: Half upper part of 4x4 array feeding network

and in-phase power. The 1x4 array is thus able to obtain sufficient bandwidth and obvious increment on gain. To extend this method, an enhanced feeding network is designed for the proposed 4x4 array and is illustrated in Fig. 4.12.

It can be seen in this feed network that, all 16 terminals are enrolled in the same circuit and each terminal has its impedance matched with antenna element input port. Several T-junction (or Y-type) power dividers are used in cascaded mode to equally distribute power from input port to each terminal. More over, quantities of quarter guided wavelength TLs are applied to match impedances at each T-junction. In this figure, Z_0, Z_a and Z_{in} are 50 ohm, Z_t is 70.7ohm, Z_b is 100ohm. In this manner, it is worth noting that, the feed network can be enlarged to enroll more terminals so as to satisfy the increment of antenna array elements.

The proposed microstrip transmission line feed network is easily realized on a TEFLON substrate using printed circuit technique. The feed board is then placed at the bottom of antenna board, probes are used here to connect feed network terminals to antenna element input ports. The entire structure has been measured and the result is given in Fig. 4.13. One can see the strong resonance exists around the central operating frequency (11.7GHz) and the achieved $VSWR \leq 2$ bandwidth ranges from 11.2GHz to 12.1GHz. However, outside this frequency band impedance mismatch could be clearly seen. The required bandwidth could not be achieved with the proposed feed network.

Let's recall that in the linear array feed network (Fig. 4.5), the achieved bandwidth is decreased when comparing to single cross-type antenna (Fig. 2.31) by using several T-junction dividers and quarter guided wavelength TLs, which are known as narrow band components. In the 4x4 array feed network, much more such components are used, therefore the achieved bandwidth has been decreased significantly.

Measurement indicates that the proposed microstrip line feeding network with

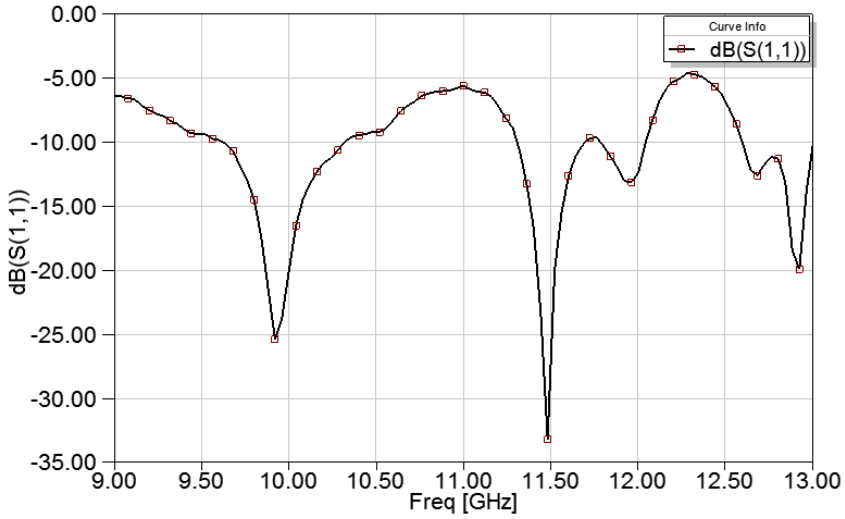

Figure 4.13: Measured return loss of 4x4 array with narrow band feeding network

T-junction and quarter guided wavelength can not satisfy required wideband applications. So we have to find substitute components which are specially for wideband use to take place of the proposed components. In the next subsection, another kind of wideband feed network designed for planar cross-type antenna array will be introduced.

4.2.3 Circuit configuration of 4x4 array feed network using Wilkinson divider

In the last section, the 4x4 cross-type antenna array feed network constructed with T-junction dividers and quarter guided wavelength TLs has been studied and found narrow band. Several other kinds of feed network have been studied, either serial [94, 95] or parallel [96, 97] or serial-parallel mixed [98] feed network have been adopted to feed our 4x4 array, but the bandwidth is still hard to obtain. In [99–101], feed networks composed of cascaded Wilkinson dividers are used to feed wideband even ultra wideband antenna arrays, good performances are reported to obtained. In this section, we would like to introduce such kind of Wilkinson feed network designed for the cross-type 4x4 antenna array.

Single Wilkinson divider

As is known to us all, Wilkinson power divider is a power splitter/combiner which has been widely used in microwave applications. The conventional two-way Wilkinson equant-power divider is a lossless three-port matched network. Input power can be split into two in-phase signals with the same amplitude [102–104]. Fig. 4.14 shows the geometry of a Wilkinson divider, in which, the impedances

have relations as follows,

$$\begin{aligned} Z_1 &= Z_2 = Z_3 \\ Z_t &= \sqrt{2} Z_1 \\ R &= 2Z_2 \end{aligned} \tag{4.1}$$

and as it is an equant and lossless divider, power received at port 2 and port 3 have the same level and equals a half of input power, as depicted in Equ. 4.2.

$$P_2 = P_3 = 1/2\ P_1 \tag{4.2}$$

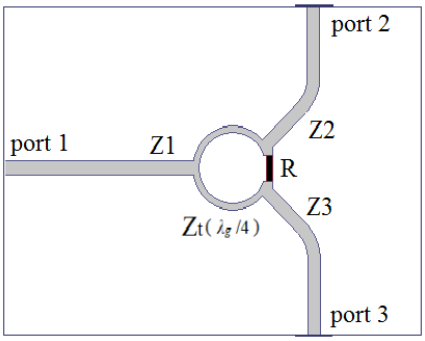

Figure 4.14: Wilkinson divider with stripline

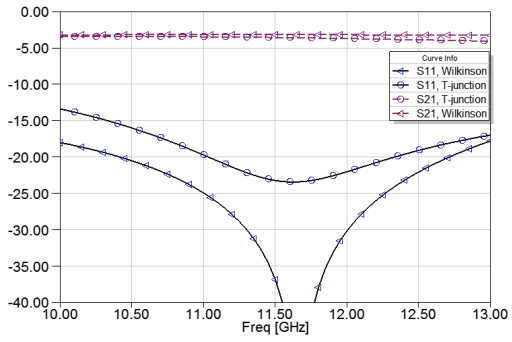

Figure 4.15: Comparisons of Wilkinson and T-junction dividers

Wilkinson divider is able to offer reasonably wide bandwidth even if it is based around the use of quarter wave transmission lines. Fig. 4.15 illustrates the comparisons between Wilkinson and T-junction power dividers. It can be seen that Wilkinson divider has better reflection coefficient along a wide bandwidth and its transmission coefficient is also a little bit higher than T-junction divider.

Cascaded Wilkinson dividers

A cascaded Wilkinson network with multi-output ports is shown in Fig. 4.16 and its simulated S-parameters are illustrated in Fig. 4.17. Obviously it can be seen that the central resonance which exists in single Wilkinson divider S_{11} is divided into two resonances and are located at both sides. Wide bandwidth could still be achieved even with cascaded Wilkinson dividers. More over, the return loss of cascaded network becomes more smooth along bandwidth compare to single divider, power division is also very stable in achieved band. To sum up, simulation indicates that Wilkinson power divider is a good choice of the corporate-fed network for antenna array.

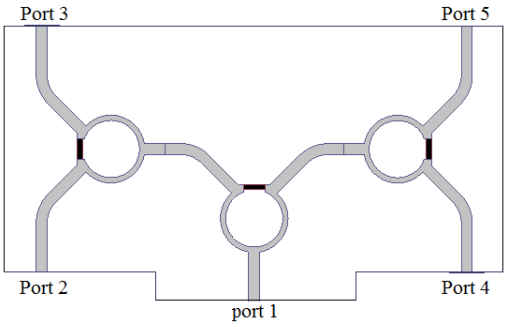

Figure 4.16: cascade Wilkinson divider

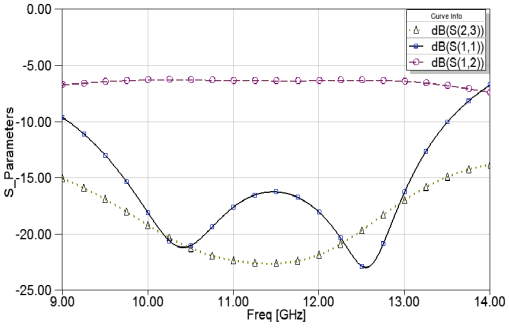

Figure 4.17: S parameters of cascaded Wilkinson divider

4x4 array feed network using cascaded Wilkinson dividers

Fig. 4.18 illustrates the circuit configuration of 4x4 cross-type antenna array feed network using Wilkinson power dividers. It can be seen that quantities of equant-division Wilkinson dividers are used in cascaded mode, and all the 16 ports in the same polarization (16 ports for horizontal polarization and another 16 ports for vertical polarization, only one polarization network is shown here) are connected in one network. Power from input port could be split into 16 ports with the same magnitude and in-phase, when the array works in emitting mode. While in receiving mode, Wilkinson components work as combiners, signals received by each antenna element will be combined and presented at the output port.

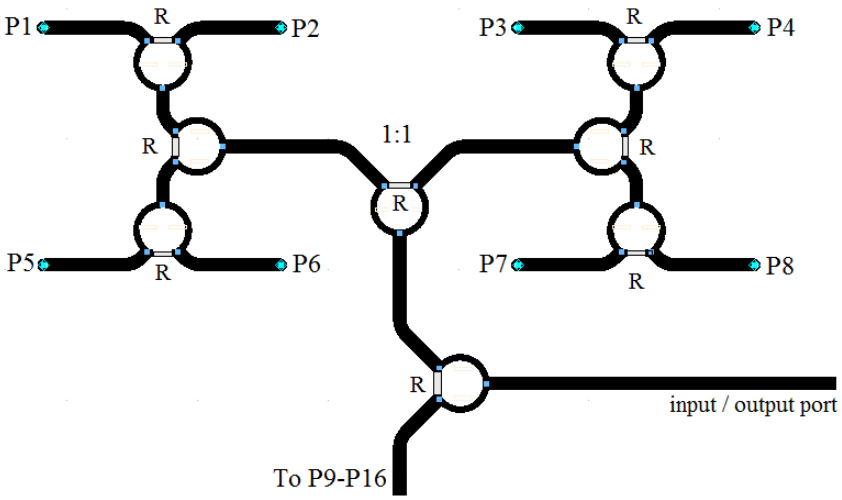

Figure 4.18: Half upper part of 4x4 array feeding network with wilkinson dividers

It is worth noting that, all the feed lines and impedance converters in the proposed Wilkinson network (Fig.4.18) are designed with strip line technology. Strip line is a kind of transmission lines like microstrip line, while the conductor is sandwiched by dielectric between a pair of ground planes. Comparing to microstrip line, strip line has less losses and thinner line width and it is also a non-dispersive line.

Transmission line radiation could also be limited by top and bottom ground planes. More over, strip line format affords more isolation between adjacent traces[105, 106].

4.2.4 Results and discussion

The proposed cross-type 4x4 antenna array fed by cascaded Wilkinson power divider network shown in Fig.4.18 has been realized. Similar with proposed feed network composed of T-junction dividers, the Wilkinson feed board is still placed at the bottom of antenna board and numerous of probes are used to connect antenna ports and feed network terminals. In addition, to maintain good isolation between terminals of Wilkinson dividers, surface mounted metal-film resistors (light-colored rectangle) are connected at output arms of each divider. The resistance R of each resistor here is 100 ohm.

Measurements are then carried out. Fig.4.19 gives the measured return loss of proposed antenna array fed with Wilkinson feed network. Very wide $S_{11} \leq -10dB$ impedance bandwidth could be observed in this figure, which ranges from 10.2GHz - 13.3GHz. Especially at around 10.8GHz, the measured S_{11} is found lower than -31dB which indicates very less power is reflected back to the main input port. The achieved band covers the band (10.7 - 12.7GHz) which satisfies the requirement of receiving all the DBS satellites signals.

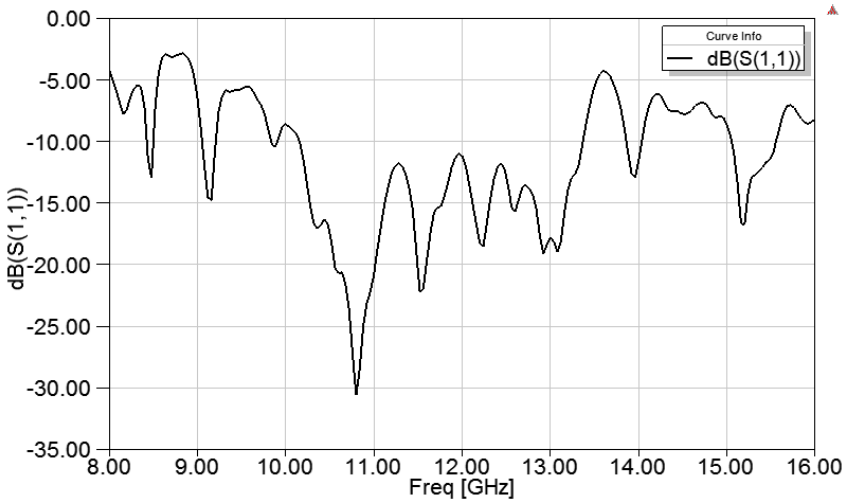

Figure 4.19: Measured return loss of 4x4 array fed by multilayer Wilkinson network

Measured radiation patterns of proposed 4x4 cross-type antenna array fed with Wilkinson network are shown in Fig.4.20. Obviously it can be seen the broadside main beams which are much higher than the other lobes. Sidelobe level is obtained 13 dB at both measured frequency. Cross-polarization can be observed 15dB lower than co-polarization at 11.04GHz and 18dB at 11.6GHz.

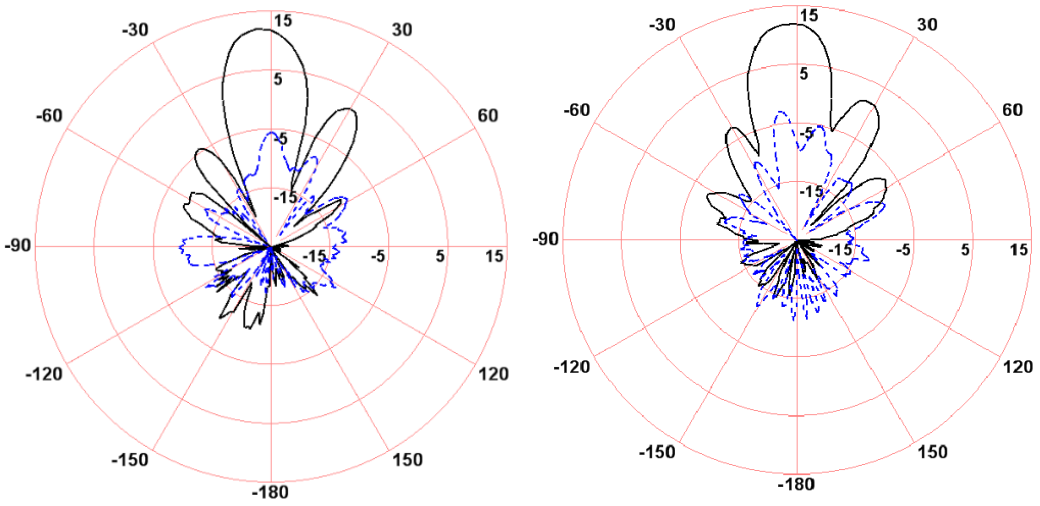

Freq = 11.04 GHz Freq = 11.6 GHz

Figure 4.20: Measured radiation patterns of 4x4 array (solid: co-polarization, dashed: cross-polarization)

As strip line technology is used in the Wilkinson divider constituted feed network, RF power is effectively limited between the pair of ground planes, thus the back radiation could be significantly decreased. The Front-to-Back Ratio (FBR) in Fig.4.20 is therefore found much higher than that of the array fed with microstrip network shown in Fig.4.6 and Fig.4.7.

4.2.5 Conclusion

In this section, cross-type antenna element is arranged into a planar array using 2-D patch sharing technique. Shared patches are able to serve adjacent elements and contribute to the entire impedance bandwidth of array. In such a 2-D array, the inter-element distance is limited to only $0.7\lambda_0$ which is even lower than the profile of single cross-type antenna. An experimental 4x4 array is designed and two kinds of network are introduced to feed the proposed array, which are the T-junction divider constituted feed network using microstrip line technology and the Wilkinson divider constituted feed network using strip line technology. Measured results indicates that T-junction divider constituted feed network suffers limited bandwidth and very high back radiation, while using Wilkinson divider constituted strip line network the required wideband is achieved and relatively high FBR is also obtained. Till now, we have successfully achieved a kind of array which provides sufficient bandwidth and which could be enlarged in infinite plane to obtain high gain. More over, this kind of antenna has flat structure with thickness only 3.2mm.

As mentioned before that dual-polarization is a necessary requirement, the proposed cross-type antenna array has also dual-polarization behavior. However, the

feed networks introduced in this section can only excite one of the two polarizations at the same time. In addition, resistors mounted on Wilkinson dividers have a thickness that insert air gaps when we tried to realize the strip line structure, which increase fabricating complexity and unstable factors to such feed network. In the next section, the multilayer structure with thin film resistor technology will be adopted to solve these problems.

4.3 Multilayer conception with thin film resistor technology

Cross-type antenna array feed networks proposed in the last section are not able to excite both polarizations at the same time when antenna elements are arranged in 2-D array. The two parallel feed networks will surely have quantities of intersections if designed on the same layer. With strip line technology, feed network is protected by a pair of ground planes, which provides us ideas of using stacked strip line to design the dual-polarization feed network. However, this method increases fabrication complexity, lumped elements are also difficult to place in such conception.

In this section, we would like to introduce a very up-to-date multilayer PCB technology with thin film resistor electroplating technique, which is able to realize stacked strip line feed network with good isolation and very thin resistor on each Wilkinson divider without soldering. Dual-polarization behavior of cross-type antenna array is thus easily obtained.

4.3.1 Geometry of multilayer PCB technology

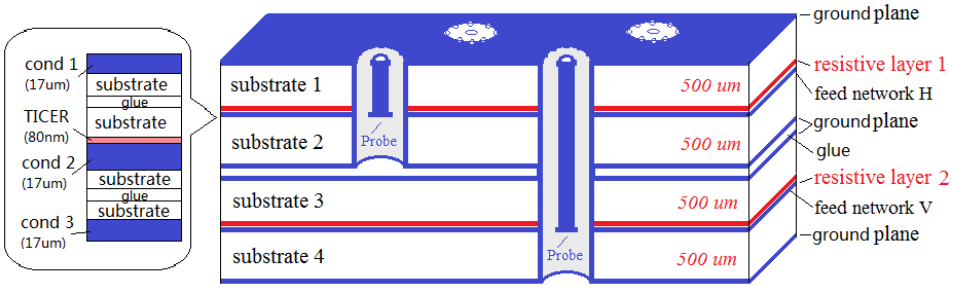

Figure 4.21: Topology of Multilayer PCB technique

Fig.4.21 illustrates the configuration of proposed multilayer PCB technology. It can be seen 6 conductive layers in this structure, which are separated by 4 dielectrics with thickness 500um. The top three conductive layers construct the horizontal strip line feed board, in which the Wilkinson dividers are distributed on the central

layer. A resistive film is tightly electroplated on the central conductive layer. Very thin resistors (80nm) are realized between the two output arms of each Wilkinson divider. The resistance is determined by the length (L) and width (W) of resistive film, as the following equation depicts,

$$R = R_0 * \frac{L}{W} \ (ohm) \tag{4.3}$$

Where R_0 is the resistance square equal to 25 Ω according to TICER PCB technology. As 100 ohm resistors are required, we just need to maintain the length to width ratio equal to 4 in this design.

In this structure, metallic Via holes act as probes are used to connect feed network and antenna elements, which has decreased the fabrication complexity. Such via holes are also used to connect strip line feed network to the main input and output port on one of the two ground planes.

Similar with horizontal feed network, the vertical feed network is placed on the fifth conductive layer while the fourth and sixth layer act as ground planes. Vertical feed board is located below the horizontal board, long via holes are used to connect the network to antenna element vertical ports. These probes are virtualized as coaxial cables where numerous small via holes act as the outer conductors and probes act as inner conductors, as shown in Fig.4.22. With this kind of structure, the two feed network will not impact on each other even if probes passed by one of the feed boards. Isolation between dual polarizations is expected to be enhanced.

4.3.2 Results and discussion

Fig. 4.23 gives the measured results of isolation between horizontal polarization port and vertical polarization port of cross-type antenna 4x4 array using proposed multilayer feed network. Very good isolation can be found in this figure when working frequency is lower than 11.7GHz (solid curve with circular flags), where transmission coefficient from port 1 (horizontal port) to port 2 (vertical port) is lower than -30dB. As frequency goes higher, S_{21} increases rapidly but in our required band from 10.7GHz to 12.7GHz, the isolation is always lower than -20dB. Comparing to single cross-type antenna, whose isolation is found as high as -16dB along working band, we can say that the method of using multilayer PCB technology is able to optimize significantly the ports isolation of cross-type antenna array.

4.3.3 Summary

In this section, cross-type antenna array dual-polarization feed network realized with multilayer PCB technology and electroplating thin film resistor technique

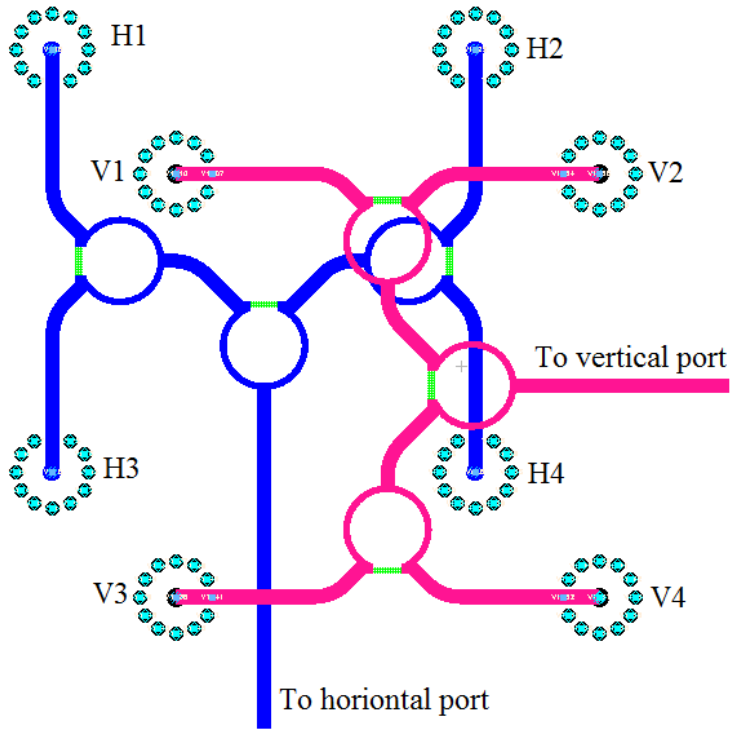

Figure 4.22: Feeding network with Wilkinson dividers for 4x4 array

is introduced. The given geometry and measured results indicate that, with such structure, not only fabricating complexity could be decreased, but also polarization isolation could be enhanced.

4.4 Conclusion

In this chapter, cross-type antenna has firstly been arranged linearly in a 1-D array and then extended to 2-D array with planar arrangement. Patch sharing technique is used in the two kinds of arrays, inter-element distance has been successfully decreased from $0.94\lambda_0$ to only $0.7\lambda_0$. Accompanying feed networks for 1-D array and 2-D array are also introduced. The feed network consists of T-junction dividers is found not able to provide sufficient impedance bandwidth therefore an optimized feed network consists of Wilkinson dividers is then introduced. With such a feed network, the cross-type antenna array operates well in the required band, very good resonating could be observed from the measured results. To obtain dual-polarization performance, a very up-to-date multilayer PCB technology with thin resistive film layer has been adopted to design the feed network of proposed antenna array. Isolation enhancement is obtained. More over, the cross-type antenna array with multilayer feed network has strictly flat structure whose entire thickness is only 3.6mm. Till now, we have successfully achieved a flat antenna which operates in the band covers 10.7GHz to 12.7GHz with horizontal polarization and vertical polarization.

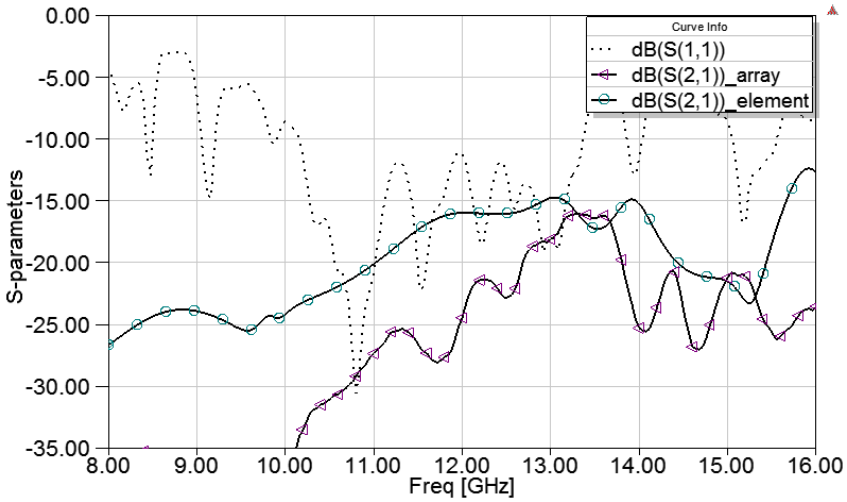

Figure 4.23: Comparison of Isolation between 4x4 array and single element

This kind of antenna can be enlarged by increasing the number of elements in infinite plane, 29dBi gain is expected to obtain.

As proposed previously, in our project, the required antenna is expected to search and focus on satellite automatically, its main beam should be steerable in sufficient angles. In the next chapter, we would like to look forward introducing a phased array based on the proposed cross-type antenna array, whose main beam shift performance will be presented.

5

Cross-type antenna array beam adjustment

In the last chapter, the cross-type antenna arrays and corresponding feed networks are introduced. Using patch sharing technique, antenna array can not only be arranged in line but also in infinite plane with the inter-element distance of only $0.7\lambda_0$. Furthermore, as shown in previous chapter, the proposed cross-type antenna array has achieved sufficient bandwidth which covers the desired band. With enhanced multilayer PCB technology with thin resistive film layer, horizontal feed network and vertical feed network are able to be realized in the same structure with good isolation, thus dual-polarization performance is also obtained for cross-type antenna array. However, to realize required beam steerable performance, more studies should be carried out.

In this chapter, we would like to firstly briefly introduce the theory of phased array in the first section. And then in the second section, the methods of realizing fixed beam shift on experimental cross-type antenna arrays will be presented. For the reason of decreasing side radiation of experimental array, the beam gathering technique is then introduced in the third section. In section IV, two kinds of voltage-controlled phase shifters will be presented and the topology of beam electronically steerable cross-type array will be given.

5.1 Phased array theory

To realize a main beam steerable antenna, we would like to start with the theory of phased array antenna.

Fig.5.1 illustrates the topology of a 1-D arranged array, which consists of N element with constant inter-element distance d. In the far field, considering an incident wave along the direction θ with respect to Z-axis, it can be inferred from Fig.5.1 that this wave is delayed on each element due to the geometrical element distribution. The phase difference ψ of adjacent elements is then expressed according to:

$$\psi = kdsin\theta \tag{5.1}$$

where $k = 2\pi/\lambda_0$ is the wave number in the medium where the field is propagating. In the case of phased array antenna, the phase difference between k and k-1 elements is then modified by introducing an electrical delay ϕ

$$\Delta\psi = \psi_{k-1} - \psi_k = kdsin\theta + \phi \tag{5.2}$$

where ϕ is the electrical phase difference of element k compared to element k-1. If we consider a homogeneous array consisted in equi-space element, it is then possible to fully synchronize the incident wave from θ direction by setting the electrical delay $\phi = -kdsin\theta$.

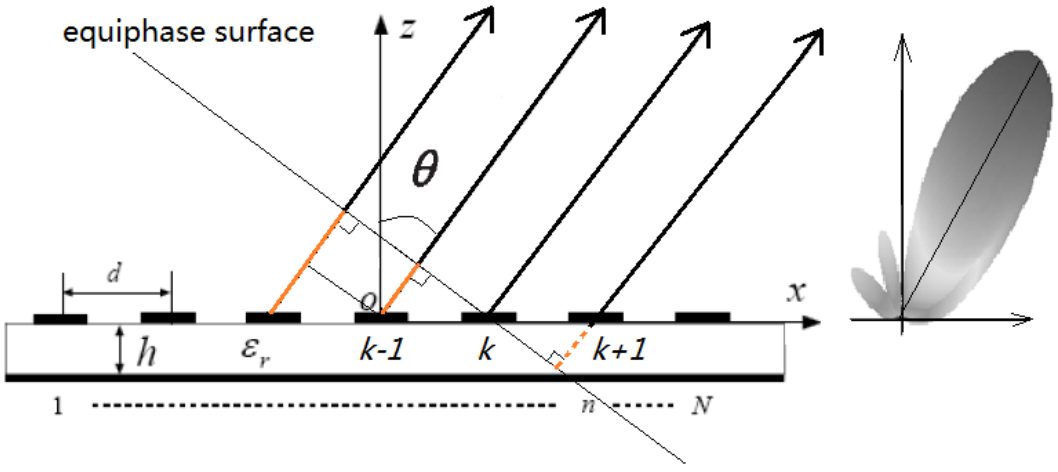

Figure 5.1: Phased array theory

Generally, the electrical phase delay ϕ in phased array is achieved by inserting phase shifting which cancels out the electrical phase difference ψ between adjacent elements. In this case, all the elements in phased array could be assumed to be located on the equiphase surface which slants at a angle of θ respect to antenna array surface, as depicted in Fig.5.1. In this manner, incident signal from θ direction could be received by each element in the array and combined in-phase. In other words, we

can say that the main beam of antenna is steered θ degrees respect to the broadside direction.

To achieve a beam steerable array and to study its beam steering ability, we propose a method of inserting fixed phase shifting in experimental antenna arrays. In the coming sections, the previously proposed 1-D and 2-D arranged cross-type antenna array with fixed phase shifted network will be introduced. Their beam steering behaviors will be studied and discussed.

5.2 Cross-type antenna phased array

In this section, the proposed 1x4 and 4x4 cross-type antenna arrays will be fed with fixed phase difference networks, in order to find their beam steering abilities. The fixed phase difference feed network can be directly printed on substrate, therefore no additional costs is needed comparing to in-phase feed network.

5.2.1 1x4 linear cross-type antenna phased array

The cross-type 1x4 linear array has already been introduced in chapter 4, which is composed of 4 dual-polarized elements and the inter-element spacing is obtained $0.7\lambda_0$ using patch sharing technique. An in-phase and balanced power division network has been applied to feed this array, as shown in Fig.4.4. In such a network, horizontal ports and vertical ports are fed separately. Each sub-ports in their network gets RF power in the same magnitude as balanced T-type power dividers are used. Several quarter-wavelength microstrip lines are applied between Z_a (Impedance of terminals, as also shown in Fig.5.2) and T-type dividers for impedance matching in a narrow band. To minimize the limitation to bandwidth of quarter-wavelength microstrip lines, tapered lines are therefore used to continuously convert impedance from Z_p to Z_0 along wideband.

To realize a beam switchable array, elements in the array should theoretically be fed with equal-difference phase shifts. A simple way to have such phase difference is to control the length of feed line, which its electrical length is expressed as below:

$$\theta = \beta l \tag{5.3}$$

where l is the length of microstrip feed line, and β is its associated propagation constant which is expressed as:

$$\beta = \frac{2\pi}{\lambda_g} \tag{5.4}$$

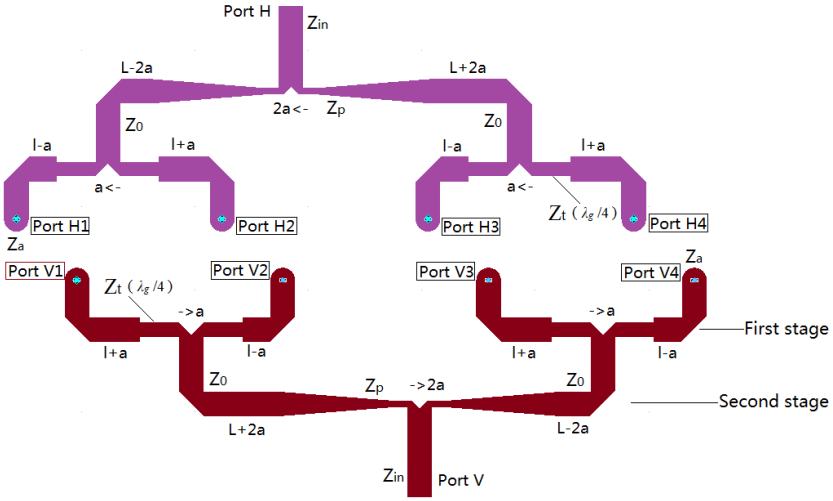

Figure 5.2: 1x4 Phased array with fixed phase difference

The Guided wavelength λ_g is known as:

$$\lambda_g = \frac{c}{f\sqrt{\varepsilon_{eff}}} \tag{5.5}$$

ε_{eff} is the effective permittivity of the waveguide line in the TEM and quasi-TEM mode approximation. Taking the central frequency of our required band f=11.7GHz into Equ.5.5, the guided wavelength is achieved about 17.56mm according to material properties and configuration.

It can be inferred from Equ.5.3 that phase varies directly as length of microstrip line changes, with operating frequency being constant. It is possible to obtain phase differences by controlling the feed line length between adjacent element in array. According to this theory, a simple phase-shifting network is thus designed, as shown in Fig. 5.2. Such a feed network is able to supply an equal-different phase shift to each element in the 1x4 array. Taking the horizontal feeding network as an example, the first stage T-dividers shift a length of a(in mm), the adjacent ports in the array should have a feed line length difference of 2a and phase shift of $\theta_1 = 2a * 2\pi/\lambda_g$. The second stage T-divider shifts a length of 2a and phase shift of $\theta_2 = 4a * 2\pi/\lambda_g$. Therefore in this 1x4 array, phase distribution could be expressed as in Tab.5.1. It can be seen that, both in horizontal and vertical feed network, elements in the array have the same equi-phase shifting of $2a * 2\pi/\lambda_g$.

This feed network has been realized and measured in our laboratory with the proposed linearly arranged cross-type 1x4 array. Very good resonance could be observed on the measured S-parameters as shown in Fig. 5.3. About 27% relative bandwidth on port H and more than 34% on port V are observed. The inter-port isolation is always higher than 18dB along our required band. Comparing to the measured results of in-phase feed network, it can be seen that the phase shifting

Table 5.1: Phase distribution of 1x4 array.

Horizontal ports		Vertical ports	
Port H1	θ	Port V1	$\theta + 6a * 2\pi/\lambda_g$
Port H2	$\theta + 2a * 2\pi/\lambda_g$	Port V2	$\theta + 4a * 2\pi/\lambda_g$
Port H3	$\theta + 4a * 2\pi/\lambda_g$	Port V3	$\theta + 2a * 2\pi/\lambda_g$
Port H4	$\theta + 6a * 2\pi/\lambda_g$	Port V4	θ

in such a network does not disturb antenna resonance too much, in contract, the resonances become better.

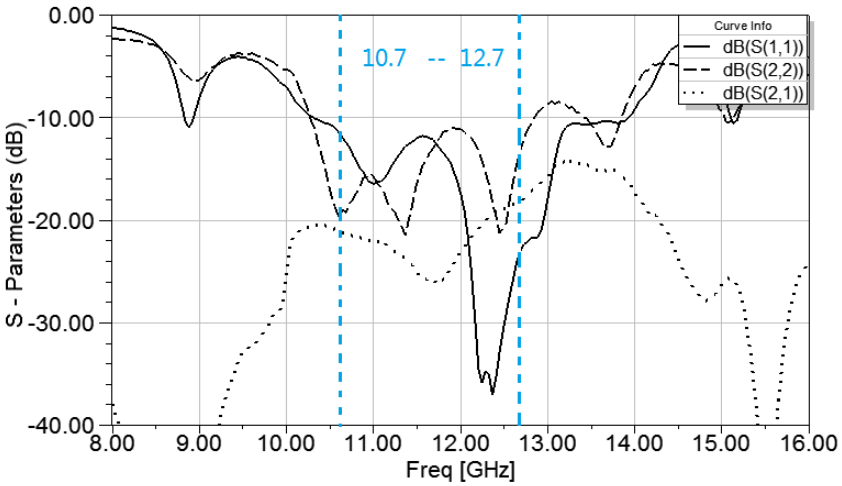

Measured S parameters of 1x4 in-phase array

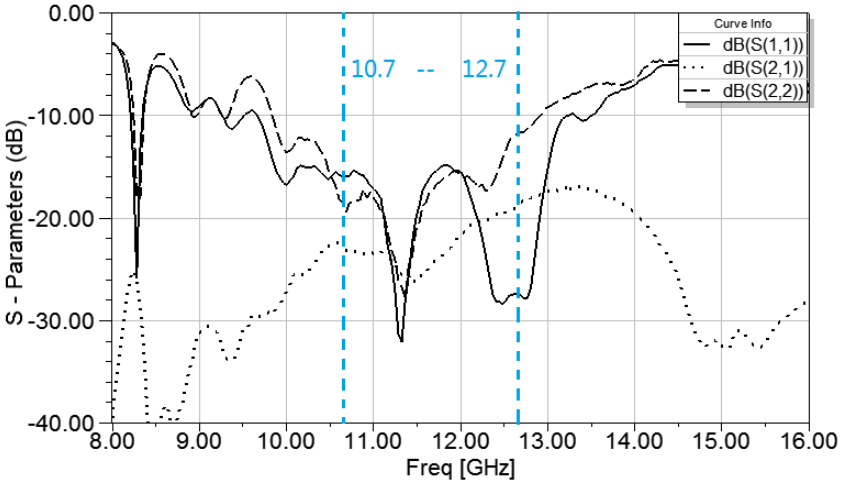

Measured S parameters of 1x4 phased array

Figure 5.3: Comparison of measured S-parameters of 1x4 in-phase array and 1x4 phased array

Radiation characteristic of 1x4 phased array fed by equal-phase shift network is measured in the anechoic chamber and the results compared with in-phase 1x4

array are illustrated in Fig.5.4 and Fig.5.5. Very good radiation performances could be observed both at H-port and V-port, the main beams are found at the broadside direction and are obviously higher than other lobes. More over, beam shifting can be observed at each pattern, about 5° beam shifting can be found at vertical port both in 10.56GHz and 11.68GHz, and more than 15° beam shifting can be found at horizontal port. Quite different beam shifting abilities are obtained at the two polarizations of experimental antenna array. This result seems quite weird as equal phase differences are applied on its dual feed networks.

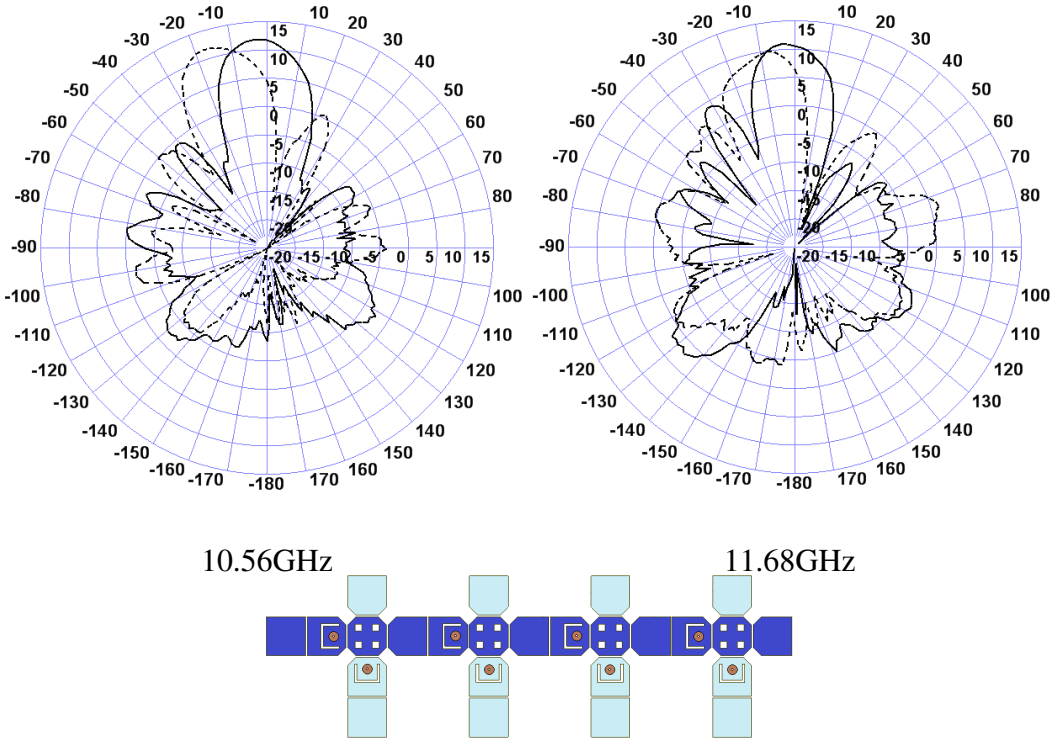

Figure 5.4: Measured radiation patterns at Horizontal port. (Solid: in-phase, dashed: phase shift)

An explanation of this is, the 1x4 antenna array does not present the same topology in vertical polarization,. comparing with horizontal polarization topology presented at the bottom of Fig.5.4, the vertical polarization (shown at the bottom of Fig.5.5) is consisted of four antenna elements which are located individually, the inter-element distance is $0.7\lambda_0$ without any shared patch. Although the horizontal polarization is consisted with the same number of antenna elements and with the same inter-element distance, but some patches are shared by two adjacent elements, phase shifting between two elements might be subdivided and becomes more contiguous and smooth. According to measured radiation patterns, we can say that, beam shifting angle could be enlarged with patch sharing technique in antenna array. To prove this, we propose to realize a two dimensional 4x4 array, which is the main purpose of the next section.

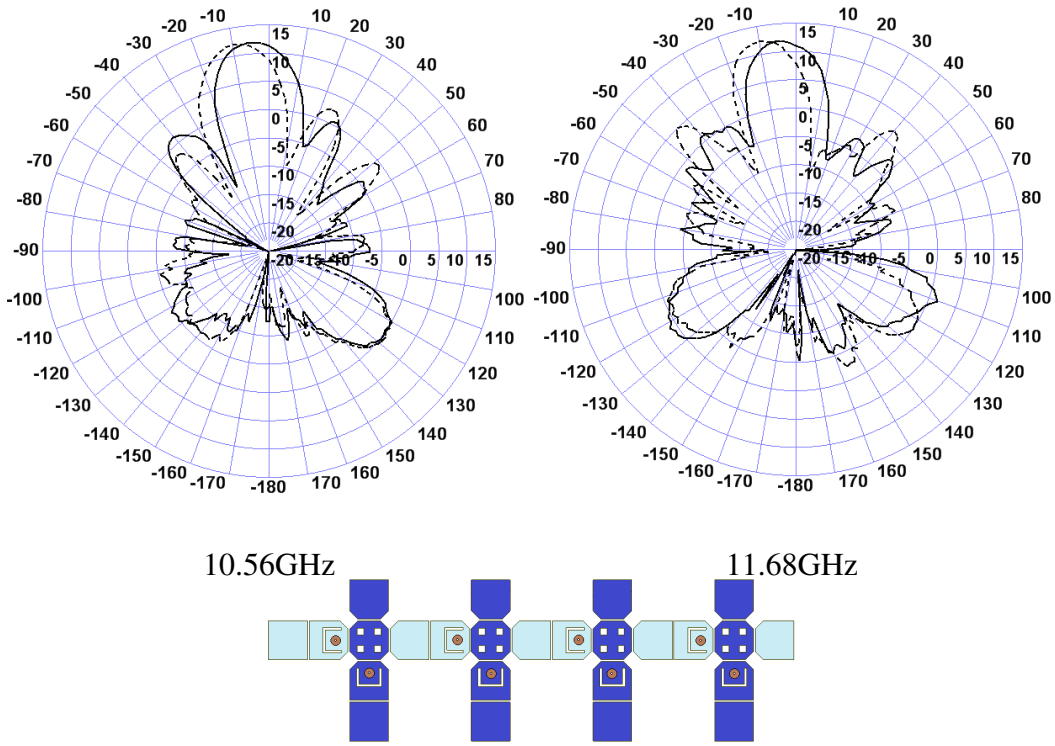

Figure 5.5: Measured radiation patterns at Vertical port. (Solid: in-phase, dashed: phase shift)

5.2.2 4x4 planar cross-type antenna phased array

In the last section, beam steering has been obtained on 1x4 cross-type antenna array when a fixed phase shifting is applied in the feed networks. About 15° beam shift on horizontal polarization is observed, which is much more than that on vertical port cause patch sharing technique is used. In this manner, we can extend this method to the 4x4 cross-type antenna array, in which patch sharing technique has been used both on horizontal polarization and vertical polarization. Big beam steering angle is expected to obtain on the two ports with quite the same behaviors.

In this section, we would like to focus on single plane (either xoz plane or yoz plane) beam steering performance to simplify the feed network conception, even if 2-D arranged array is used.

Fig.5.6 illustrates a fixed equal-different phase shifting network for 4x4 phased array cross-type antenna, which is based on the original in-phase feed network as shown in Fig.4.18. In this feed network, the locations of Wilkinson dividers are shifted a (mm) to $-x$ direction, therefore adjacent horizontal ports have a fixed phase difference of $2a * 2\pi/\lambda_g$, and beam shifting in xoz plane is expected. In each column, antenna elements are in phase, thus no beam shifting in yoz plane. This kind of feed network has been fabricated and used to feed the dual polarizations of cross-type antenna 4x4 array, measured radiation patterns are shown in Fig.5.7. As

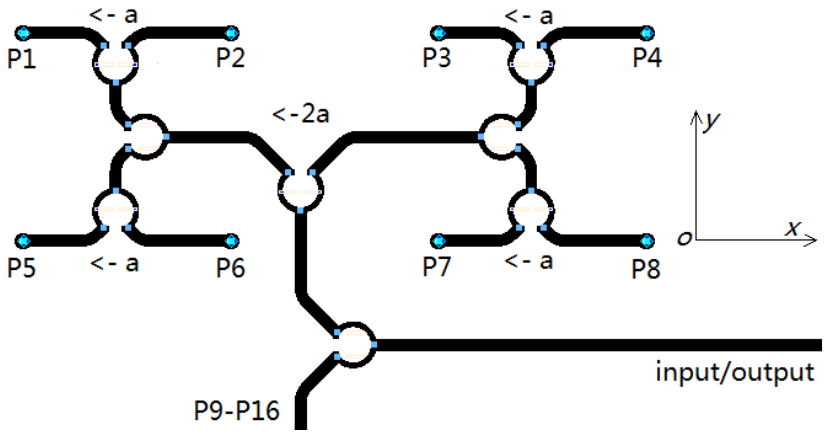

Figure 5.6: Fixed phase shift network (half upper part)

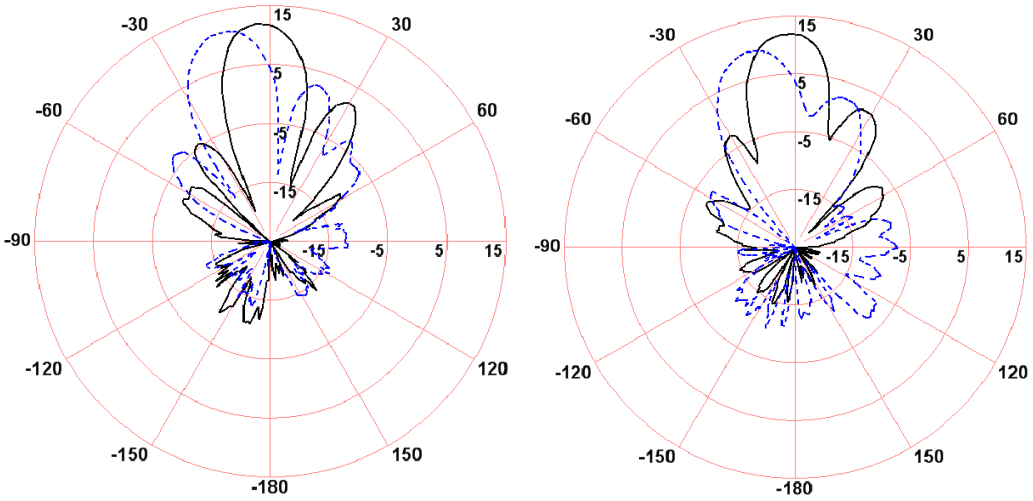

Freq = 11.04 GHz Freq = 11.6 GHz

Figure 5.7: Beam steering with fixed phase shift (Solid: in-phase, dashed: phase shift)

the two polarization are totally symmetric, their radiation performances are almost the same, so here we give only the radiation patterns of vertical polarization.

From Fig.5.7, it can be seen obviously beam shifting in the measured radiation patterns. The dashed curves indicate the radiation of 4x4 cross-type antenna array when the proposed fixed phase shifting network is used, while the solid one corresponds to the in-phase case. The main beams are steered more than 15° with respect to the normal direction at both measured frequencies. Comparing to the beam shifting angle of vertical polarization of 1x4 phased array which is only about 5°, improvement is obviously seen as patch sharing technique has been carried out in this polarization. These results are consistent with those observed with the previous 1x4 array.

5.2.3 Conclusion

For the application of reception of Ku-band satellite direct broadcast, a dual-polarized and beam switchable patch antenna array is studied and introduced in this section. The proposed array is formed with cross-type antenna unit cell and fed by a phase variable power division network. By tuning the length of paths in the feeding network, equal-different phase shift takes place among units. Therefore beam-shifting could be obviously observed on the measured radiation patterns, which indicates that the main beam of the proposed array is switchable as expected. It is worth while noting that, as patch sharing technique is used in the array arrangement, not only the inter-element distance is significantly decreased but also the beam-shifting angle is distinctly enlarged in the case of same phase-shifting.

However, with such fixed phase shifting network, the main beam can only be switched from broadside direction to a fixed angle. A beam continuously steerable phased array is expected. In the coming section, we would like to introduce such arrays integrated with voltage-controlled phase shifters which are able to supply continuous phase shifting.

5.3 Beam continuously steerable array

Although beam shifting has been obtained for cross-type antenna array by realizing fixed equal-different phase in the feed network, but the beam shifting angle is not continuously steerable. To solve this problem, we have to use some kinds of electrically-tunable phase shifters.

A lot of microwave companies provide commercial phase shifters which satisfy the requirement of applying continuously voltage-controlled phase differences [107, 108]. However, these phase shifters are extremely costly, which are not suitable to be used in our cost-sensitive antenna. We would like to find cheap ways to obtain phase shifting.

In this section, two kinds of phase shifters constituted of microwave circuit and varactor diode will be introduced, no exceptional cost is needed using PCB technology. The circuit geometries of cross-type antenna array integrated with such phase shifters will be presented.

5.3.1 Voltage-controlled phase shifters

Taichiro et al. have introduced us a simple structure Ku-band directional phase shifter in [109], which consists of a $\pi/2$ hybrid circuit and two varactor diodes, as depicted in Fig.5.8 (a). A thin branch line (150ohm) connected to the main transmission line is used to provide bias DC voltage for varactor diodes and decouple

DC supply and microwave circuit. This kind of phase shifter has been simulated in HFSS and its prototype has been optimized according to our working band, results are presented in Fig.5.8 (b). In (b) it can be seen that the simulated reflection coefficient is always lower than -10dB along our required band (10.7-12.7GHz). However the transmission coefficient raises slowly at the lower band until the central frequency and decreases rapidly as frequency goes higher. About 10dB loss is observed at around 12.3GHz, which indicates that this kind of phase shifter has high insertion loss.

By adjusting the bias voltage from 0 volt to 20 volts, the capacitance of varactor diodes in this phase shifter could be continuously tuned (normally, the capacitance decreases as voltage increases.), thus phase difference happens between port 1 and port 2. About 56° phase shift is reported by Taichiro, as referred from Fig. 5.8 (c).

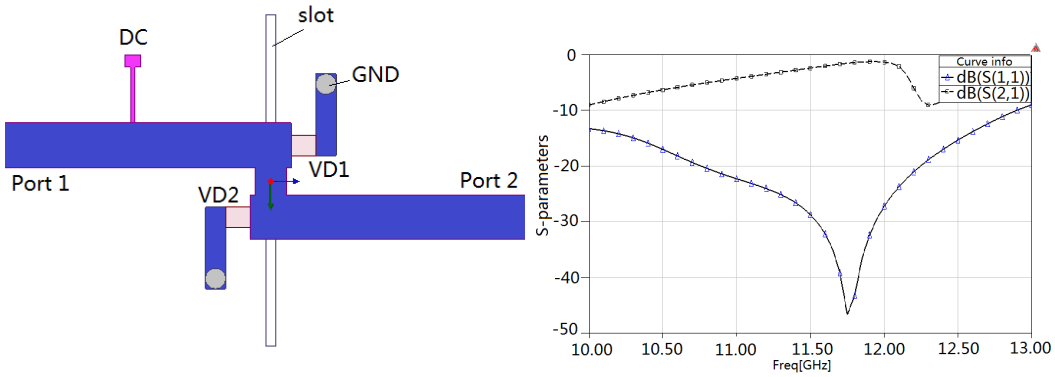

(a)Geometry (b)Simulated S-parameters

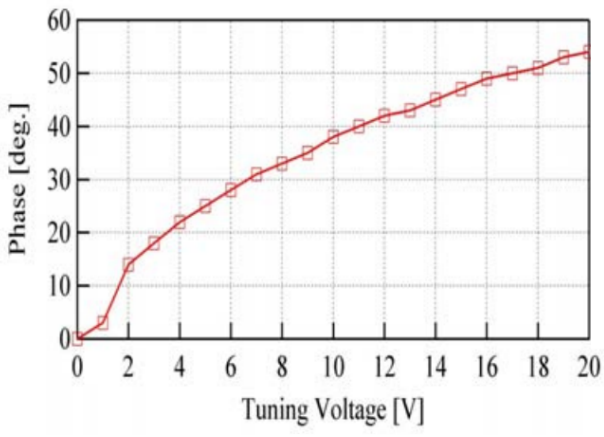

(c)Phase shifting [109]

Figure 5.8: Proposed directional phase shifter

Even though the directional phase shifter is simple in structure and easy in fabrication, but its insertion loss remains very high, moreover, the achieved phase shifting can not provide sufficient phase difference for our antenna array.

In [110], the 90° branch-line coupler based phase shifters is introduced. Varactor

diode is also used as active element to tuning phase shifting by adjusting the input DC voltage. The geometry of basic branch-line phase shifter is shown in Fig.5.9(a). 109° phase shifting with an insertion loss of 1.8 ± 0.3dB was obtained in Ku-band by Chang-Lee et al. in [110] with only one varactor diode in each tuning arm. And 180° phase shifting is reported in [13].

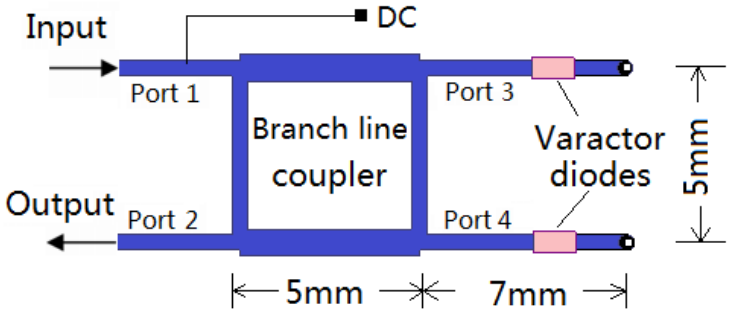

(a)Geometry

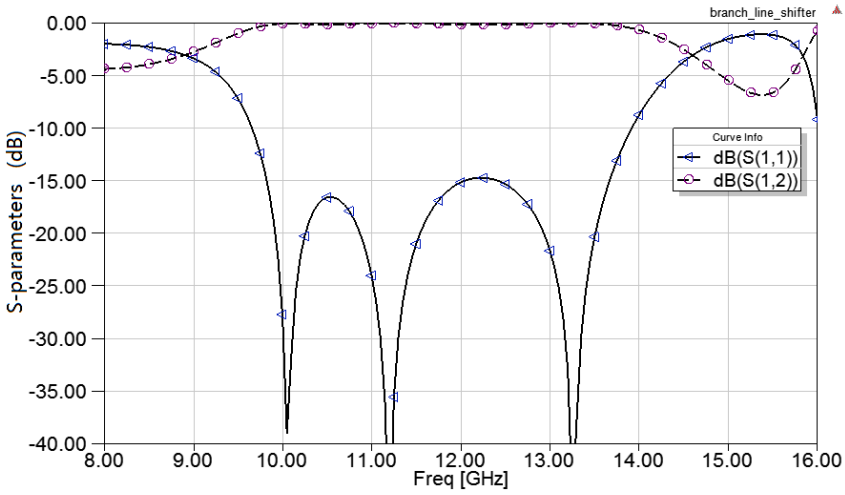

(b)simulated S-parameters of branch-line phase shifter

Figure 5.9: Basic Branch-line phase shifter

This basic branch-line phase shifter is simulated and the S-parameters are shown in Fig.5.9 (b). Very wide operating band can be observed in this figure which covers entirely our required band. Meanwhile, the transmission coefficient is very high along whole band which indicates very low insertion loss using branch-line phase shifter (about 0.5 dB).

In [13], Lambard et al. have optimized the branch-line phase shifter by using two parallel varactor diodes, both in series with a quarter wavelength line and a third varactor diode, as depicted in Fig.5.10 (a). More than 360° phase shifting between 11.5 and 12.5GHz has been obtained in (b), while at 12 GHz the $3.3 \pm 0.5dB$ insertion loss is reported in their work.

The proposed branch-line phase shifter with one or three varactor diodes are able to provide continuous phase shift by adjusting the input DC voltage, which

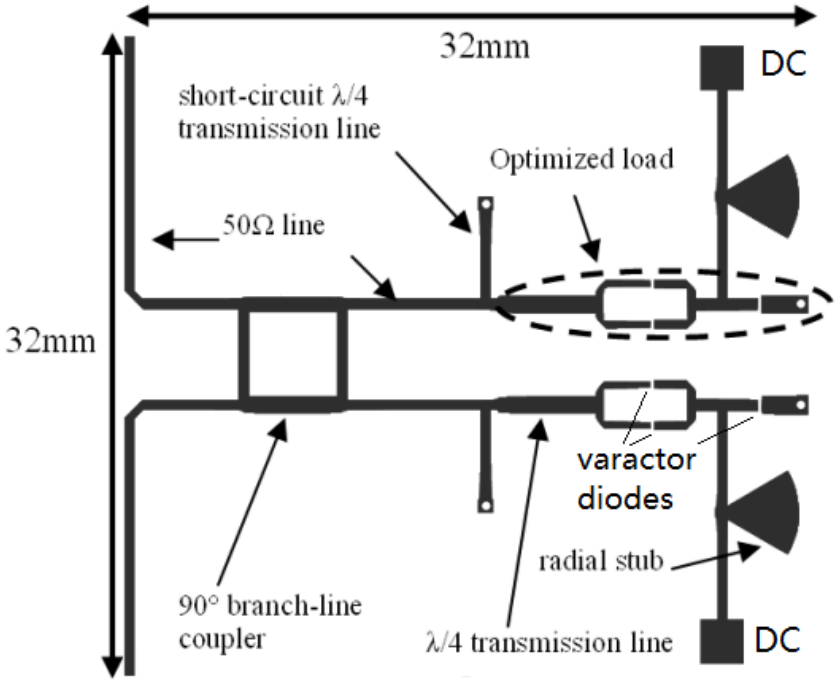

(a)Geometry

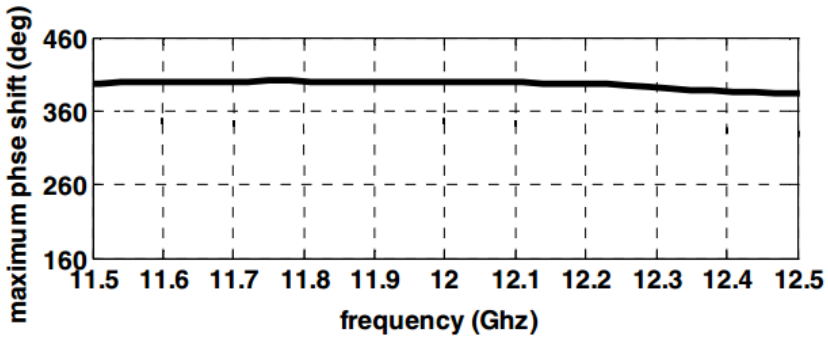

(b)Phase shifting angle

Figure 5.10: Proposed branch-line phase shifter [13]

provide us ideal options in designing the beam continuously steerable cross-type antenna array. Although the optimized branch-line phase shifter could provide more phase shifting, its size becomes much bigger than the basic one, which increases the complexity to integrate into our feed network. By considering 180° phase shifting is enough for our experimental 4x4 array, we decide to adopt the basic type branch-line phase shifter to realize the beam electrically steerable antenna array. In the next subsections, the geometry of the 4x4 cross-type antenna array integrated with the proposed phase shifter will be presented.

5.3.2 Beam electrically steerable array

The branch-line coupler and varactor diode based phase shifter is able to provide continuously 0° to 180° phase shifting while tuning the driving voltage on varactor

diode. This kind of phase shifter is thus adopted in the experimental 4x4 cross-type antenna array. Fig.5.11 gives the circuit geometry of 4x4 array feed network integrated with branch-line phase shifters. To avoid overlap displaying, only one polarization feed network is illustrated here, the other feed network is absolutely the same.

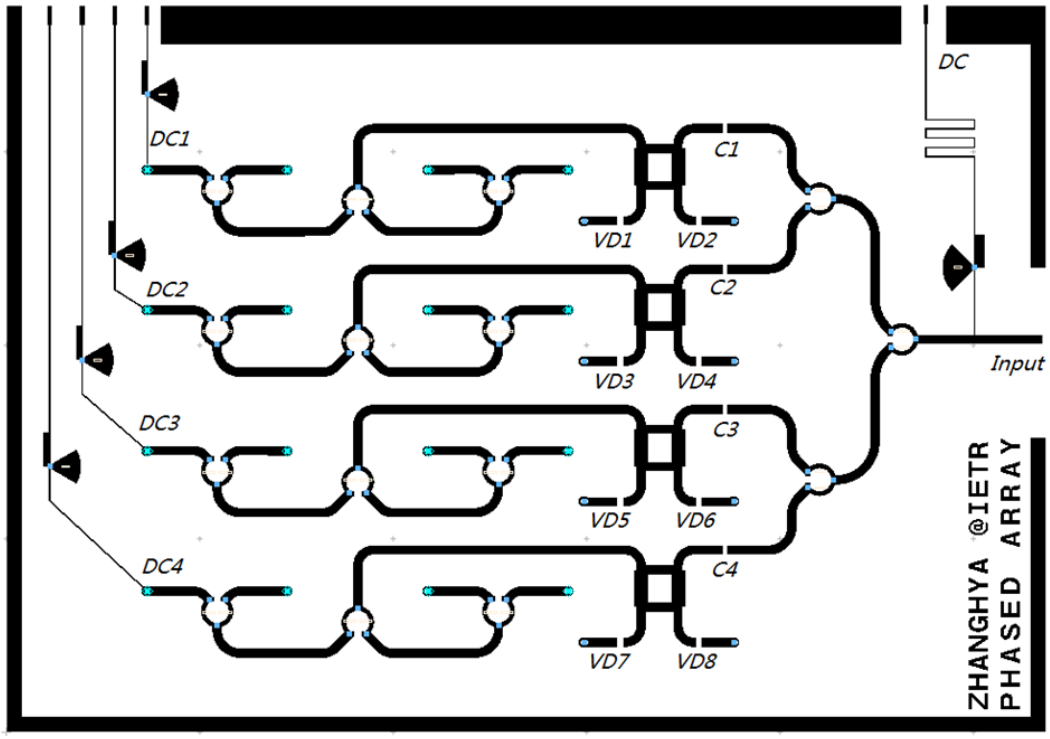

Figure 5.11: Geometry of 4x4 beam continuously steerable array

It can be seen in this feed network that every four antenna ports be connected in a branch and one branch-line phase shifter is used to adjusting the phase of each branch. As branch-line phase shifter provides continuous phase shifting by tuning the driving voltage, the 4x4 array is thus expected to obtain continuous beam shifting performance. In this circuit, C1-C4 are capacitors which are used to decouple input power with each branch. VD1-VD8 are varactor diodes and DC1-DC4 are adjustable DC suppliers for corresponding branch-line phase shifters.

With High-Performance Calculating (HPC) performance of HFSS, the entire structure of antenna array and feeding network are able to be simulated entirely with the software. (The method of configuring HPC function is detailedly introduced in Annex 3.) In Fig.5.12, the simulated radiation patterns of 4x4 array with proposed phase shifting network are presented. It can be obviously seen beam shifting in the figure. The main beam at the broad side direction is able to be shifted while phase differences taking place in this feed network. When 100° phase difference is added in the feed network, the beam can be steered about 25° clockwise (negative phase shifting will lead to counter-clockwise steering). However the sidelobe level can be

seen increasing rapidly. A method to improve the sidelobe level is introduced in the next section

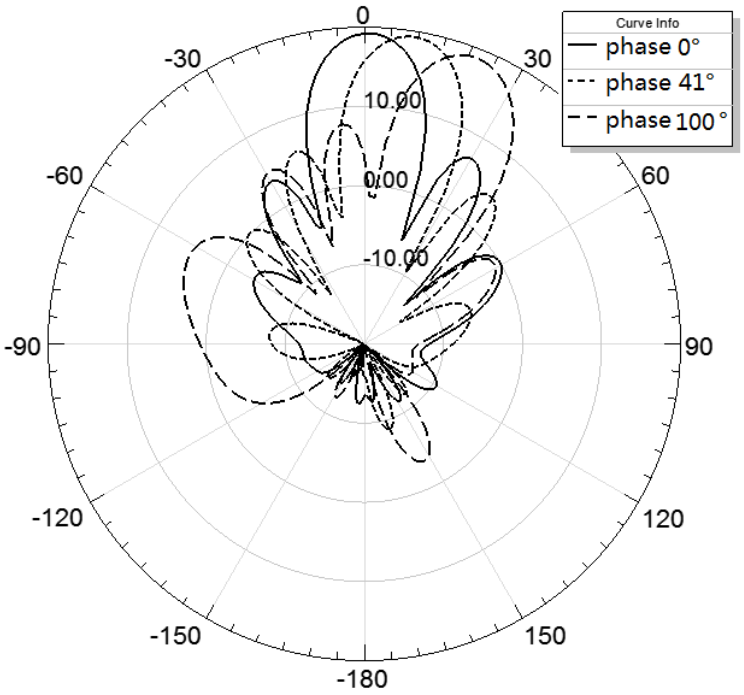

Figure 5.12: Beam shifting of 4x4 phased array

5.3.3 Conclusion

In this section, two kinds of voltage-controlled phase shifters have been introduced, which are able to provide continuous phase shifting when the driving voltage varies. With the integration of such kinds of phase shifters, the main beam of the proposed cross-type antenna array is electrically steerable, which enables cross-type antenna the abilities of searching and focusing on satellite with its main beam. However, it can be found relatively high sidelobe level when antenna array enlarges. In the next section, we would like to introduce a method to control antenna array sidelobe level by managing the power distribution.

On the other hand, in order to stably receive satellite signal, the gain of cross-type antenna array need to be increased to as high as 29 dBi. The most common way is to increase the number of antenna elements, as well as the number of phase shifters. In such a case, if each phase shifter has an independent power supply, the circuit geometry might be too complex and these power suppliers will be too difficult to adjust. To simplify the phase shifter management, a module based on microprocessor and digital-potentiometer to automatically manage the antenna beam is introduced detailedly in the fourth annex. Nevertheless, we have proved the efficiency of this kind of array for automatically steer the main beam of such an array.

5.4 Power gathered array

It can be seen from the measured radiation patterns of experimental 4x4 array (Fig.5.12) that the sidelobe level is relatively high, which is only about 13dB less with respect to the main beam. As mentioned previously, the 4x4 array adopts an equal-magnitude feed network, that is, all the antenna elements in this array receive power from the input port with the same level, radiation from elements around the array edge contribute much to the sidelobe level. To solve this problem, we would like to propose a new power distribution of antenna array. Antenna elements in the array center are assigned with more power than the ones around the edge, shown in Fig.5.13. It can be seen that the 16 elements in the array are distributed with three scales of power. The central 4 elements with deep color are assigned with power px. In the second scale, 8 elements are assigned with power $px * ratio$ ($ratio$ is a variable to manage power distribution). And at the outer scale, the 4 elements are assigned with power $px * ratio^2$. As the input power is 1, we have an equation as depicted below if taking no account of losses.

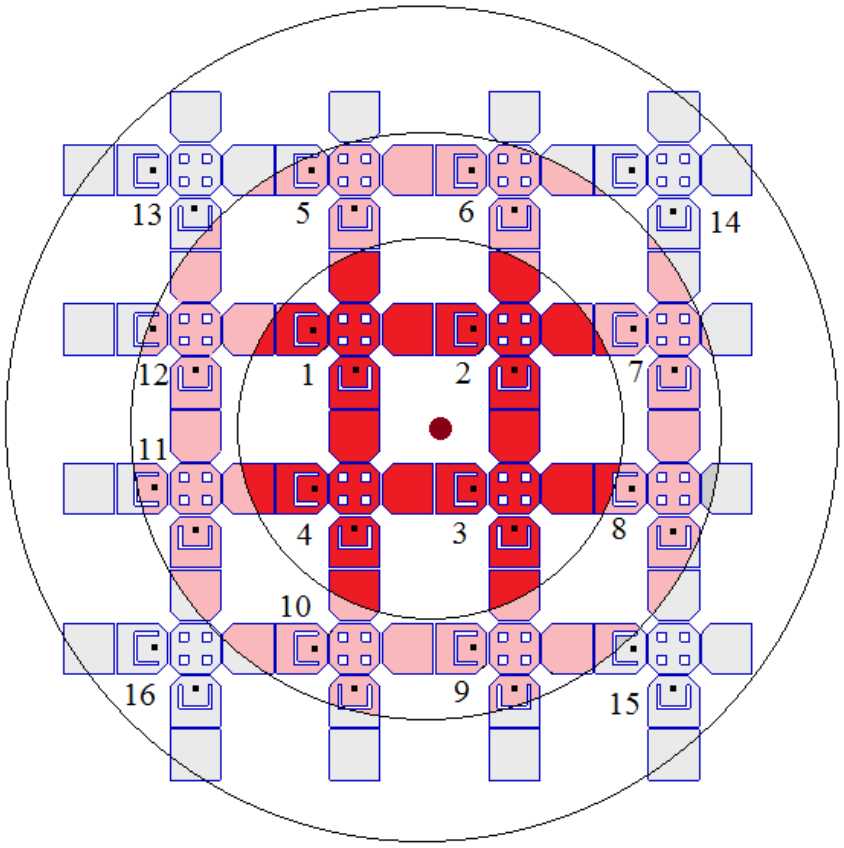

Figure 5.13: power distribution in a 4x4 array

$$4 * px + 8 * px * ratio + 4 * px * ratio^2 = 1 \tag{5.6}$$

yields:

$$px = \frac{1}{4(1+ratio)^2} \tag{5.7}$$

Where $0 < ratio \leq 1$, when $ratio = 1$, we will obtain the proposed equal-power distributed array. The variable $ratio$ enables us easily manage the power distribution in the simulation. On the other hand, we have a variable t_phase to manage the phase distribution of the array. To simplify the description, we have listed Table 5.2 and Table 5.3 to show the power and phase distribution of the two polarizations of experimental 4x4 array. With proposed High-Performance Calculating (HPC) of HFSS v15.0, the entire geometry of 4x4 array with two parameters to manage power and phase could be rapidly and effectively resolved.

Table 5.2: Power and Phase distribution of 4x4 array Horizontal polarization.

Port H13	Port H5	Port H6	Port H14
$Power = px * ratio^2$	$Power = px * ratio$	$Power = px * ratio$	$Power = px * ratio^2$
$Phase = t\_phase * 3$	$Phase = t\_phase * 3$	$Phase = t\_phase * 3$	$Phase = t\_phase * 3$
Port H12	Port H1	Port H2	Port H7
$Power = px * ratio$	$Power = px$	$Power = px$	$Power = px * ratio$
$Phase = t\_phase * 2$	$Phase = t\_phase * 2$	$Phase = t\_phase * 2$	$Phase = t\_phase * 2$
Port H11	Port H4	Port H3	Port H8
$Power = px * ratio$	$Power = px$	$Power = px$	$Power = px * ratio$
$Phase = t\_phase$	$Phase = t\_phase$	$Phase = t\_phase$	$Phase = t\_phase$
Port H16	Port H10	Port H9	Port H15
$Power = px * ratio^2$	$Power = px * ratio$	$Power = px * ratio$	$Power = px * ratio^2$
$Phase = 0$	$Phase = 0$	$Phase = 0$	$Phase = 0$

Fig.5.14 illustrates the simulated radiation pattern of proposed 4x4 array with power re-managed. Comparing to equal-power distributed array (dashed curve), the solid curve indicates very low sidelobe level which is as low as 25dB and about 12dB improved. However, the main beam becomes wider and it can be seen that the gain is decreased about 2dB. The method of power re-management sacrifices a little antenna gain for better sidelobe level. Fig.5.15 gives the simulated radiation pattern of antenna array when the parameter t_phase is set to 41° and $ratio = 0.25$. Obviously beam shifting can be seen from this figure, and compare to equal-power distributed array (dashed curve), the steered beam also indicates extremely low sidelobe level.

Table 5.3: Power and Phase distribution of 4x4 array Vertical polarization.

Port V13 $Power = px * ratio^2$ $Phase = t\_phase * 3$	Port V5 $Power = px * ratio$ $Phase = t\_phase * 2$	Port V6 $Power = px * ratio$ $Phase = t\_phase$	Port V14 $Power = px * ratio^2$ $Phase = 0$
Port V12 $Power = px * ratio$ $Phase = t\_phase * 3$	Port V1 $Power = px$ $Phase = t\_phase * 2$	Port V2 $Power = px$ $Phase = t\_phase$	Port V7 $Power = px * ratio$ $Phase = 0$
Port V11 $Power = px * ratio$ $Phase = t\_phase * 3$	Port V4 $Power = px$ $Phase = t\_phase * 2$	Port V3 $Power = px$ $Phase = t\_phase$	Port V8 $Power = px * ratio$ $Phase = 0$
Port V16 $Power = px * ratio^2$ $Phase = t_phase * 3$	Port V10 $Power = px * ratio$ $Phase = t\_phase * 2$	Port V9 $Power = px * ratio$ $Phase = t\_phase$	Port V15 $Power = px * ratio^2$ $Phase = 0$

Summary

In this section, the method of re-manage power distribution in cross-type antenna array is introduced. With this method, more power is assigned to the central elements and less power to the elements around edge. Simulated results indicate that obvious decreasing on sidelobe level could be observed. Even though the method of power re-management sacrifices a little gain to improve sidelobe level, the total gain of 4x4 antenna array is also as high as 18dBi and can be enlarged by utilizing more elements. To realize the method of power re-management, unbalanced Wilkinson power divider is the best candidate. The work of improving cross-type antenna array performances could be extended in this way in the future.

5.5 Conclusion

In this chapter, the theory of realizing cross-type antenna beam steering with equal-different phase shifting in the feed network is firstly introduced. To obtain such kind of phase difference in the feed network, feed line length is modified both in the experimental 1x4 array feed network and 4x4 feed network, obvious main beam steering have been observed. With this method, fixed phase shifting could be provided thus the beam can be simply steered to a fixed angle. Moreover, measured results indicated that the cross-type antenna array beam shifting angle can be increased by using patch sharing technique, which is another advantage of this technique excepting decreasing inter-element distance. Due to using voltage-controlled and varactor diode based phase shifters, the phase shifting in feed network could be continuously obtained. More over, as the micro-processor and digital potentiometer

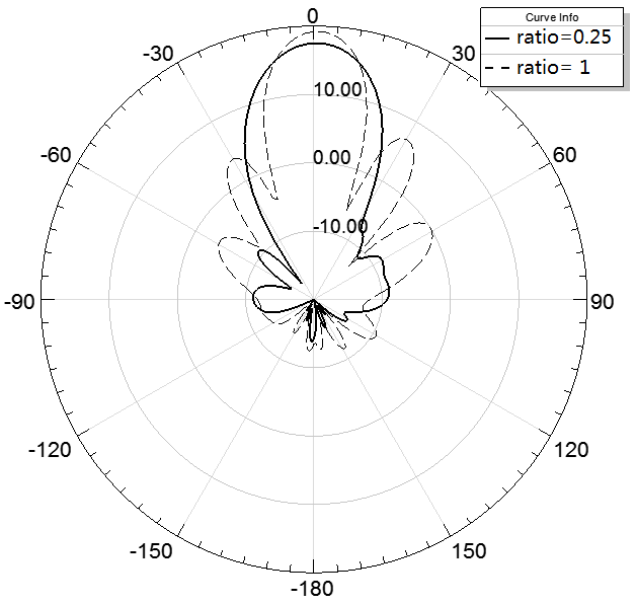

Figure 5.14: Radiation patterns $t\_phase = 0$

have been adopted, the main beam of the proposed array could be electrically and automatically steerable. To decrease sidelobe level of cross-type antenna array, the method of power re-management is introduced. By adjusting power distribution, elements in the array center are assigned with more power than the ones at the edge, simulation indicates that obvious improvement on sidelobe level could be obtained.

In pursuit of the required performances of antenna in our project, till now, we have found the cross-type antenna array which applies sufficient bandwidth ranges from 10.2GHz to 13.3GHz with dual polarizations. Using patch-sharing technique, this kind of antenna array is able to be arranged in plane with inter-element distance only $0.7\lambda_0$. The experimental 1x4 array has a gain about 12.6dBi and the gain of 4x4 array reaches up to 18.9dBi. The gain can be increased by enlarging the array with more elements. A 29dBi gain is expected with a 16x16 cross-type antenna array, if taking no account of feed network losses. With the integration of voltage-controlled phase shifters in the feed network, the proposed array is able to achieve continuous beam shifting, which applies the cross-type antenna array with possibilities to realize satellite searching and focusing functions. As the proposed beam management unit has adopted micro-processors and digital potentiometers to manage all the phase shifters in feed network, the main beam of cross-type antenna array could be managed automatically and accurately.

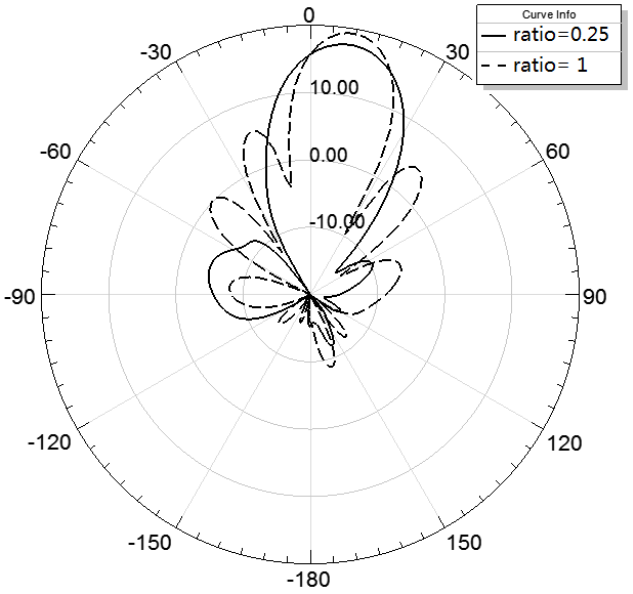

Figure 5.15: Radiation patterns $t\_phase = 41°$

6

Conclusion and perspectives

To replace beam fixed and non-planar parabola antenna, a low-cost, wide-band, dual-polarized and beam steerable antenna is expected for TV signal reception of Direct-Broadcast from Satellite (DBS) system. A mass of studies have been carried out, finally microstrip patch antenna which has flat structure with low cost and could be fabricated easily with PCB technology is adopted.

At the beginning of our study, a wideband, dual polarized and low profile CPW-fed antenna is introduced. This antenna has inherently wide bandwidth as a monopole antenna, even more, parasitical patch and arc slot are used to maintain bandwidth. Therefore in a low profile as small as 6.2 mm in diameter, the CPW-fed antenna achieves the required band which is from 10.7 to 12.7GHz. To achieve higher gain, CPW-fed antenna has been arranged both in 1-D and 2-D arrays. Dolph-Chebyshev current distribution method has been used to assign power to each element in both kinds of arrays. However, as quantities of quarter-wavelength TLs are used in array feed network, the bandwidth is hard to maintain. Nevertheless, if more studies are carried out, the CPW-fed monopole antenna array with Dolph-Chebyshev magnitude distribution feed network is expected to have better performance.

As studies went on, a cross-type patch antenna consists of 2 driven patch and 5 parasitical patches to expand bandwidth was obtained. This antenna has a relative bandwidth more than 38% which covers the required band (10.7-12.7GHz). Due to its symmetric structure and orthogonal feeding method, dual polarizations are also obtained [111]. The cross-type antenna is printed on a 1.524mm thickness Teflon substrate and the feed part is on a 0.8mm thickness Teflon substrate, hence the entire structure is flat and very thin. As we all know that the applied Teflon substrate is

cheap and easy to find, therefore the cost and fabrication complexity of cross-type antenna are both very low.

Since cross-type antenna has attractive performances, it is then adopted as element and arranged in arrays. Cross-type antenna has firstly been arranged linearly in a 1-D array and then extended to 2-D array with planar arrangement. Patch sharing technique is used in the two kinds of arrays, inter-element distance has been successfully decreased from $0.94\lambda_0$ to only $0.7\lambda_0$ [93]. Accompanying feed networks for 1-D array and 2-D array are also introduced. The feed network consists of T-junction dividers is found not able to provide sufficient impedance bandwidth therefore an optimized feed network consists of Wilkinson dividers is then introduced. With such a feed network, the cross-type antenna array operates well in the required band, very good resonating could be observed from the measured results. To obtain dual-polarization performance, a very up-to-date multilayer PCB technology with thin resistive film layer has been adopted to design the feed network of proposed antenna array, isolation enhancement could be obtained. More over, the cross-type antenna array with multilayer feed network has strictly flat structure whose entire thickness is only 3.6mm. The required flat antenna which operates in the band covers 10.7GHz to 12.7GHz with horizontal polarization and vertical polarization is successfully achieved. The experimental 4x4 cross-type antenna array achieves a gain about 18.9dBi. This gain of cross-type antenna array can be continuously enlarged by increasing elements.

To realize main beam steerable ability, fixed and equal-different phase shift network has firstly been carried out on cross-type antenna arrays, obvious beam shift could be observed on measured radiation patterns [112] of 1x4 array and 4x4 array. With the help of voltage-controlled and varactor diode based phase shifter, the main beam of cross-type antenna array can be steered continuously and electrically, which applies the cross-type antenna array with possibilities to realize satellite searching and focusing functions.

During our studies, a simple method to stabilize radiation pattern over a large bandwidth was found very useful to suppress side radiation of patch antenna. The proposed method is composed of a conductor ring and circular slot both with the width of a quarter wavelength, while the antenna part is located at the center of ring. With this method, obvious decreasing on sidelobe level could be observed on measured radiation patterns [75]. Patch sharing technique, to the author's knowledge, is the first time proposed in patch antenna array arrangement. With this technique, not only inter-element distance of antenna array could be significantly decreased, but also the main beam shifting angle is obviously enlarged according to measured results [93]. In addition, we found that, by using the power re-management method, elements in the array center are assigned with more power than the ones at the edge,

sidelobe level could be significantly decreased. With the development of phased array antenna, there is a demand of simple method to control dozens of phase shifters in feeding network. A new method which is able to transmit phase shifter controlling and polarization selecting commands associated with DC power supply and RF signal all in one coaxial cable is also achieved in our studies (see Annex 4).

Cross-type antenna array was proved well satisfying the requirements of our project. A much bigger array which consists of 256 elements in the form of 16x16 is in perspective, in that case, about 26dBi gain is expected to obtain thus satellite signal reception experiment will be carried out. Although hundreds of cross-type antenna elements are used, the 16x16 array will have a dimension of only 30cm by 30cm and with a thickness of 4.7mm. Moreover, a prototype of electrically beam steerable antenna has to be realized and measured. Further studies will be carried out on phase shifters, gain controlled amplifier and unbalanced wideband Wilkinson power divider. On the other hand, we can also propose to model the cross-type antenna (in circuit view) as a filter to quantify power and phase on each element (especially the parasitic patches) to show if optimization could be done on the command to steer the main beam with the minimum phase shift variation.

This kind of cross-type antenna is attractive and we are sure it will be a powerful competitor of parabola antenna in TV signal reception of Direct-Broadcast from Satellite (DBS) application in the future.

Publications

Journal papers

[1]. Haiyang Zhang, Yann Mahe, Tchanguiz Razban, and Serge Toutain, "A Simple Method to Stabilize Radiation Pattern over a Large Bandwidth," International Journal of Microwave Science and Technology, vol. 2014, Article ID 712735, 5 pages, 2014. doi:10.1155/2014/712735.

[2]. Haiyang Zhang, Yann Mahe, Tchanguiz Razban, "Low-Cost Ku-Band Dual-Polarized and Beam Switchable Cross-Type Antenna Array for Satellite Communications," Microwave and Optical Technology letters, Vol. 56, No. 11, Article ID MOP28670, pp. 2656-2659, Aug. 2014. doi: 10.1002/mop.

Conference papers

[3]. Haiyang ZHANG, Yann MAHE, Tchanguiz RAZBAN, "A novel wideband and dual-polarized cross-antenna for satellite communications," in PIERS 2013, Stockholm, Suède, Aug. 2013, p. PIERS 2013.

[4]. Haiyang ZHANG, Yann MAHE, Tchanguiz RAZBAN, "Ku-band Dual-polarized Patch Antenna Array Arrangement Using Patch Sharing Technique," EUMC 2014, Rome, ITALY, Oct. 2014.

Bibliography

[1] ZHI NING CHEN AND MICHAEL Y. W. CHIA. *Broadband planar antennas: design and applications*, **TK7871**. John Wiley & Sons Ltd, 2005. xiii, 19

[2] NC. **Systèm de réception multi-satellite**. *Lycée Notre Dme de Bel Air*, pages 1–15, 2001. xv, 2, 3

[3] FROM LYNGSAT MAPS. **Astra 1L at 19.2° E**. http://www.lyngsat-maps.com/maps/astra1l.html. xv, 4

[4] FROM LYNGSAT MAPS. **Hot bird 6 at 13.0° E**. http://www.lyngsat-maps.com/maps/astra1l.html. xv, 4

[5] D.ORBAN AND G. J. K. MOERNAUT. **The Basics of Patch Antennas**. *RF Globalnet newsletter*, pages 1–20, September 2009. xv, 13, 14, 42

[6] IP RESEARCH & COMMUNITIES. **High efficiency slot fed microstrip patch antenna**. http://www.freepatentsonline.com/6842140.html. xv, 19, 20

[7] KAI FONG LEE, S. L. S YANG, KISHK A. A., AND KWAI MAN LUK. **The Versatile U-Slot Patch Antenna**. *Antennas and Propagation Magazine, IEEE*, **52**(1):71–88, Feb 2010. xv, 20

[8] ZHI NING CHEN AND MICHAEL Y. W. CHIA. *Broadband planar antennas: design and applications*, **TK7871**. John Wiley & Sons Ltd, 2005. xv, 15, 20, 21

[9] HORNG-DEAN CHEN. **Broadband CPW-fed square slot antennas with a widened tuning stub**. *Antennas and Propagation, IEEE Transactions on*, **51**(8):1982–1986, Aug 2003. xv, 22

[10] R. YAHYA AND T.A. DENIDNI. **Compact CPW-fed antenna with ultra-wideband and dual polarization**. In *Mediterranean Microwave Symposium (MMS), 2011 11th*, pages 110–112, Sept 2011. xv, 22, 23, 41, 42, 43

[11] JUNG-HAN KIM, JOONG-KWAN KIM, YONG-JIN KIM, AND HONG-MIN LEE. **High Gain Antenna using Parasitic Shorted Annular Patch Structure**. In *Microwave Conference, 2007. APMC 2007. Asia-Pacific*, pages 1–4, Dec 2007. xv, 25

[12] H. VETTIKALLADI, O. LAFOND, AND M. HIMDI. **High-Efficient and High-Gain Superstrate Antenna for 60-GHz Indoor Communication**. *Antennas and Wireless Propagation Letters, IEEE*, **8**:1422–1425, 2009. xv, 25

[13] T. LAMBARD, O. LAFOND, M. HIMDI, H. JEULAND, AND S. BOLIOLI. **A novel analog 360° phase shifter design in Ku and Ka bands**. In *Antennas and Propagation (EuCAP), 2010 Proceedings of the Fourth European Conference on*, pages 1–4, April 2010. xviii, 97, 98

[14] FROM WIKIPEDIA. **Direct-Broadcast satellite**. http://en.wikipedia.org/wiki/Direct-broadcast_satellite. 1

[15] FROM WIKIPEDIA. **Orbite geostationnaire**. http://fr.wikipedia.org/wiki/Orbite_geostationnaire. 2

[16] X. Y. PENG AND K. Y. PAN. **Satellite communications and geo-stationary orbits distribution**. *NCP newsletter*, **19**:11–13, september 2010. 2

[17] J. ETHIER, M.R. CHAHARMIR, J. SHAKER, AND D. LEE. **Development of Novel Low-Cost Reflectarrays [Antenna Applications Corner]**. *Antennas and Propagation Magazine, IEEE*, **54**(3):277–287, June 2012. 11

[18] DAVID M. POZAR, STEPHEN D. TARGONSKI, AND H. D. SYRIGOS. **Design of millimeter wave microstrip reflectarrays**. *Antennas and Propagation, IEEE Transactions on*, **45**(2):287–296, Feb 1997.

[19] J. SHAKER, M.R. CHAHARMIR, M. CUHACI, AND A. ITTIPIBOON. **Reflectarray research at the communications research centre Canada**. *Antennas and Propagation Magazine, IEEE*, **50**(4):31–52, Aug 2008. 11

[20] A.G. ROEDERER. **Reflectarray antennas**. In *Antennas and Propagation, 2009. EuCAP 2009. 3rd European Conference on*, pages 18–22, March 2009. 11

[21] P.BHARTIA, K.V.S.RAO, AND R.S.TOMAR. *Millimeter-wave microstrip and printed circuit antennas*. Artech House, 1991. 13, 14, 125

[22] AGILENT TECHNOLOGIES. **MLIN(Microstrip Line)**. http://edocs.soco.agilent.com/pages/viewpage.action?pageId=58330348. 13

[23] ALA SHARAIHA. *Planar Antennas for Microwave Applications*. IETR, University of Rennes 1, May 2012. 13, 14, 28

[24] ANTENNA THEORY COM. **Microstrip antenna - Feeding Methods**. http://www.antenna-theory.com/antennas/patches/patch3.php. 14

[25] BANALIS C.A. *Antenna Theory: Analysis and Design, 2ND ED*. John Wiley & Sons Ltd, 1997. 14

[26] ANTENNA THEORY.COM. **Bandwidth**. http://www.antenna-theory.com/basics/bandwidth.php. 15, 16, 17

[27] MATS GUSTAFSSON AND SVEN NORDEBO. **Bandwidth, Q factor, and resonance models of antennas**. *LUTEDX*, **TEAT**(7138):1–16, september 2005. 15

[28] L. J. CHU. **Physical limitations of Omni-Directional antennas**. *Phys.*, **1**(19):1163–1175, 1948.

[29] R. F. HANSEN. **Time Harmonic Electromagnetic Fields**. *McGraw-Hill*, 1961.

[30] A. D. YAGHIJIAN AND S. R. BEST. **bandwidth, and q of antennas**. *IEEE Trans. Antennas Propagat.*, **53**(4):1298–1324, 2005. 15

[31] MICROWAVES101.COM. **Microstrip Patch Antennas**. http://www.microwaves101.com/encyclopedias/789-microstrip-patch-antennas. 16

[32] T. LAMBARD, O. LAFOND, M. HIMDI, H. JEULAND, S. BOLIOLI, AND L. LE COQ. **Design of a KA-band wide scanning phased array antenna**. In *Antennas and Propagation, 2009. EuCAP 2009. 3rd European Conference on*, pages 1247–1251, March 2009. 17

[33] GUSTAVO ADOLFO SOTELO BAZÀN. *Design of a circularly polarized patch antenna for satellite communications in L-band*. PhD thesis, Universitat politécnica de catalunya, december 2010. 17

[34] M.F. ISMAIL, M.K.A. RAHIM, M.R. HAMID, AND H.A. MAJID. **Dual-fed circular polarization compact array antenna**. In *Applied Electromagnetics (APACE), 2012 IEEE Asia-Pacific Conference on*, pages 116–119, Dec 2012.

[35] M.I. SABRAN, S. K A RAHIM, M. S A RANI, AND M. Z M NOR. **A single band dual-fed circular polarization microstrip antenna for RFID application**. In *RF and Microwave Conference (RFM), 2011 IEEE International*, pages 137–140, Dec 2011. 17

[36] D.M.POZAR AND D.H.S.(ED). *Microstrip Antennas: Analysis and Design*. John Wiley & Sons Ltd. 19

[37] N. JAYASUNDERE AND T. S M MACLEAN. **Omnidirectional radiation patterns from body mounted microstrip antennas**. In *Antennas and Propagation, 1989. ICAP 89., Sixth International Conference on (Conf. Publ. No.301)*, pages 187–190 vol.1, Apr 1989.

[38] E. LEVINE, G. MALAMUD, S. SHTRIKMAN, AND DAVID TREVES. **A study of microstrip array antennas with the feed network**. *Antennas and Propagation, IEEE Transactions on*, **37**(4):426–434, Apr 1989.

[39] A.E. GERA. **The radiation resistance of a microstrip element**. *Antennas and Propagation, IEEE Transactions on*, **38**(4):568–570, Apr 1990.

[40] ZAIPING NIE, WENG CHO CHEW, AND Y.T. LO. **Analysis of the annular-ring-loaded circular-disk microstrip antenna**. *Antennas and Propagation, IEEE Transactions on*, **38**(6):806–813, Jun 1990.

[41] D. THOUROUDE, M. HIMDI, AND J. P DANIEL. **CAD-oriented cavity model for rectangular patches**. *Electronics Letters*, **26**(13):842–844, June 1990.

[42] DAVID M. POZAR AND B. KAUFMAN. **Design considerations for low side-lobe microstrip arrays**. *Antennas and Propagation, IEEE Transactions on*, **38**(8):1176–1185, Aug 1990.

[43] G.P. GAUTHIER, A. COURTAY, AND G.M. REBEIZ. **Microstrip antennas on synthesized low dielectric-constant substrates**. *Antennas and Propagation, IEEE Transactions on*, **45**(8):1310–1314, Aug 1997. 25

[44] M.I. AKSUN, SHUN-LIEN CHUANG, AND Y.T. LO. **On slot-coupled microstrip antennas and their applications to CP operation-theory and experiment**. *Antennas and Propagation, IEEE Transactions on*, **38**(8):1224–1230, Aug 1990. 19

[45] T. HUYNH AND K. F. LEE. **Single-layer Single-patch Wideband Microtrip Antenna**. *Electronics letters*, **31**(16):1310–1312, 1995. 19

[46] K. F. TONG, K. M. LUK, K. F. LEE, AND R. Q. LEE. **A Broadband U-Slot Rectangular Patch Antenna on a Microwave Substrate**. *IEEE Transactions on Antennas and Propagation*, **AP-48**(6):954–960, 2000. 20

[47] AARON K. SHACKELFORD, KAI-FONG LEE, AND K. M. LUK. **Design of Small-Size Zide-Bandwidth Microstrip-Patch Antenna**. *Antennas and Propagation Magazine, IEEE*, **45**(1):75–83, Feb 2003. 20

[48] T.A. DENIDNI AND M.A. HABIB. **Broadband printed CPW-fed circular slot antenna**. *Electronics Letters*, **42**(3):135–136, Feb 2006. 22

[49] SANTANU MONDAL AND PARTHA P.SARKAR. **a novel design of compact wideband hexagonal antenna**. *Mrcrowave and optical technology letters*, **55**(1):1–4, January 2013. 22

[50] ZHANTAO YANG, LI LI, AND HUAZHI WANG. **Investigation on ultra-wideband printed circular monopole antenna with frequency-notched**. In *Microwave and Millimeter Wave Technology, 2008. ICMMT 2008. International Conference on*, **4**, pages 1858–1861, April 2008. 22

[51] JIANXIN LIANG, C.C. CHIAU, XIAODONG CHEN, AND C.G. PARINI. **Study of a printed circular disc monopole antenna for UWB systems**. *Antennas and Propagation, IEEE Transactions on*, **53**(11):3500–3504, Nov 2005.

[52] M.J. AMMANN AND ZHI-NING CHEN. **A wide-band shorted planar monopole with bevel**. *Antennas and Propagation, IEEE Transactions on*, **51**(4):901–903, April 2003.

[53] BROADBAND PLANAR RECTANGULAR MONOPOLE ANTENNAS. **A wide-band shorted planar monopole with bevel**. *Microwave Opt. Technol Lett*, **28**(1):55–59, 2001.

[54] O. AHMED, A.A. ABUMAZWED, AND A.-R. SEBAK. **A trapezoidal printed monopole antenna with bell-shaped cut with 5.0-6.0GHz band rejection**. In *Antennas and Propagation, 2009. EuCAP 2009. 3rd European Conference on*, pages 1459–1463, March 2009.

[55] BINGGANG XIAO, XIUMIN WANG, JIXIANG ZHAO, AND DONGPING ZHANG. **Compact ultra-wideband printed monopole antenna with a**

trapezoidal radiator. In *Information Science and Engineering (ICISE), 2010 2nd International Conference on*, pages 1919–1922, Dec 2010. 22

[56] T.A. DENIDNI AND M.A. HABIB. **Broadband printed CPW-fed circular slot antenna**. *Electronics Letters*, **42**(3):135–136, Feb 2006. 22

[57] A. ADRIAN AND D.H. SCHAUBERT. **Dual aperture-coupled microstrip antenna for dual or circular polarisation**. *Electronics Letters*, **23**(23):1226–1228, November 1987. 23

[58] S.B. CHAKRABARTY, F. KLEFENZ, AND A. DREHER. **Dual polarized wide-band stacked microstrip antenna with aperture coupling for SAR applications**. In *Antennas and Propagation Society International Symposium, 2000. IEEE*, **4**, pages 2216–2219 vol.4, July 2000. 23

[59] C.H. TSAO, Y.M. HWANG, F. KILBURG, AND F. DIETRICH. **Aperture-coupled patch antennas with wide-bandwidth and dual-polarization capabilities**. In *Antennas and Propagation Society International Symposium, 1988. AP-S. Digest*, pages 936–939 vol.3, June 1988. 23

[60] S. GAO, L.W. LI, M.S. LEONG, AND T.S. YEO. **A broad-band dual-polarized microstrip patch antenna with aperture coupling**. *Antennas and Propagation, IEEE Transactions on*, **51**(4):898–900, April 2003. 23, 43

[61] P. BRACHAT AND J.-M. BARACCO. **Printed radiating element with two highly decoupled input ports**. *Electronics Letters*, **31**(4):245–246, Feb 1995. 24

[62] FROM WIKIPEDIA. **Microstrip antenna**. http://en.wikipedia.org/wiki/Microstrip_antenna. 24

[63] H. BOUTAYEB AND T.A. DENIDNI. **Gain Enhancement of a Microstrip Patch Antenna Using a Cylindrical Electromagnetic Crystal Substrate**. *Antennas and Propagation, IEEE Transactions on*, **55**(11):3140–3145, Nov 2007. 25

[64] R.G. ROJAS AND K. W. LEE. **Surface wave control using nonperiodic parasitic strips in printed antennas**. *Microwaves, Antennas and Propagation, IEE Proceedings*, **148**(1):25–28, 2001.

[65] A.K. BHATTACHARYYA. **Characteristics of space and surface waves in a multilayered structure [microstrip antennas]**. *Antennas and Propagation, IEEE Transactions on*, **38**(8):1231–1238, Aug 1990.

[66] D.R. JACKSON, J.T. WILLIAMS, A.K. BHATTACHARYYA, R.L. SMITH, S.J. BUCHHEIT, AND S.A. LONG. **Microstrip patch designs that do not excite surface waves**. *Antennas and Propagation, IEEE Transactions on*, **41**(8):1026–1037, Aug 1993. 25

[67] HON TAT HUI. **Antenna Arrays**. http://www.ece.nus.edu.sg/stfpage/elehht/Teaching/EE6832/Lecture%20Notes%5CAntenna%20Arrays.pdf. 25

[68] ATEF AL NUKARI. *Contribution to the design and the realization of compact RF power transmitters*. PhD thesis, Ecole Polytechnique de l'Universite de Nantes, december 2010. 28, 126

[69] J. P. TURPIN, Q. WU, D. H. WERNER, B. MARTIN, M. BRAY, AND E. LIER. **Low cost and broadband dual-polarization metamaterial lens for directivity enhancement**. *IEEE Transactions on Antennas and Propagation*, **60**(12):5717–5726, 2012. 36

[70] Z. B. WENG, N. B. WANG, Y. C. JIAO, AND F. S. ZHANG. **A directive patch antenna with metamaterial structure**. *Microwave and Optical Technology Letters*, **49**(2):456–459, 2007. 36

[71] Z. FANGMING, L. QINGCHUN, AND H. JUN. **Adirective patch antenna with metamaterial structure**. *Asia-Pacific Microwave Conference (APMC 05)*, **3**, 2005. 36

[72] Y. LEE, X. LU, Y. HAO, S. YANG, J. R. G. EVANS, AND C. G. PARINI. **Narrow-beam azimuthally omni-directional millimetre-wave antenna using freeformed cylindrical woodpile cavity**. *IET Microwaves, Antennas and Propagation*, **4**(10), 2010. 37

[73] Y. LEE, X. LU, AND Y. HAO. **Rapid prototyping of ceramic millimetre-wave metamaterials simulations and experiments**. *IET Microwaves, Antennas and Propagation*, **29**(9), 2007. 37

[74] X. LU, Y. LEE, AND S. YANG. **Fabrication of electromagnetic crystals by extrusion freeforming**. *Metamaterials*, **2**(1), 2008. 37

[75] H.ZHANG, Y. MAHE, T.RAZBAN, AND S. TOUTAIN. **A Simple Method to Stabilize Radiation Pattern over a Large Bandwidth**. *International Journal of Microwave Science and Technology*, **2014**(712735), April 2014. 38, 108

[76] MICROWAVES101.COM. **Coplanar waveguide**. http://www.microwaves101.com/encyclopedia/coplanarwaveguide.cfm. 44

[77] HE-XIU XU, GUANG-MING WANG, AND KE LU. **Microstrip Rat-Race Couplers**. *Microwave Magazine, IEEE*, **12**(4):117–129, June 2011. 51

[78] M. CAILLET, M. CLENET, A. SHARAIHA, AND Y.M.M. ANTAR. **A Compact Wide-Band Rat-Race Hybrid Using Microstrip Lines**. *Microwave and Wireless Components Letters, IEEE*, **19**(4):191–193, April 2009.

[79] TING TING MO, QUAN XUE, AND CHI-HOU CHAN. **A Broadband Compact Microstrip Rat-Race Hybrid Using a Novel CPW Inverter**. *Microwave Theory and Techniques, IEEE Transactions on*, **55**(1):161–167, Jan 2007.

[80] K.-K.M. CHENG AND FAI-LEUNG WONG. **A novel rat race coupler design for dual-band applications**. *Microwave and Wireless Components Letters, IEEE*, **15**(8):521–523, Aug 2005.

[81] K.-K.M. CHENG AND F.-L. WONG. **Dual-band rat-race coupler design using tri-section branch-line**. *Electronics Letters*, **43**(6):41–42, March 2007. 51

[82] V. RABINOVICH AND N. ALEXANDROV. *Antenna Array and Automotive Applications*. Springer Science, 2013. 54, 68

[83] A. SAFAAI-JAZI. **A new method for the analysis and design of Chebyshev arrays**. In *System Theory, 1994., Proceedings of the 26th Southeastern Symposium on*, pages 157–161, Mar 1994. 55

[84] A. KORETZ AND B. RAFAELY. **Dolph-Chebyshev Beampattern Design for Spherical Arrays**. *Signal Processing, IEEE Transactions on*, **57**(6):2417–2420, June 2009.

[85] Y. J. LIU AND C. H. CHEN. **A Low-sidelobe and Low-Backlobe Antenna**. In *China Academic Journal Electronic Publishing House*, pages 26–28, June 2003.

[86] L. FENG AND S. LI. **Design of 5.8 GHz dual-polarized microstrip antenna array with low-sidelobe and series feed**. In *China Academic Journal Electronic Publishing House*, pages 9–12, Feb 2011. 55

[87] A. BRESLER. **A new algorithm for calculating the current distributions of dolph-chebyshev arrays**. *Antennas and Propagation, IEEE Transactions on*, **28**(6):951–952, Nov 1980. 55

[88] WIDIPEDIA. **Power dividers and directional couplers**. http://en.wikipedia.org/wiki/Power_dividers_and_directional_couplers. 61

[89] SHIH-KAI LIN AND YI-CHENG LIN. **A Compact Sequential-Phase Feed Using Uniform Transmission Lines for Circularly Polarized Sequential-Rotation Arrays**. *Antennas and Propagation, IEEE Transactions on*, **59**(7):2721–2724, July 2011. 68

[90] SHI-GANG ZHUO AND TAN-HUAT CHIO. **Dual-wideband and dual-polarized shared aperture antenna**. In *Antennas and Propagation (ISAP), 2012 International Symposium on*, pages 798–801, Oct 2012. 68

[91] SHI-GANG ZHUO AND TAN-HUAT CHIO. **A wideband, low profile P- and Ku-band Dual Polarized shared aperture antenna**. In *Antennas and Propagation (ISAP), 2012 International Symposium on*, pages 794–797, Oct 2012. 68

[92] KAINAN ZHAO, JIAWEN SUN, WENHUA CHEN, AND ZHENGHE FENG. **Effect of inter-element spacing on performance of planar switched parasitic array antenna**. In *Microwave and Millimeter Wave Technology, 2008. ICMMT 2008. International Conference on*, **3**, pages 1189–1192, April 2008. 68

[93] HAIYANG ZHANG, YANN MAHE, AND TCHANGUIZ RAZBAN. **Ku-band Dual-polarized Patch Antenna Array Arrangement Using Patch Sharing Technique**. In *European Microwave Week Conference (EUMC) 2014, Rome, Italy*, Oct 2014. 69, 108

[94] E.E. OKON AND C.W. TURNER. **Design of broadband microstrip series array for mm-wave applications**. *Electronics Letters*, **38**(18):1036–1037, Aug 2002. 78

[95] T. METZLER. **Microstrip series arrays**. *Antennas and Propagation, IEEE Transactions on*, **29**(1):174–178, Jan 1981. 78

[96] A. YOSEAF, N. FAHOUM, AND H. MATZNER. **A linear microstrip antenna array having low sidelobe level**. In *Antennas and Propagation, 2009. EuCAP 2009. 3rd European Conference on*, pages 1166–1170, March 2009. 78

[97] HONGQI XIANG, XING JIANG, AND SIMIN LI. **Design of a High Gain Low Sidelobe Microstrip Antenna Array at Ku-band**. In *Communications and Mobile Computing, 2009. CMC '09. WRI International Conference on*, **1**, pages 29–32, Jan 2009. 78

[98] K. WINCZA AND S. GRUSZCZYNSKI. **Microstrip Antenna Arrays Fed by a Series-Parallel Slot-Coupled Feeding Network**. *Antennas and Wireless Propagation Letters, IEEE*, **10**:991–994, 2011. 78

[99] M. STRACKX, K. JANSSEN, E. D'AGOSTINO, G.A.E. VANDENBOSCH, P. REYNAERT, AND P. LEROUX. **Ultra-wideband antipodal vivaldi antenna array with Wilkinson power divider feeding network**. In *Ultra-Wideband (ICUWB), 2011 IEEE International Conference on*, pages 1–4, Sept 2011. 78

[100] K.P. RAY, K. NIRMALA, S.S. KAKATKAR, N.S. MADAKA, AND C. PRINCE. **Broadband modified Wilkinson power divider fed antipodal Vivaldi antenna array**. In *Microwave and Photonics (ICMAP), 2013 International Conference on*, pages 1–4, Dec 2013.

[101] LUNG-FAI TUEN AND CHING-LIEH LI. **Design and optimization for the satellite Ku-band CP array antennas**. In *Applications of Electromagnetism and Student Innovation Competition Awards (AEM2C), 2010 International Conference on*, pages 274–278, Aug 2010. 78

[102] RADIO-ELECTRONICS.COM. **Wilkinson Power Divider/ Splitter/ Combiner**. http://www.radio-electronics.com/info/rf-technology-design/coupler-combiner-splitter/wilkinson-splitter-combiner-divider.php. 78

[103] MICROWAVES101.COM. **Wilkinson Power Splitters**. http://www.microwaves101.com/encyclopedia/Wilkinson_splitters.cfm.

[104] DANIEL D. HARTY. **Novel design of a wideband ribcage-dipole array and its feeding network**. *Worcester polytechnic institute*, pages 3–15, December 2010. 78

[105] MICROWAVES101.COM. **Stripline**. http://www.microwaves101.com/encyclopedia/stripline.cfm. 81

[106] N.C. **Microstrip Versus Stripline: How to make the choice**. http://mwexpert.typepad.com/rog_blog/2010/12/

microstrip-versus-stripline-how-to-make-the-choice.html. 81

[107] HITTITE MICROWAVE CORPORATION. **410° analog phase shifter, 8-12GHz**. http://www.hittite.com/content/documents/data_sheet/hmc931lp4.pdf. 95

[108] HITTITE MICROWAVE CORPORATION. **600° analog phase shifter, 6-15GHz**. http://www.everythingrf.com/products/analog-phase-shifters/hittite/626-4-hmc-c010. 95

[109] T. HAMA, K. KAWASAKI, T. TANAKA, AND M. AIKAWA. **A Ku band push-push oscillator array using directional phase shifter**. In *Microwave Conference Proceedings (APMC), 2010 Asia-Pacific*, pages 582–585, Dec 2010. 95, 96

[110] CHANG-LEE CHEN, W.E. COURTNEY, LEONARD J. MAHONEY, M.J. MANFRA, A CHU, AND H.A ATWATER. **A Low-Loss Ku-Band Monolithic Analog Phase Shifter**. *Microwave Theory and Techniques, IEEE Transactions on*, **35**(3):315–320, Mar 1987. 96, 97

[111] HAIYANG ZHANG, YANN MAHE, AND TCHANGUIZ RAZBAN. **A novel wideband and dual-polarized cross-antenna for satellite communications**. In *PIERS 2013*, page PIERS 2013, Stockholm, Suède, August 2013. 107

[112] HAIYANG ZHANG, YANN MAHE, AND TCHANGUIZ RAZBAN. **Low-cost Ku-band dual-polarized and beam switchable cross-type antenna array for satellite communications**. In *Microwave and Optical Technology Letters (MOTL)*, JUNE 2014. 108

[113] CHEMANDY ELECTRONICS LTD. **Velocity of Propagation**. http://chemandy.com/technical-articles/sitting-waves/standing-waves-article6.htm. 125

[114] MATLAB CENTRAL. **Electromagnetic Waves & Antennas Toolbox**. http://www.mathworks.com/matlabcentral/fileexchange/4456-electromagnetic-waves---antennas-toolbox/content/chebarray.m. 129

[115] JOHN SILVESTRO. **HPC Optionsfor HFSS**. In *ANSYS Advantage, Analysis Tools*, **4**, pages 41–43, 2010. 133

Annex 1: Dielectric measurement

A.1 Substrate relative permittivity measuring approach

Electromagnetic waves propagate at a speed that is dependent on the electrical properties of the surrounding medium. In air, or vacuum, the velocity of propagation is the speed of light. In a dielectric material, the velocity of propagation is slower. The velocity of propagation and the effective dielectric constant have a relation depicted in the following formula [113].

$$v_p = \frac{c}{\sqrt{\varepsilon_{eff}}} \tag{A.1}$$

Where v_p is the velocity of propagation in m/s and c is the speed of light 3x$10^8 m/s$. The effective dielectric constant is therefore expressed as:

$$\varepsilon_{eff} = \left(\frac{c}{v_p}\right)^2 \tag{A.2}$$

and as we all know that in a substrate, the effective dielectric constant can also be obtained by [21]:

$$\varepsilon_{eff} = \frac{\varepsilon_r + 1}{2} + \frac{\varepsilon_r - 1}{2}\left(1 + \frac{10h}{W}\right)^{-1/2} \tag{A.3}$$

Thus, the relative dielectric constant of substrate ε_r could be yielded from equation A.2 and A.3 if the velocity of propagation in such substrate is known. A method to obtain the velocity of propagation in a substrate is to measure the propagation de-

lay for a known length line, as illustrated in Fig.A.1. The two narrow and wide line have the same length $L = 100mm$. Using a Vector Network Analyzer, the reflection coefficient for each transmission line could be measured, which are given in Fig.A.2 and Fig.A.3. The velocity of propagation could be obtained with the following expression and two random adjacent resonate frequency points from Fig.A.2 and Fig.A.3 [68].

$$v_p = 2 \cdot L \cdot (f_k - f_{k-1}) \tag{A.4}$$

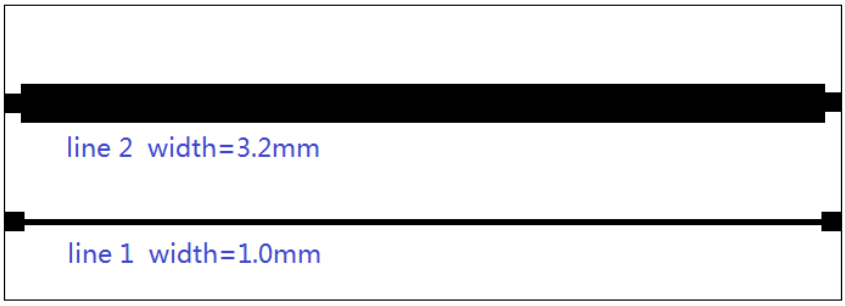

Figure A.1: Layout of narrow and wide transmission lines

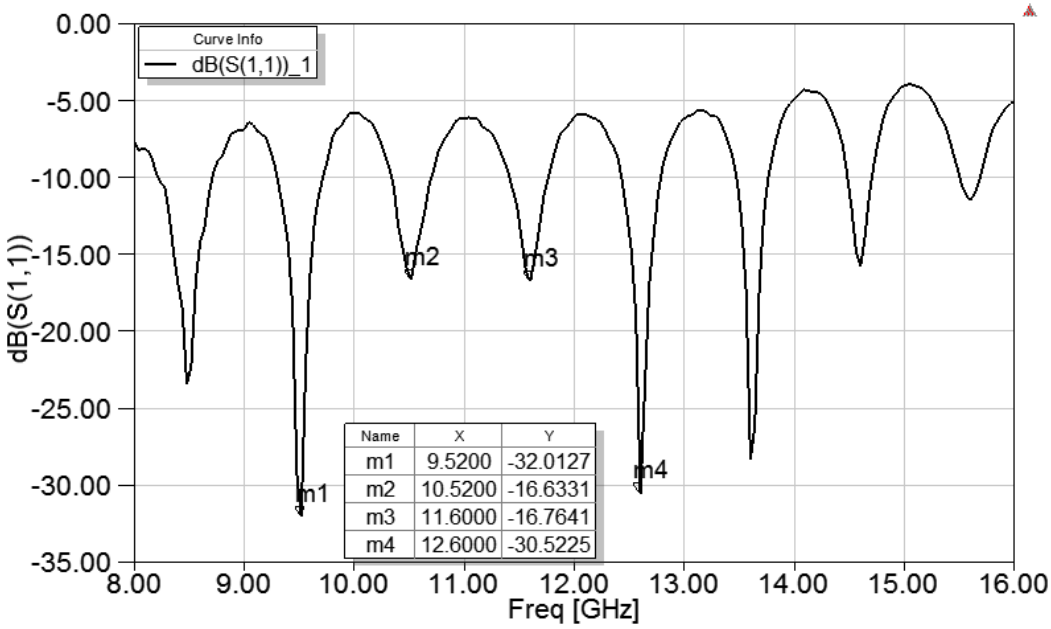

Figure A.2: Measured reflection coefficient of narrow transmission line

With equation A.2, A.3, A.4 and Fig.A.2 A.3, the relative permittivity of given substrate is able to achieved. In the band ranges from 10GHz to 13GHz, the average ε_{eff} of the measured substrate is about 2.875.

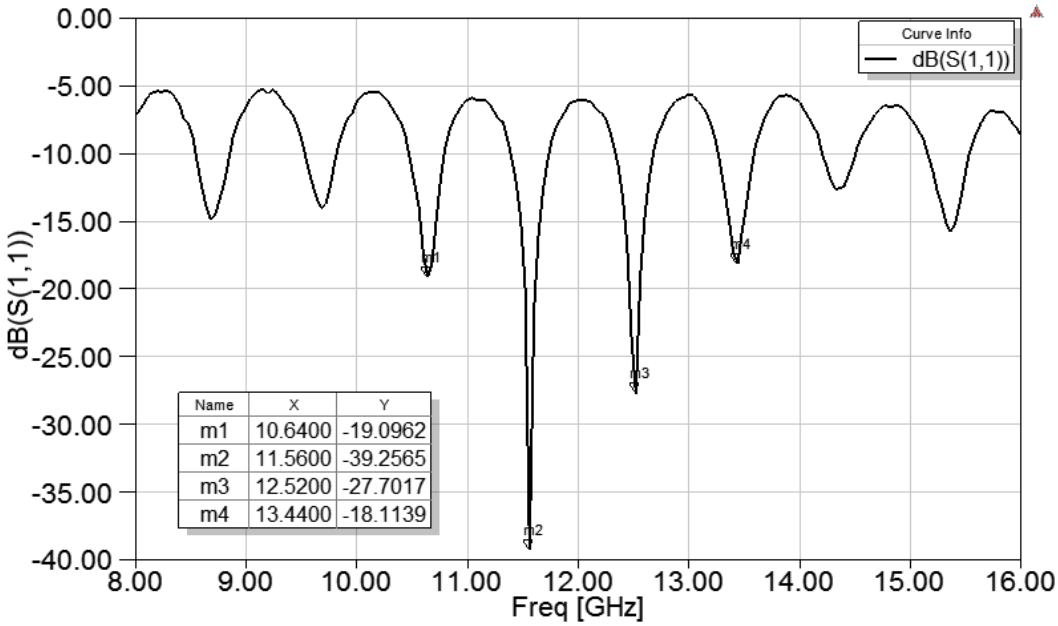

Figure A.3: Measured reflection coefficient of wide transmission line

A.2 Matlab function to calculate substrate relative permittivity

Here in this section, we give an example Matlab program which helps calculating the average relative permittivity automatically if transmission line length and width is given and the measured s*p file output by VNA is specified.

```
clear all;clc;

h=0.8e-3; % substrate thickness (m)
c=3e8; % light speed in free space (m/s)
%————————————————————————————————
% transmission line characteristics
W=1.0e-3; % transmission line width (m)
L=100e-3; % transmission line length (m)
h_w=(1+10*h/W)^(-1/2);
%————————————————————————————————
% import measured file
%————————————————————————————————
A=importdata('your file.s2p',' ',7); % load file and change the value of start line
data=A.data;
clear A;
freqA=data(:,1);
```

```
S11A=10.^(data(:,2)/20).*exp(1i*data(:,3)*pi/180);
dBS11A=data(:,2);
S21A=10.^(data(:,4)/20).*exp(1i*data(:,5));
figure(1);plot(freqA,dBS11A);grid
ylabel('dB(S(1,1))');xlabel('freq'); hold on;
[pksA, locsA]=findpeak(-dBS11A,'MINPEAKDISTANCE',5,'NPEAKS',20);
MINA=zeros(length(locsA),3);
for i=1:length(locsA)
MINA(i,1)=freqA(locsA(i));
MINA(i,2)=S11A(locsA(i));
MINA(i,3)=dBS11A(locsA(i));
end

plot(MINA(:,1),-pksA,'k^','markerfacecolor',[1 0 0]);
hold off;

freq_point=MINA(:,1);
Eps=zeros(length(locsA),1);
F1=freq_point(1);
Eps_total=0;
freq_lowband=0;
for j=2:length(locsA)
F2=freq_point(j);
EpsEff=(c/(2*L*(F2-F1)))^2;
Eps(j)=(EpsEff-1/2+h_w/2)/(1/2+h_w/2);
F1=F2;
if(F2<1.6E+10)
freq_lowband=freq_lowband+1;
Eps_total=Eps_total+Eps(j);
end
end
figure(2);
plot(freq_point,Eps);grid
hold off;
freq_eps=zeros(length(locsA),2);
freq_eps(:,1)=freq_point;
freq_eps(:,2)=Eps;
Eps_average=Eps_total/(freq_lowband)
```

B

Annex 2: Chebyshev array weights

B.1 Matlab function for obtaining Chebyshev array weights

chebarray.m [114].

```
function coefs = chebarray(M, sldb)

%CHEBARRAY Compute chebyshev excitation coefficients for a linear array.
%
% Calling sequence: coefs = chebarray(M, sldb)
%
% Input arguments:

    % M The number of elements in the array.
% sldb The sidelobe level in dB. Note sldb > 0.
%
% Output arguments:
% coefs A vector of length M containing the real excitation
% coefficients of the array. They are normalized so that the end
% elements' excitation is unity.
%
```

```
% Language: Matlab 6.x
% Author: Peter S. Simon
% Date: 12/21/2003
% Reference: A. D. Bresler, "A new algorithm for calculating the current
% distributions of Dolph-Chebyshev arrays," IEEE Trans.
% Antennas Propagat., vol. AP-28, no. 6, November 1980.
%
% Copyright 2003 Peter S. Simon, peter_simon@ieee.org
% This routine may be used by anyone for any purpose. I simply ask
% that acknowledgement be made to me.


if (sldb <= 0)
error('sldb must be positive!')
end

N = floor(M/2);
Meven = (M == 2*N); % True if even # elements in array.
sigma = 10 ^ (sldb/20); % Side lobe level as a voltage ratio.
Q = acosh(sigma);
beta = (cosh(Q/(M-1))) ^ 2;
alpha = 1 - 1/beta;
if Meven
nend = N-1;
I = zeros(1,N); % Storage for half the array coefficients.
else
nend = N;
I = zeros(1,N+1); % Storage for half the array coefficients.
end
I(1) = 1;

for n = 1:nend
np = 1;
for m = 1:(n-1)
f_m = m * (M-1-2*n + m) / ((n-m) * (n+1-m));
np = np * alpha * f_m + 1;
end
I(n+1) = (M-1)*alpha * np;
end
```

```
if Meven
coefs = [I fliplr(I)];
else
coefs = [I(1:end-1) fliplr(I)];
end

return
```

C

Annex 3: HFSS fast and efficient simulation

C.1 HFSS High-Performance Computing (HPC) options

The latest HFSS release contains a wide array of powerful new features and enhancements. Included are some dramatic additions to the product's high-performance computing (HPC) capability. These improvements allow efficient simulation of large, complex problems and enhanced insight that would be difficult or impossible to obtain any other way. HFSS offers three HPC solution options: multiprocessing (MP) and the domain decomposition method (DDM), both used for exploiting multiple cores for a single simulation, and the distributed solve option (DSO), which enables consideration of multiple design points using distributed processors. All three options are designed to make efficient use of multicore and networked processing power [115].

MP and DDM options can be executed on a single machine with several cores, nevertheless, by using high speed network, DDM and DSO options will accelerate the solution and save much time which manage more processors into computing. Fig.C.1

In our studies, we have big antenna array with quantities of elements and dozens of parameters to be solved in HFSS, one can imagine the complexity and time consumption if the solution is calculated in a single machine. Thanks to the help of HPC

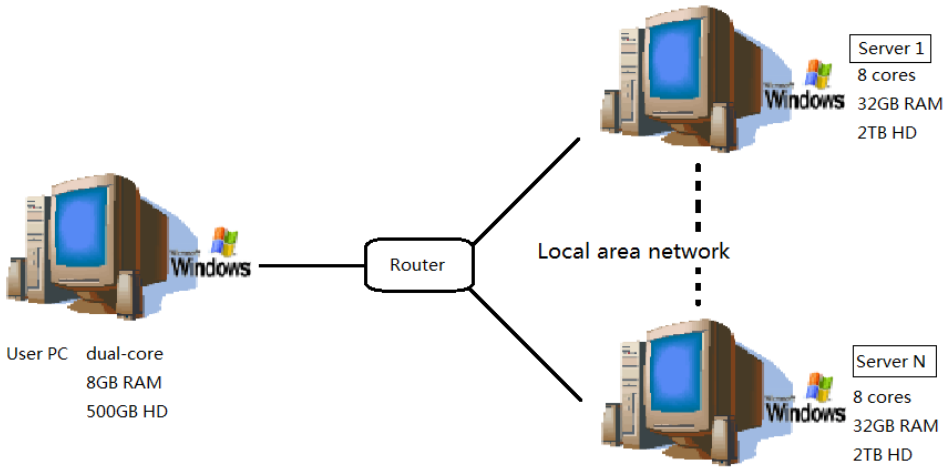

Figure C.1: Network topology for HPC

options and the wonderful workstations in our laboratory, we have finally achieved very good simulation results. We would like to introduce the configurations and setups to experience HPC options.

C.2 Experience HPC options

In this section, we would like to introduce the steps of constructing both Multi-processing computing and distributed analysis in the same computer, to experience the fast and efficient simulation and parametric optimization.

Firstly, we have to install Ansoft Remote Simulation Manager (RSM) both in user computer and workstations. Remote Simulation Manager allows users to remotely solve HFSS designs from any machine in the lab or one of the other powerful lab workstations. In order to take advantage of this feature, several settings must be configured in the HFSS desktop application.

Then we have to configure the user computer. From the menu bar of HFSS, choose Tools -> Options -> General Options, choose Analysis Options, select Distributed as the value of Analysis Machine Options. Then edit the distributed machine configurations via IP address, as depicted in Fig.C.2.

In addition, we have to tell the software the total number of processors which will take part in the solution. Simply by choose Tools -> Options -> HFSS options -> Solver, and set the number corresponding to the total number of processors we actually use, as shown in Fig.C.3. Fig.C.4 illustrates the screen when solution is in calculation and we can see 9 threads are executing in parallel.

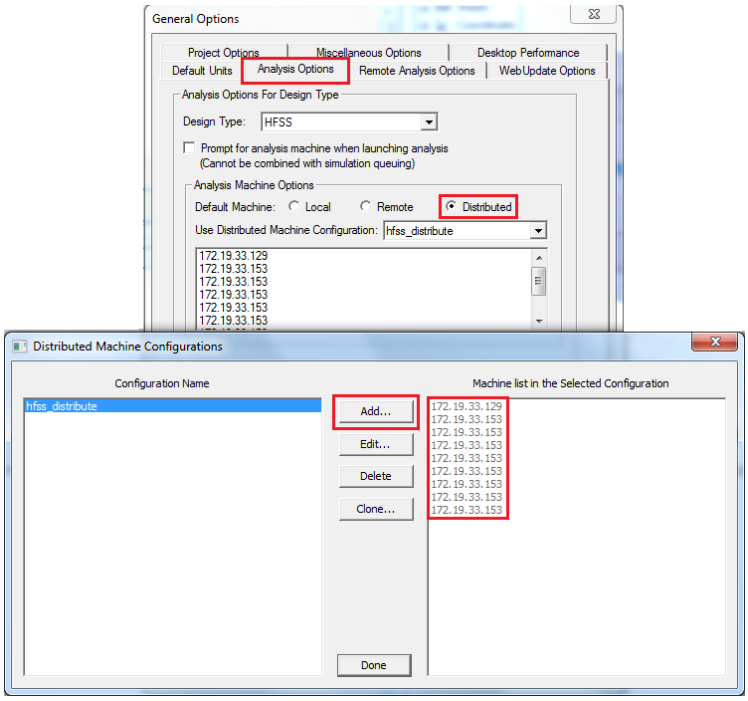

Figure C.2: Configuration for distributed analysis

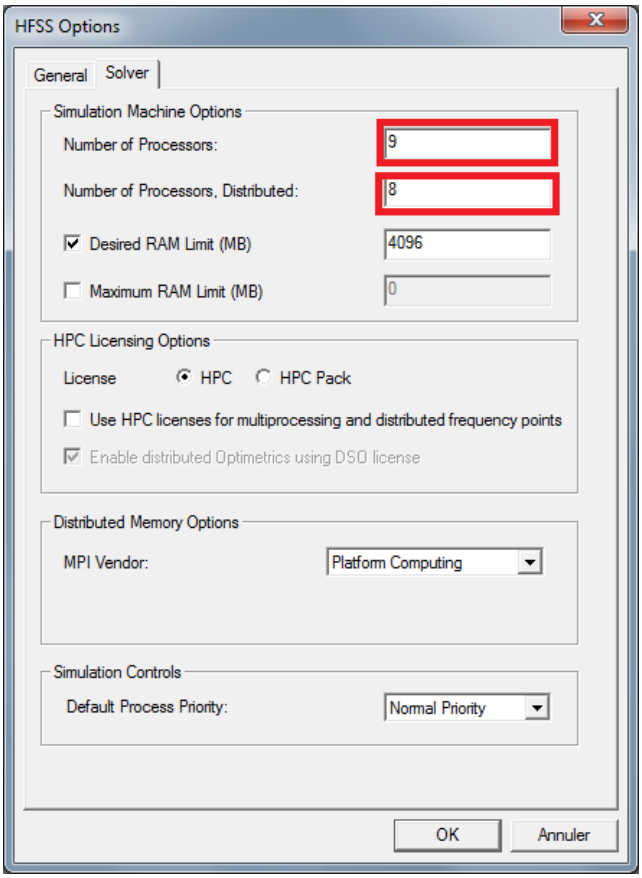

Figure C.3: Configuration for multi-processing

Figure C.4: Distributed analysis

D

Annex 4: Beam management unit

Due to the reason of enlarging cross-type antenna array gain by increasing elements, a big quantity of voltage-controlled phase shifters will be used, which increases also the circuit complexity of entire system. One problem seems very difficult, which is to provide the same quantity of power suppliers with phase shifters. In addition, to manage all the phase shifters at the same time so as to construct the steered beam is also a challenge.

In this section, we would like to introduce a microwave and digital circuit integrated module which is able to manage antenna array phase shifters by using a serial of digital potentiometers. Therefore only one DC voltage is needed which will be distributed to each phase shifter by the potentiometers. A micro-processor is used in this module to manage all the digital potentiometers and communicate with user device to obtain beam shifting commands. In addition, a circuit which enables intermediate frequency signal, DC power and phase shifter command transmit in the same coaxial cable will also be introduced.

D.1 Circuit configuration of Beam management unit

Fig.D.1 illustrates the topology of proposed beam management module, in which it can be seen the integration of microwave and digital circuits. The microwave circuit is consisted of transmission lines, power dividers and quantities of phase shifters, which provides paths for RF signal transmission between input port and cross-type antenna array. The digital circuit is consisted of micro-processor and numerous of digital-potentiometers, commanded through an I^2C (Inter-Integrated

Circuit) Bus. As each potentiometer MCP4662 has an hardware-programmable address, so commands transmission between micro-processor and each potentiometer is timely separated. Once a beam steering command is sent to the micro-processor from user device, the processor will rapidly calculate the phase difference and obtain the phase distribution table, which corresponds to the phase shifter driving voltage table. At last, the processor will command each digital potentiometer and send the corresponding voltage value through I^2C Bus.

The digital circuit is directly connected with the LNB (Low-noise block) input port, thus DC voltage is able to feed the micro-processor and potentiometers, commands from user device can also be received by processor. A capacitor is used between microwave network and input port to stop DC current flowing into microwave network. With this kind of circuit, there is no need to feed each phase shifter with different power suppliers while only one DC voltage is enough to distribute automatically to phase shifters with the help of micro-processor.

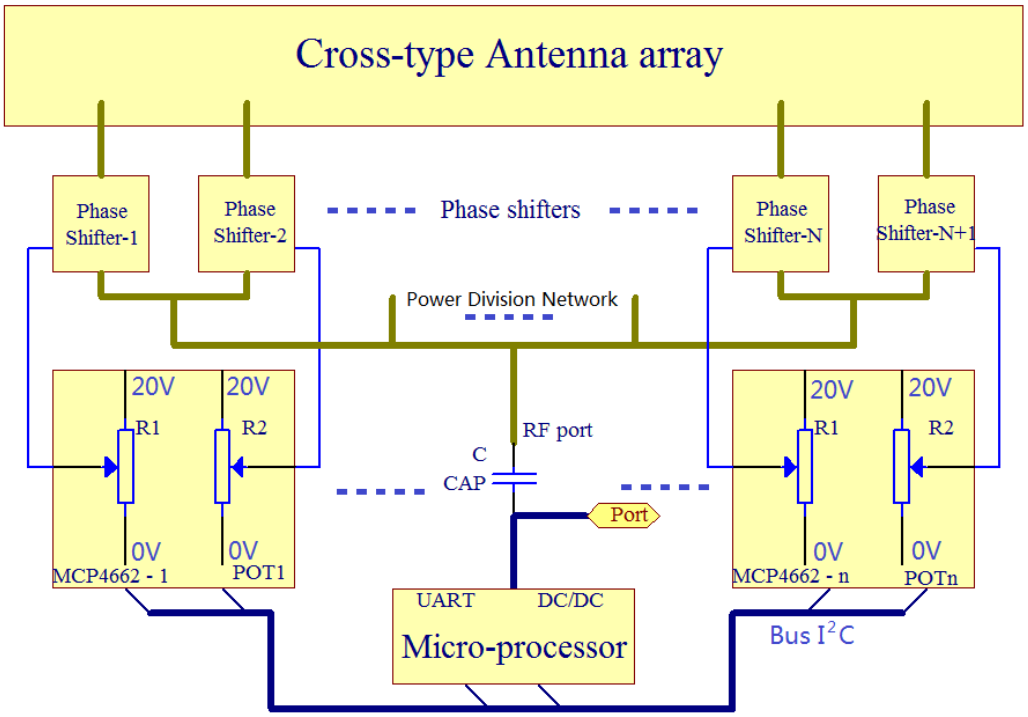

Figure D.1: Topology of entire system

D.2 Optical-isolated Command transmitting circuit

Beam steering command is executed by micro-processor by adjusting phase distribution in the feed network. Normally, we should have a DC power supply separated with command transmission path. however, to avoid using numerous of cables, we have specially designed an optical-isolated command transmission circuit

integrated with DC power supply and IF signal transmission, therefore only one coaxial cable is sufficient to connect phased antenna array and reception device. The schematic of the proposed circuit is presented in Fig.D.2.

From Fig.D.2, it can be seen the command transmitting circuit is separated into two parts which are the sending part and the receiving part. The unique coaxial cable is used as the transmission channel of all three kinds of signals. At the sending part, commands are modulated and then loaded on a couple of DC voltages which are 14V and 19V. DC voltage will be transmitted directly to the receiving part via coaxial cable. At the receiving part, the DC voltage difference will cause the transistor Q1 turns on and off, therefore commands will be selected out from other signals. Commands will finally be demodulated in the micro-processor of receiving part. The DC voltage load on coaxial cable provides enough power consumption for the receiving part, potentiometers, phase shifters and other components.

With the decoupling function of capacitors, IF signal can be easily separated from DC voltage even though they are transmitted in the same cable.

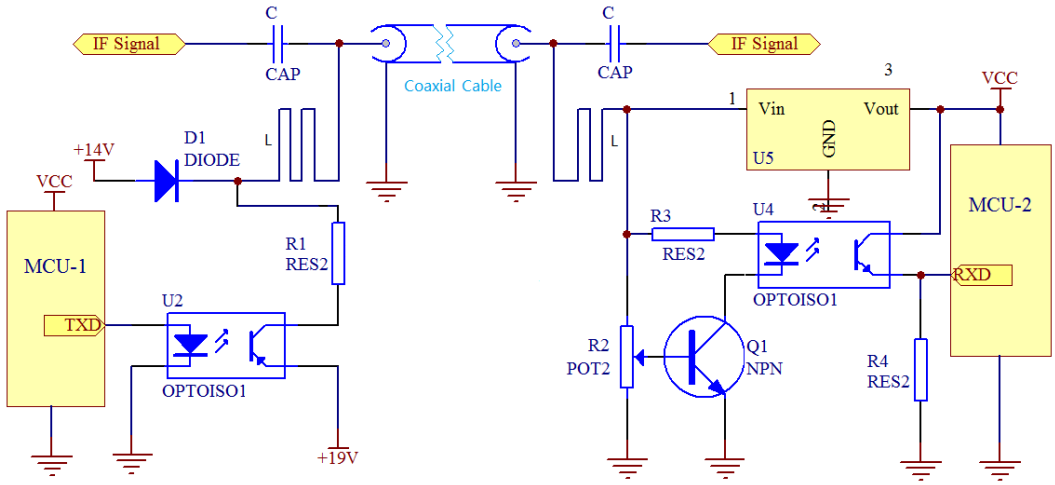

Figure D.2: Schematic of command transmission circuit

D.3 Command format

The previous section applies us an economic and simple method to transmit command integrated with DC supply and IF signal from user device to phased array antenna. To control the radiation of the proposed cross-type phased array antenna which operates in Ku-band with wide bandwidth and dual polarizations, the commands should contain plenty of information. Here we have constructed a standard of command format, which has been presented detaildly in Tab.D.1.

Table D.1: Command format table

Head 1 byte	Commands	Value	CNT 1 byte	CRC 1 byte
0x55	ASCII Codes	ASCII Codes		
All commands start with 0x55	Polarization	0 H V 0	Sum of total byte numbers	Cyclic Redundancy Check
	Beam_location	+ degree - degree		
	Beam_shift	+ degree - degree		
	Oscillator	0 L H 0		

It can be inferred from Tab.D.1 that each command begins with a head byte $0x55$ and ends with total byte count and one Cyclic Redundancy Check byte, to ensure the accuracy of command transmission. Considering the required function of our antenna, we have summed up four kinds of commands to control antenna radiation and local oscillators (generally two oscillators are used in antenna Low-noise Block, reserved to cover wideband, as already depicted in Chapter 1).

D.3.1 command code: Polarization

This command code is used to set the current polarization of cross-type antenna array. The optional values are Horizontal (0 H) and Vertical (V 0).

$$e.g. \qquad Polarization : 0H$$

D.3.2 command code: Beam_location

This command code is used to locate the main beam of antenna array, the beam angle has a accuracy of 0.1° and has a flag to determine beam shifting direction (CW or CCW).

$$e.g. \qquad Beam\_location : +10.1$$

to tell the slave micro-processor to shift antenna array beam to 10.1° CW.

D.3.3 command code: Beam_shift

This command is to ask the slave micro-processor to shift antenna array beam with a relative angle. A flag is also needed to determine the shifting direction (CW or CCW).

$$e.g. \qquad Beam\_shift : -1.5$$

to tell the slave micro-processor to shift antenna array beam 1.5° CCW relative to the current beam direction.

D.3.4 command code: Oscillator

This command code is used to choose the local oscillators. Generally, there are two oscillators in LNB, which are 9.75GHz and 11.6GHz. The value 0L is to choose the 9.75GHz oscillator and H0 is to choose the 11.6GHz oscillator.

$$e.g. \qquad Oscillator : 0L$$

D.4 Results and discussion

The experimental command transmitting modules are realized in our laboratory and the photograph is presented in Fig.D.3 (DC power supplier and potentiometers array are not illustrated here). Measured S-parameters are plotted in Fig.D.4, in which we can see the command transmitting modules are well optimized in Ku-band, very low reflection coefficient is obtained. It is worth noting that about 6dB loss in transmission coefficient because of using dual capacitors and long transmission cable, however this loss could be made up by Low-Noise Amplifiers in LNB.

Fig.D.5 illustrates the measured voltage level at the sending module and receiving module with oscilloscope, which indicates that the commands loaded on the couple of DC voltages could be accurately detected by the receiving module.

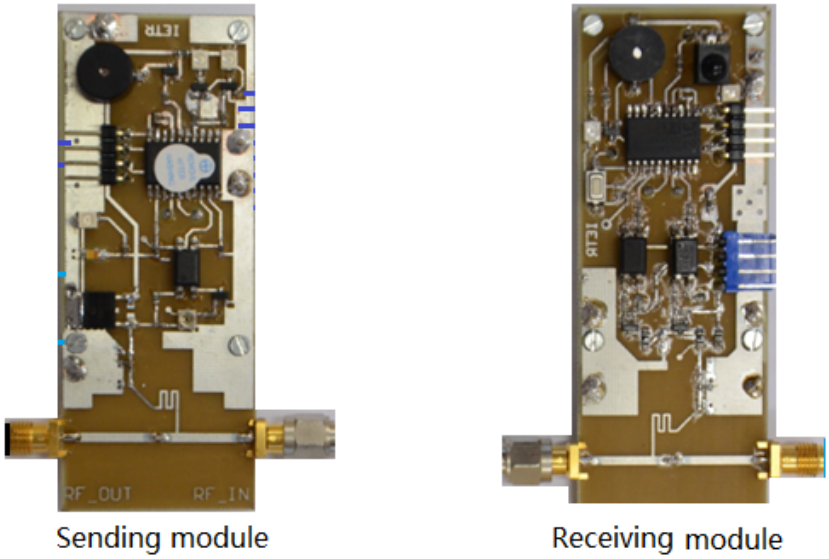

Figure D.3: Realized command transmitting modules

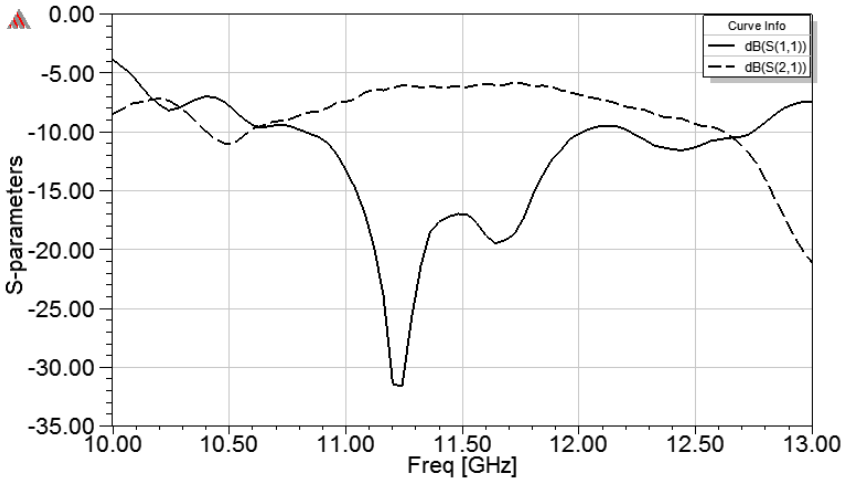

Figure D.4: measured S-parameters

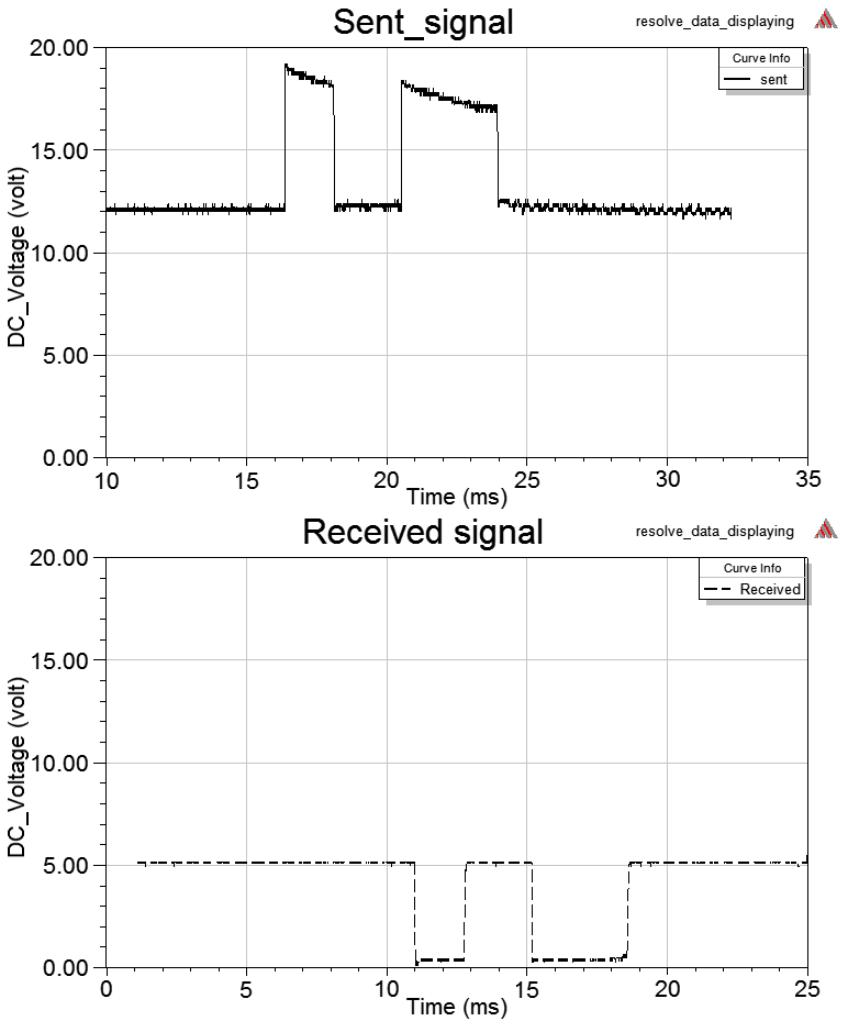

Figure D.5: Measured voltage level of sent and received command

l'université nantes angers le mans
COMMUNAUTÉ D'UNIVERSITÉS ET ÉTABLISSEMENTS

UNIVERSITÉ DE NANTES

Thèse de Doctorat

Haiyang ZHANG

Conception et Réalisation d'un Réseau d'antennes à pointage électronique pour les communications par satellite

Design and realization of an auto-focus antenna array for satellite communications

Résumé

Actuellement, la réception des signaux émis par les satellites géostationnaires s'effectue à l'aide d'antennes paraboliques. Cette antenne est largement utilisée en raison de ses performances et de son coût. Cependant, celle-ci souffre de défauts inhérents à sa conception (antenne 3D, faisceau fixe).Afin de trouver une alternative à l'existant, la conception d'une antenne planaire, large bande (20% de BP), bi-polarisation, de gain élevé (29dBi), à pointage électronique et à faible coût est envisagée pour la réception TV par satellite (système DBS).

Pour répondre aux critères de faible encombrement et de faible coût, la technologie microruban a été retenue. Deux topologies d'antennes élémentaires ont été étudiées, optimisées et mises en réseau pour répondre aux autres critères de ce projet : une antenne monopole alimentée par accès coplanaire et une antenne microruban à résonateurs couplés en croix.

Ces travaux ont abouti à un certain nombre de résultats originaux. La mise en oeuvre d'une méthode simple a permis d'établir qu'il était possible de stabiliser le diagramme de rayonnement dans le demi-espace supérieur sur une large bande passante et d'atténuer le rayonnement arrière. Un autre apport de ces travaux réside dans le principe de partage des résonateurs lors de la mise en réseau de l'antenne croix. Cette technique permet de limiter la distance inter-éléments (limitation des lobes de réseau) mais aussi, pour un gradient de phase donné, de réaliser un dépointage plus important. Ces travaux prouvent qu'un tel réseau d'antennes est une alternative crédible aux antennes paraboles.

Mots clés

Antenne réseau, large bande et double polarisation, communications par satellite, réception TV.

Abstract

Nowadays, receiving signals from geostationary satellites is performed using parabolic antennas composed of a metal reflector and a LNB (Low Noise Block) placed at the focus of the parabola. This antenna is widely used because of its performance and cost. However, this kind of antenna suffers from inherent shortcomings (3D antenna, fixed beam).

To find an alternative to the existing, design of a planar, broadband (20% BP), dual-polarization, high gain (29dBi), electronically steerable and low cost antenna is proposed for the reception of TV signals from satellite (DBS system).

To meet the criteria of compactness and low cost, microstrip technology is chosen. Two topologies of unitary antenna have been studied, optimized and arrayed to meet the requirements of this project: one coplanar fed monopole antenna and one cross-type multi-resonator antenna.

This work has led to numbers of original results. The development of a simple method shows that it is possible to stabilize the radiation pattern in the upper half space over a wide bandwidth and to decrease the rear radiation part. Another contribution of this work lies in the principle of sharing resonators when arraying cross shaped antenna. This technique not only reduces the inter-element distance (grating lobes appearance), but also, for a given phase gradient, achieves a greater beam steering. This proves the feasibility of such an antenna to be a credible solution.

Key Words

Phased array antenna, Wideband & Dual-Polarization, Satellite Communications, Television Reception.